

ABSTRACT

Title of Dissertation: ANALYSIS OF *ARABIDOPSIS* ABCB AUXIN TRANSPORTER MUTANTS REVEALS A PRIMARY ROLE IN MEMBRANE EXCLUSION

Mark Kubo Jenness, Doctor of Philosophy, 2018

Dissertation directed by: Professor Angus S. Murphy, Department of Plant Science and Landscape Architecture

Polar transport of the phytohormone auxin regulates multiple of aspects of plant growth and development. A subset of plant ATP-binding cassette subfamily B (ABCB) transporters mediate cellular auxin export. Loss of these transporters results in reduced polar auxin movement and altered plant architecture but no significant defects in embryogenesis or organ formation. Several of lines of evidence suggest that isotropically-localized ABCB transporters mediate auxin exclusion from the plasma membrane and prevention of reuptake after directional PIN-mediated efflux. Examination of the *Arabidopsis* auxin transporters ABCB1 and ABCB19 indicates a primary role in exclusion from small auxin producing cells in apical regions and prevention of leakage from polar auxin transport streams. Analysis of *abcb* mutants identifies a contribution from ABCB21 in restricting auxin to within the root vasculature in seedlings. In mature tissues, ABCB6, ABCB21, and ABCB11 make

additional contributions to polar auxin transport in inflorescence stems, leaves, and flowers, respectively. The results presented herein reflect an evolutionarily conserved function for ABCB transporters in maintaining polar transport streams and prevention of cellular reuptake via exclusion.

ANALYSIS OF *ARABIDOPSIS* ABCB AUXIN TRANSPORTER MUTANTS
REVEALS A PRIMARY ROLE IN MEMBRANE EXCLUSION

by

Mark Kubo Jenness

Dissertation submitted to the Faculty of the Graduate School of the
University of Maryland, College Park, in partial fulfillment
of the requirements for the degree of
Doctor of Philosophy
2018

Advisory Committee:
Professor Angus Murphy, Chair
Professor David Hawthorne
Professor Jianhua Zhu
Professor Wendy A. Peer
Professor Gary Coleman

© Copyright by
Mark Kubo Jenness
2018

Preface

I would first like to start by thanking Dr. Murphy and Dr. Peer for giving me the opportunity to participate in their summer internship program at Purdue while I was an undergraduate at California State University, Monterey Bay. During that internship I assisted a Master's student, Deepti Sanjai, in her characterization of the *Arabidopsis* AMINOPEPTIDASE P1 (APP1) that is involved in auxin signaling. My time spent in the Murphy and Peer labs during that internship opened my eyes to plant research and is what I consider to be the start of my scientific career. Without this experience and the support of Dr. Murphy and Dr. Peer I'm not sure I would have had the opportunity to pursue my Ph.D.

When I was applying for graduate school Dr. Murphy said if I chose to join his lab at Purdue University he had a project that would be great for me. The project was doing a structural and functional analysis of plant ABCB transporters. In mammals these transporters have broad specificity and contribute to chemotherapeutic drug resistance. However, in plants they appeared to have very narrow specificities, transporting the phytohormone auxin and a few other small organic anions. If these two sets of transporters utilize ATP hydrolysis to power substrate translocation across membranes in the same manner and share a highly conserved overall protein structures, then how do they perform such different functions? The project was to identify putative substrate binding sites in the *Arabidopsis* auxin transporters, create site-directed mutants within these sites, then test transport activity when expressed in the fission yeast *Schizosaccharomyces pombe*. Things were generally going according to plan when two years into my

project our lab relocated to University of Maryland. While moving was difficult, the failure of the yeast system I relied upon could not have been anticipated. Despite the efforts of several lab members to troubleshoot the issues, the system remains non-functional.

Around that time a paper was published showing that *Arabidopsis* ABCB21 transports auxin in leaf protoplasts and when expressed in yeast, however the authors were unable to report any phenotypic differences in plants. Previously at Purdue, I had taken over analysis of ABCB21 from a past Ph.D. student and a post-doc in the lab. I decided to repeat some of the past experiments and found a new allele of *abcb21* that showed phenotypic differences in root growth. This ultimately led to the analysis of a conserved exclusionary function shared by ABCB auxin transporters presented in this dissertation.

In Chapter 3, I analyzed ABCB transporters for roles in auxin transport in *Arabidopsis* seedlings. Considering the levels of *ABCB19* expression and activity compared to the others, it became apparent that ABCB19 is the primary ABCB auxin transporter in seedlings and any contribution from others would be supplementary. In this analysis I establish a primary function for ABCB21 in the root. ABCB19 and ABCB21 maintain the rootward auxin transport stream by excluding auxin from entering bounding tissues. Analysis of several other ABCB transporters indicate they are more likely to contribute to transport in mature tissues.

In Chapter 4, I investigated the contributions of ABCB transporters to auxin transport in mature tissues. In this chapter I establish that ABCB transporters function primarily by excluding auxin from small auxin producing cell in shoot and leaf

apices. A detailed phenotypic analysis of light-dependent phenotypes again point to the exclusionary function of ABCB19 being primary. Further, I identify contributions other ABCB transporters, including ABCB21, make to auxin transport in inflorescence stems, leaves, and flowers. Like with what is observed in seedlings, their contributions to auxin transport are supplementary to that of ABCB19.

In the previous chapters I established ABCBs contribute to auxin transport primarily by an exclusionary mechanism. One question that remains a challenge to answer is how ABCB transporters recognize auxin as a substrate. In Chapter 5, I collaborated with Dr. Ken-Ichiro Hayashi to investigate the use of fluorescently-tagged auxins as a tool for auxin transport studies. I tested to see if the fluorescent auxins were indeed substrates for long-distance transport, however, my conclusion was that they are not substrates of the primary ABCB and PIN long-distance auxin transporters.

In Chapter 6, I use homology modelling and heterologous expression systems to identify structural features that contribute to ABCB transporter specificity and activity. These analyses identified putative substrate binding sites that support a primary function of ABCB transporters in exclusion of auxin from the membrane. Analysis of the contribution of these binding sites to specificity and activity are ongoing as attempts to adapt systems established for other organisms to plant transporters remains a challenge.

At this time, I would like to thank my advisor, Dr. Angus Murphy. I am thankful for your guidance and support. You taught me not only how to become an independent researcher and critical thinker, but also gave me professional

development and leadership skills that will be indispensable in my future endeavors. Thank you to Dr. Wendy Peer for your continual expertise, encouragement, and always delicious baked snacks. To all my committee members, I truly appreciate your advice, time, criticisms, and patience. To all the current and past members of the Murphy and Peer labs, thank you for all of your company, support, assistance and contributions. Thank you to my family and friends for your continued love and support, and understanding of me being away for so long. Finally, I would like to thank my mom. We have encountered many difficult times but together we've always pulled through. You have always pushed me to do my best and encouraged me to pursue my dreams. Your strength and support have allowed me to get to where I am today.

Mark Jenness

April 2018

Dedication

In memory of my dad, Guy William Jenness, and step-dad, Thomas Ray Murphy.

Contributions to this dissertation

Chapter 3: ABCB19-GFP was imaged with help from Candace Pritchard. *ABCB21* and *ABCB11* promoters were cloned by Nicola Carraro. Auxin quantifications were performed by Dr. Angus Murphy, Dr. Bruce Cooper and Dr. Reuben Tayengwa with consultations and discussions from Dr. Joshua Blakeslee and Jinshan Lin. Seedling transport assays were done by Dr. Angus Murphy and Yan Cheng. *abcb21* phototropic bending was conducted by Candace Pritchard. RNAi lines were generated and analyzed by Dr. Haibing Yang. qRT-PCR was done in collaboration with Dr. Wiebke Tapken.

Chapter 4: Inflorescence and leaf transport assays by Dr. Angus Murphy. Auxin quantifications were performed by Dr. Angus Murphy, Dr. Bruce Cooper and Dr. Reuben Tayengwa with consultations and discussions from Dr. Joshua Blakeslee and Jinshan Lin. *ABCB21* and *ABCB11* promoters were cloned by Dr. Nicola Carraro. Leaf transport data were analyzed by Dr. Wiebke Tapken. Triple mutant phenotypic analysis was performed with equal contribution from Dr. Wiebke Tapken. Triple mutant cell sizes were measured by Changxu Pang.

Chapter 5: The majority of experiments in this chapter were performed by Dr. Ken-ichiro Hayashi and colleagues. My contributions to this chapter are analysis of the fluorescent auxins distribution in wild type and *abcb/pin* mutants, the decapitated seedling transport assays, and writing and review of the manuscript.

Table of Contents

Preface.....	ii
Dedication.....	vi
Contributions to this dissertation	vii
List of Tables	x
List of Figures.....	xi
List of Abbreviations	xiii
Nomenclature.....	xiv
Chapter 1. General Introduction	1
Discovery of Auxin.....	1
Auxin Metabolism	2
Auxin signaling.....	3
Auxin induces cell division and cell expansion.....	3
Auxin transport	4
AUXIN1/LIKE-AUXIN1 uptake permeases	7
PIN-FORMED (PIN) efflux carriers	8
ATP-binding cassette subfamily B (ABCB) efflux transporters	10
<i>Conserved ABC Transporter structure</i>	11
<i>Plant ABCB transporters</i>	14
<i>Function of ABCBs in polar auxin transport</i>	15
<i>Interaction with FKBP42/TWD1</i>	17
<i>Substrate specificity and specific activity</i>	18
Research Objectives.....	20
Chapter 2. Evolution of transport directionality in ABCBs.....	21
Summary	21
Introduction.....	22
Discovery of plant ABCB uptake transporters	25
Phylogeny of putative uptake transporters and functional divergence	30
Structural features unique to putative uptake transporters.....	32
Mechanism of uptake and conditional “reversibility”	34
Re-Evaluation of the Data: Truly Reversible or Simply Control of Efflux?	36
Conclusion	40
Chapter 3. <i>Arabidopsis ABCB21</i> contributes to rootward auxin streams by regulating auxin levels in the seedling pericycle	42
Summary	42
Introduction.....	42
Results.....	46
<i>Exclusion of auxin mediated by ABCBs at the plasma membrane</i>	46
<i>ABCB21 maintains auxin transport streams by restricting auxin to within the vasculature</i>	49
<i>ABCB transporter expression</i>	59
<i>Auxin transport in cluster specific ABCB-RNAi lines</i>	61
<i>Phenotypes and transport in ABCB single mutant lines</i>	64
<i>Characterization of ABCB11</i>	67
Discussion.....	71

Materials and Methods.....	76
Chapter 4. ABCB regulation of auxin transport in <i>Arabidopsis</i> stems, leaves and flowers.....	81
Summary.....	81
Introduction.....	81
Results.....	85
<i>ABCB1 and ABCB19 function by excluding auxin from the shoot apex in inflorescences</i>	85
<i>Light dependent phenotypes in abcb1 and abcb19 mutants</i>	87
<i>ABCB6 mediates auxin transport in inflorescence stems</i>	91
<i>Analysis of ABCB11 and ABCB21 in aerial tissues</i>	96
<i>Analysis of abcb11 and abcb21 triple mutants</i>	101
Discussion.....	108
Materials and Methods.....	111
Chapter 5. Auxin transport sites are visualized in planta using fluorescent auxin analogs	113
Summary.....	114
Introduction.....	115
Results.....	118
<i>Design and Synthesis of Fluorescently Labeled Auxin Analogs</i>	118
<i>Fluorescent Auxin Functions as an Auxin Analog Specific for Auxin Transport</i>	120
<i>Auxin Transport System Regulates the Distribution of Fluorescent Auxin</i>	123
<i>Distribution of Fluorescent Auxin at the Root Apex</i>	126
<i>Fluorescent Auxin Distribution Mimics Native Auxin Accumulation in Vivo</i> ..	128
<i>Subcellular Distribution of Fluorescent Auxins</i>	129
Discussion.....	131
Materials and Methods.....	133
Acknowledgements.....	134
Chapter 6. Computational modelling and heterologous expression	136
Summary.....	136
Introduction.....	136
Results.....	137
<i>Sequence analysis of Arabidopsis ABCB transporter NBDs</i>	137
<i>Computational modelling predicts auxin binding sites</i>	139
<i>Mutational analysis of ABCB19 in Schizosaccharomyces pombe</i>	142
<i>Analysis of ABCB19 in Lactococcus lactis</i>	144
Discussion.....	147
Materials and Methods.....	149
Conclusions.....	152
Appendices.....	155
Appendix A. Supplementary information for Chapter 5	155
Appendix B. Lines used in this dissertation.....	181
Appendix C. Primers used in this dissertation.....	181
Bibliography	184

List of Tables

Table 3.1. Single mutant phenotypes

List of Figures

- Figure 1.1. Chemiosmotic model of auxin transport
Figure 1.2. Wildtype and *pin1* *Arabidopsis* inflorescence stems
Figure 1.3. Structural features of ABC transporters
Figure 2.1. ABCB4 regulates root hair elongation in *Arabidopsis*
Figure 2.2. Phylogenetic tree of plant ABCB transporters
Figure 2.3. Proposed model for ABCB4 mediated accumulation and activation of efflux
Figure 3.1. Cellular exclusion is a primary function of ABCB19
Figure 3.2. Activity and expression of *ABCB21*
Figure 3.3. Loss of ABCB21 reduces the supply of auxin to emerging lateral roots
Figure 3.4. Cotyledon-hypocotyl auxin transport and phototropic bending in *abcb21*
Figure 3.5. Root twisting in *b1b19b21* and expression of ABCB transporters in seedlings
Figure 3.6. Expression and transport in *ABCB-RNAi* lines
Figure 3.7. Auxin transport assays in *abcb* mutants seedlings
Figure 3.8. Expression and activity of *ABCB11*
Figure 3.9. Model for ABCB21 function in the root
Figure S3.1. Isolation of *abcb21-2*
Figure S3.2. Lateral root number in 10-day seedlings
Figure S3.3. Primary root growth in *abcb* triple mutants is *twd1*-like
Figure S3.4. *ABCB* transporter expression in seedlings from the TraVA RNA-seq database
Figure S3.5. Compensatory expression of *ABCB19* in *abcb1* but not *abcb11* or *abcb21*
Figure S3.6. *ABCB12* does not compensate for loss of *ABCB11*
Figure 4.1. ABCB1 and ABCB19 exclude auxin out of the shoot apex in inflorescences
Figure 4.2. Leaf angles and areas in *abcb1* and *abcb19* mutants with varying light
Figure 4.3. Inflorescences of *abcb1* and *abcb19* mutants with varying light
Figure 4.4. *ABCB* transporter expression in inflorescence stems
Figure 4.5. Auxin transport in inflorescence segments
Figure 4.6. Expression of *ABCB11* and *ABCB21*
Figure 4.7. ABCB21 activity in leaves
Figure 4.8. ABCB triple mutant leaf phenotypes
Figure 4.9. Triple mutant inflorescence phenotypes
Figure S4.1. Comparison of *abcb1abcb19* and *twd1*
Figure S4.2. *ABCB* transporter expression in inflorescence stems from the TraVA RNA-seq database
Figure S4.3. *ABCB* transporter expression in leaves and flowers from the TraVA RNA-seq database
Figure S4.4. *proABCB21:GUS* is expressed after wounding
Figure S4.5. Intact triple mutant flowers
Figure 5.1. Distribution of fluorescent auxin analogs in *Arabidopsis* root
Figure 5.2. Effects of NBD-auxins on SCF^{TIR1} auxin signaling

Figure 5.3. Auxin transport system affects the distribution of fluorescent auxin in roots

Figure 5.4. Auxin maxima in the root apex

Figure 5.5. Distribution of fluorescent auxin mimics the native auxin gradient

Figure 5.6. Subcellular localization of NBD-NAA

Figure 6.1. Comparison of ABCB6 and Sav1866 nucleotide binding domain (NBD) dimer organization

Figure 6.2 Docking of IAA to the inner leaflet associated binding sites

Figure 6.3. Amino acid residues associated auxin binding in ABCB19

Figure 6.4 Mutations in ABCB19 binding pockets reduce transport activity

Figure 6.5. Schematic of assays in *L. Lactis* membrane vesicles

Figure 6.6. ABCB19 exhibits auxin efflux activity that is sensitive to transport inhibitors in *L. Lactis* whole cells

Figure 6.7. ABCB19 exhibits auxin efflux activity that is sensitive to transport inhibitors in *L. Lactis* whole cells

Figure 6.8. ABCB19 exhibits auxin transport activity in *L. Lactis* inverted membrane vesicles

List of Abbreviations

ABC	ATP-binding cassette
ADP	adenosine-diphosphate
ATP	adenosine-triphosphate
BA	benzoic acid
BP	base pair
cDNA	complementary deoxyribonucleic acid
CDS	coding sequence
DPM	disintegrations per minute
ER	endoplasmic reticulum
GUS	β -glucuronidase
GFP	green fluorescent protein
IAA	indole-3-acetic acid
MDR	multidrug resistance
MRP	multidrug resistance relate protein
NBD	nucleotide-binding domain
PCR	polymerase chain reaction
PDR	pleiotropic drug resistance
PGP	P-glycoprotein
PM	plasma membrane
RPM	revolutions per minute
qRT-PCR	quantitative real-time polymerase chain reaction
TMD	transmembrane domain
TMH	transmembrane helices

Nomenclature

The nomenclature used in this dissertation follows the Community standards for *Arabidopsis* genetics (Meinke and Koornneef, 1997).

<i>UPPERCASE ITALICS</i>	wild-type gene
<i>lowercase italics</i>	mutant gene
UPPERCASE	wild-type protein
lowercase	mutant protein

Chapter 1. General Introduction

Unlike animals, plants lack a central nervous system that allows for long distance signaling between tissues and organs. Instead, plants have developed mechanisms for cell-to-cell hormone movement and communication. One of the primary plant growth regulators, or phytohormones, that is transported in this manner is auxin.

Discovery of Auxin

Studies of chemical messengers in plants have been conducted for over 250 years. In 1758, experiments by Henri-Louis Duhamel du Monceau suggested movement of sap from leaves controlled root growth (Duhamel du Monceau, 1758). In 1868, German botanist Julius von Sachs, who many consider the father of plant physiology, suggested that “organ-forming substances” were made by the plant and transported to different parts where they controlled growth and development (von Sachs, 1868). In The Power of Movement in Plants, Charles Darwin described a diffusible element that caused asymmetric growth of grass coleoptiles in response to light (Darwin, 1880). Later, in 1927, Fritz Went isolated this “growth regulator” by collecting the substance in agar blocks and showing that it could re-initiate growth when placed on decapitated oat coleoptiles (Went, 1926). The substance was later identified as indole-3-acetic acid (IAA) and termed “auxin” from the Greek word “auxien” meaning “to grow/to increase” (Kögl and Haagen-Smit, 1931). Since then the establishment of localized and global gradients of auxin have been shown to be important for a variety of aspects of growth and development including

embryogenesis, organogenesis, cell/tissue/organismal polarity, phyllotaxis, and tropic responses (reviewed in Zazimalová *et al.*, 2010).

Auxin Metabolism

The primary auxin in plants is indole-3-acetic acid (IAA). Several other naturally occurring auxins have been identified including indole-3-butyric acid (IBA) (Cooper, 1935), 2-phenylacetic acid (PAA) (Koepfli *et al.*, 1938), and 4-chloroindole-3-acetic acid (4-Cl-IAA) (Porter and Thimann, 1965), however their roles plants are not well understood. IAA is primarily synthesized from tryptophan in a two-step reaction (Mashiguchi *et al.*, 2011; Stepanova *et al.*, 2011). First TRYPTOPHAN AMINO TRANSFERASE of ARABIDOPSIS (TAA) and TAA-Related (TAR) proteins convert tryptophan into indole-3-pyruvic acid (IPyA). Then one of the eleven YUCCA members catalyze the rate-limiting step of converting IPyA into IAA. IAA can also be synthesized in a tryptophan-independent pathway, however, the enzymes involved have yet to be identified (reviewed in Zhao, 2018). In addition to biosynthesis, the levels of free IAA, or IAA available for auxin signaling, within a cell are controlled by auxin conjugation and oxidation. Several enzymes catalyze the conjugation (addition) and hydrolysis (removal) of methyl groups (methyl-IAA), glucose (IAA-Glc), or one of several amino acids (IAA-ala, IAA-Asp, etc.) to reversibly inactivate and reactivate auxin (reviewed in Zhang & Peer, 2017). IAA can also be inactivated irreversibly through oxidation by DIOXYGENASE FOR AUXIN OXIDATION (DAO) (Mellor *et al.*, 2016; Porco *et al.*, 2016; Zhang *et al.*, 2016). Additionally, while auxin biosynthesis occurs on the cytosolic surface of the endoplasmic reticulum (ER), the majority of auxin hydrolases are localized within the

ER lumen (Campanella et al., 2003), pointing to compartmentalization as being an important mechanism for auxin homeostasis.

Auxin signaling

Cells respond to auxin transcriptionally via the SUPPRESSOR OF KINETOCHORE PROTEIN1 (SKP1)-CULLIN1-F-box (SCF) E3 ubiquitin ligase complex in the nucleus (reviewed in Ma *et al.*, 2018). When cellular auxin is below threshold levels, AUXIN/INDOLE-3-ACETIC ACID (Aux/IAA) proteins bind to transcription factors called auxin response factors (ARFs). This represses transcription by preventing ARFs from binding to auxin response elements (AuxREs) in promoters of auxin responsive genes. Aux/IAs associated with DNA-bound ARFs also trigger recruitment of the histone de-acylases TOPLESS (TPL) and (TOPLESS RELATED (TPR), which cause DNA condensation and further prevention of transcription (Korasick et al.; Han et al., 2014). When cellular auxin reaches threshold concentrations, IAA binds to the auxin receptor TRANSPORT INHIBITOR RESPONSE 1 (TIR1) F-box protein and acts like a “molecular glue” to promote association of Aux/IAs with the SCF^{TIR1} complex (Tan et al., 2007; Calderón Villalobos et al., 2012). This triggers poly-ubiquitination and degradation of Aux/IAs and release of the ARFs to allow for transcriptional activation (reviewed in Weijers & Wagner, 2016). In some cases, free ARFs act as transcriptional repressors but the mechanisms are not well understood.

Auxin induces cell division and cell expansion

Auxin promotes two primary cellular responses: cell division and cell expansion. Transcriptional regulation caused by localized auxin gradients in meristematic tissues maintain stem cell niches and induce organ formation and patterning (reviewed in Wang & Jiao, 2018). In these cells, complex cross-talk between auxin and cytokinin, a phytohormone that regulates cell division and differentiation, dictates cell fate specifications during embryo- and organogenesis (Chandler and Werr, 2015).

During cell expansion, auxin induces expression of SMALL AUXIN UPREGULATED RNAs (SAURs) (reviewed in Ren & Gray, 2015). The SAURs interact with several PP2C-D protein phosphatases to inhibit their activity (Spartz et al., 2014). This results in activation of the H⁺-ATPases that acidify the apoplast, ultimately leading to cell wall loosening and cell expansion (reviewed in Arsuffi & Braybrook, 2018). One example of this mechanism in action is phototropism, the classical physiological response that led to the discovery of auxin by Charles and Francis Darwin. During phototropism auxin is differentially transported to the shaded side of coleoptiles, hypocotyls, or stems. This causes activation of H⁺-ATPases and cell expansion, resulting in elongation of the shaded side of the stem and growth toward the light source. Achievement of these responses requires the ability to move of auxin from cell to cell.

Auxin transport

As the early discoverers of auxin all noted, the sites of IAA biosynthesis and the sites of response and signaling are typically separated by space and time. IAA is primarily synthesized in young tissues in shoot and root meristems and in the tips of

young leaves. According to the chemiosmotic model of auxin transport IAA is transported from sites of synthesis to sites of action by a combination of diffusion and the activities of several auxin uptake and efflux proteins (Fig. 1.1) (Rubery and Sheldrake, 1974; Raven, 1975; Goldsmith, 1977). At apoplastic pH (pH 5.5) about 15% of IAA (pKa 4.75) is protonated (IAAH) and can cross the plasma membrane (PM) through lipophilic diffusion. The remaining 85% remains anionic (IAA⁻) and requires uptake mediated by an AUXIN1/LIKE-AUXIN1 (AUX1/LAX) auxin-proton symporter to cross the PM (reviewed in Swarup & Péret, 2012). Once inside the cell (pH 7.0) greater than 99% of IAA is anionic and requires the activities PIN-FORMED (PIN) efflux carriers and ATP-binding cassette subfamily B (ABCB) transporters to mediate movement back out of the cell (reviewed in Geisler *et al.*, 2017).

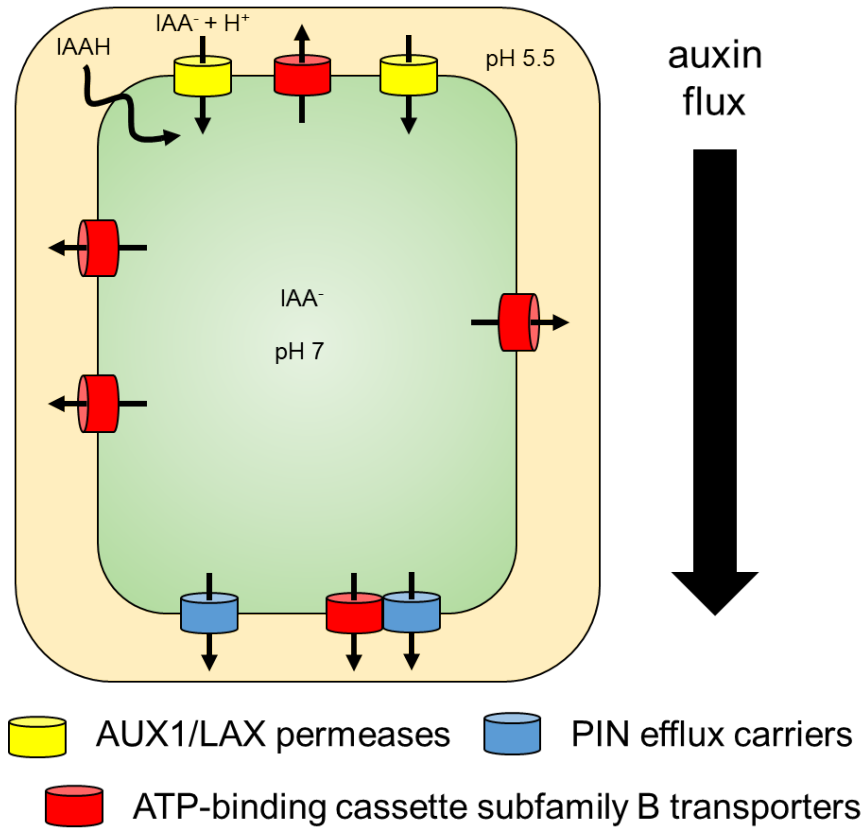


Figure 1.1. Chemiosmotic model of auxin transport auxin. (IAA) can enter cells through lipophilic diffusion or proton-coupled uptake mediated by AUX1/LAX permeases. At cytosolic pH auxin is anionic and trapped must be exported by PIN efflux carriers or ATP-binding cassette subfamily B (ABCB) transporters. Figure by the author of this dissertation.

In addition to AUX1/LAXs, PINs, and ABCBs a few other proteins have been implicated in auxin transport. On the PM, NITRATE TRANSPORTER 1.1 (NRT1.1) has been suggested to act as a dual function nitrate/auxin uptake transporter (Ho et al., 2009; Krouk et al., 2010). Two members of the ATP-binding cassette subfamily G (ABCG) transporters, ABCG36 and ABCG37, have been suggested to transport the IAA precursor IBA across the PM (Růžicka et al., 2010). While these proteins do exhibit some characteristics of auxin transport, direct evidence of auxin as a substrate and their physiological roles in auxin transport *in planta* remain unclear. Several other proteins have also been shown to regulate cellular auxin homeostasis by compartmentalization. The PIN-LIKES (PILS) transport auxin into and out of the ER (Barbez et al., 2012). WALLS ARE THIN1 (WAT1) and the multidrug and toxic compound extrusion (MATE) transporter ADP1 have been suggested to regulate intracellular auxin homeostasis by mediating auxin transport out of the vacuole and in post-golgi endomembrane compartments, respectively (Ranocha et al., 2013; Li et al., 2014b). Little is known about the function of the short PINs and other endomembrane auxin transporters, however, their localization to internal membranes points to compartmentalization of auxin being an important aspect during growth and development.

AUXIN1/LIKE-AUXIN1 uptake permeases

In *Arabidopsis*, the AUX1/LAX family is comprised of four highly conserved proteins: AUXIN1 (AUX1) and LIKE-AUXIN1 (LAX) LAX1, LAX2 and LAX3 (reviewed in Swarup & Péret, 2012). Although AUX1/LAX proteins share considerable similarity to amino acid permeases, uptake of tryptophan or other amino

acids has not been demonstrated (Zazimalová et al., 2010). AUX1 is localized apically on the PM in auxin conducting cells, supporting a coordination of uptake with basally localized efflux transporters in auxin transport streams (Swarup et al., 2001). AUX1/LAX proteins have been shown to be important for a variety of developmental processes and responses including embryogenesis, apical hook formation, root gravitropism, lateral root development, root hair development, and leaf phyllotaxis (reviewed in Swarup & Péret, 2012). However, even the *aux1lax1lax2lax3* quadruple mutant develops only minor phenotypic defects (Bainbridge et al., 2008).

PIN-FORMED (PIN) efflux carriers

The PIN-FORMED (PIN) efflux carriers are unique to plants. The name PIN-FORMED originates from the first mutant isolated (*pin1*), which has an inflorescence stem that lacks floral organs resulting in a structure that resembles that of a pin (Fig. 1.2) (Okada et al., 1991). This pin-like structure is phenocopied by treatment with the polar auxin transport inhibitors 9-hydroxyfluorene-9-carboxylic acid (HFCA) or N-1-naphthylphthalamic acid (NPA), strongly suggesting a role for PIN1 in regulating polar auxin transport (Okada et al., 1991). The *Arabidopsis* genome encodes eight *PIN* family members that are divided into 'long' PINs and 'short' PINs, based on the length of a hydrophilic loop that connects two transmembrane domains (Křeček et al., 2009).

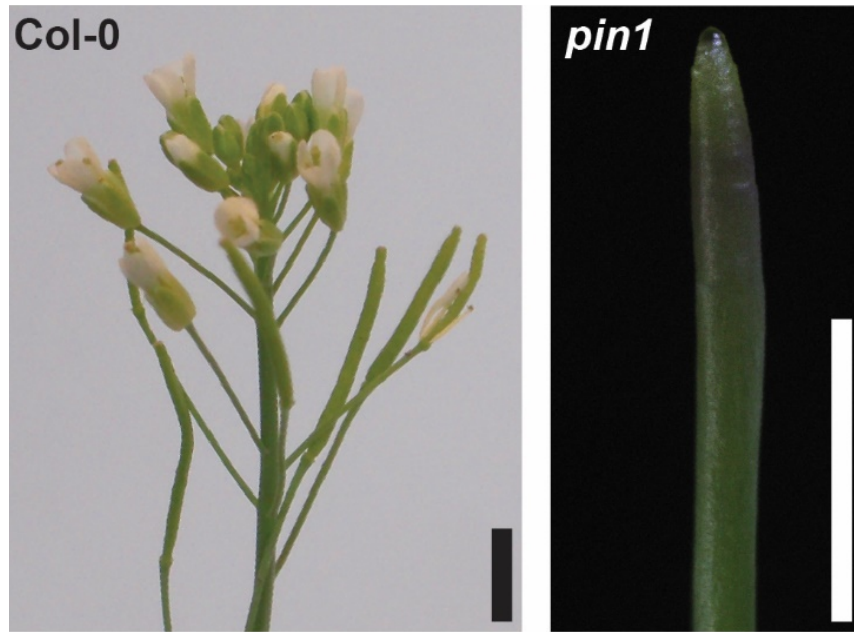


Figure 1.2. Wildtype and *pin1* *Arabidopsis* inflorescence stems. Bars = 2.5 mm.

Figure by the author of this dissertation. *pin1* image kindly provided by Candace Pritchard.

The ‘long’ PINS (PIN1-4 and PIN7) are polarly localized on the PM where they mediate directional auxin transport necessary for embryogenesis, organogenesis, phototropism, and gravitropism (reviewed in Adamowski & Friml, 2015). Although PINs are best known for their polarity, non-polar localizations are also common, particularly in non-auxin conducting tissues. Additionally, PINs are not static on the PM and apolar localization can rapidly become polar with various environmental cues. For example, within minutes of gravistimulation of roots, PIN3 changes localization from apolar to the basal side of cells to allow for differential auxin transport and growth with the new gravity vector (Friml et al., 2002). These rapid

trafficking events are dependent on the vesicular trafficking regulator GNOM, and PIN phosphorylation status regulated by PID, WAG, and D6PK (Weller et al., 2017).

The 'short' PINs (PIN5 and PIN8) have significantly reduced central loops (~50 amino acids) compared to the 'long' PINs (~300 amino acids). Short PINs localize to the ER membrane and are proposed to function in concert with the PILS to regulate auxin homeostasis (Mravec et al., 2009; Ding et al., 2012). PIN6, which has an intermediate length central loop (~250 amino acids), was recently shown to cycle between the ER and PM (Simon et al., 2016). This suggests PIN6 may have a role distinct from typical short and long PINs and supports evidence that loop modifications (phosphorylation) regulate trafficking and activity (reviewed in Adamowski & Friml, 2015).

Despite having critical roles during growth and development the mechanism for how PINs mediate auxin transport remains elusive. Activity of PIN1 is believed to be driven by the electrochemical gradient across the PM but direct evidence for the mechanism of action has not been fully demonstrated. Determination of a PIN protein structure by X-ray crystallography or cryo-electron microscopy would be a tremendous asset in understanding how they work.

ATP-binding cassette subfamily B (ABCB) efflux transporters

In plants, ABCB transporters are believed to play a primary role in maintaining PIN-mediated auxin transport streams. The best studied ABCB transporter is mammalian P-glycoprotein (PGP/ABCB1). The activity of PGP, a polyspecific, lipophilic-drug exporter, is best known for contributing to multidrug resistance in tumor cells (Ambudkar et al., 2006). PGP is constitutively expressed

throughout most tissues but expression is increased in cells surrounding transport streams (pulmonary, respiratory, and digestive) and vital organs (reviewed in Schinkel, 1997). For example, PGP functions in keeping toxic compounds from entering the brain by bounding capillaries at the blood-brain barrier and excluding them surrounding endothelial cells (Jodoin et al., 2003). This exclusionary mechanism is also hypothesized to be the primary mode of action for plant ABCBs during auxin transport.

While ABC transporters can mediate export or import of substrates, the majority of ABC transporters are exporters. Uptake transporters are only found in prokaryotes, in which a periplasmic substrate binding protein sequesters the substrate, then binds to the transporter for uptake (Higgins, 1992). Since prokaryotic importers have structures distinct from exporter type transporters, focus from here on will remain on canonical ABC exporter type transporters. The only transporters that have been shown to exhibit bidirectional transport activity are the *Arabidopsis* auxin transporters ABCB4 and ABCB21. A detailed analysis of these transporters and the mechanism of conditional transport directionality is provided in Chapter 2.

Conserved ABC Transporter structure

The overarching ABC superfamily of transporters share a common protein structure, despite having a diverse array of functions and substrates. Fully functional transporters all contain two transmembrane domains (TMDs) consisting of two sets of six transmembrane helices (twelve total), and two nucleotide-binding domains (NBDs) (Fig. 1.3 A) (Xiong et al., 2015). Transporters can be synthesized either as half-length transporters or full-length transporters. Half-length transporters, which are

arranged as (TMD-NBD) or (NBD-TMD) must homo- or hetero-dimerize to form a functional (TMD-NBD)-(TMD-NBD) or (NBD-TMD)-(NBD-TMD) transporter. Full-length transporters, which encode fused pseudo-symmetric halves connected with a linker, can be organized (TMD-NBD-TMD-NBD) or (NBD-TMD-NBD-TMD). All members of the PM localized ABCB transporters known to date are arranged (TMD-NBD-TMD-NBD) (Kang et al., 2011).

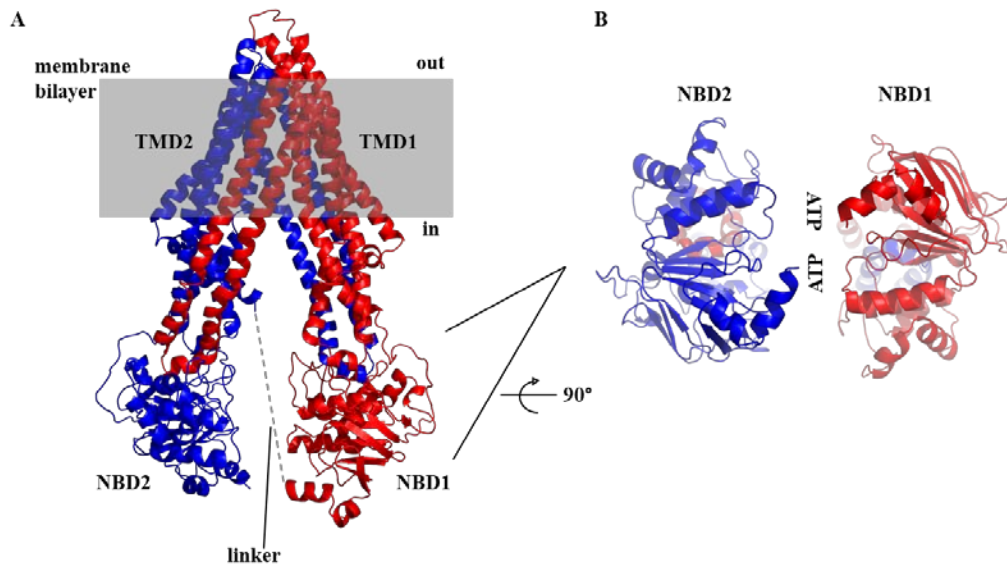


Figure 1.3. Structural features of ABC transporters. (A) Inward-facing conformation of *Arabidopsis* ABCB19 threaded on mammalian ABCB1 (PDB 4M1M). (B) Nucleotide-binding domain “sandwich dimer.” Figure by the author of this dissertation. Protein model visualized using PyMol.

The energy to drive substrate translocation is harvested from ATP within the nucleotide binding cassettes for which the protein family was named (Fig. 1.3 B). The core of the catalytic center consists of several highly conserved motifs that facilitate

ATP binding and hydrolysis (Rees et al., 2009; Wilkens, 2015). ATP is positioned within one NBD by a Walker motif (GXXGXXGKS/T) which interacts with the α - and β -phosphates of ATP, a conserved tyrosine residue (A-loop, Y) that positions ATP through base stacking with the adenine ring, and a Walker B motif ($\Phi\Phi\Phi\Phi$ DE, where Φ is hydrophobic) that provides a glutamine needed for catalysis of ATP. The ATP is positioned between the Walker A, A-loop, and Walker B from the NBD on one half of the transporter and a signature sequence motif (LSGGQ) from the opposing NBD in what is known as a “sandwich dimer.” The H-loop (H), or “switch” motif, stabilizes the geometry of the catalytic site during the transition-state. Q-loop (Q) and D-loops (SALD) provide contact point between the NBDs and TMDs to couple hydrolysis to transport.

In canonical ABC exporters, each TMD has 6 transmembrane α -helices for a total of 12 in a full transporter (Fig. 1.3A) (Rees et al., 2009; Wilkens, 2015). The organization of the α -helices results in a transmembrane pore that allows entry of substrates from the cytoplasm or from within the membrane bilayer. Unlike what is observed with the NBDs, highly-conserved sequence motifs have not been associated with the TMDs. This is likely what contributes to the diversity of substrates ABC transporters are able to move.

Substrate translocation is achieved by coupling ATP hydrolysis in the NBDs with conformational changes in the TMDs (reviewed in Locher, 2016). An alternating access model is the most widely accepted hypothesis for how substrates bind on one side of a membrane and are subsequently released on the other. In this model, substrate binds to the transporter in a binding pocket within the TMDs that is exposed

to only one side of the membrane. Subsequent ATP binding and hydrolysis causes a conformational change in the TMDs that alternates exposure of the binding pocket to the opposite side of the membrane. A change in affinity between the substrate and the transporter allows for substrate release. After substrate translocation, hydrolysis of ATP and release of ADP + P_i resets the system. Several varying hypotheses of this general scheme exist and a number of questions remain unanswered including whether ATP molecules in each NBD are required and if each ATP hydrolysis occurs concurrently or successively.

Plant ABCB transporters

Plant ABCB transporters were first studied to determine if they have a similar function to mammalian PGP that could be exploited to enhance herbicide resistance (Dudler and Hertig, 1992). However, it was shown that plant homologs of PGP are not polyspecific detoxifiers and are of little use for this purpose (Sidler et al., 1998). Analyses of other plant ABCB transporters indicate that these proteins are not primarily xenobiotic exporters, instead cellular detoxification is associated with plasma membrane-localized members of the pleiotropic drug resistance (PDR/ABCG) and tonoplast-localized multidrug resistance associated protein (MRP/ABCC) families (Remy and Duque, 2014).

The best characterized *Arabidopsis* ABCB transporters are the auxin transporters ABCB1, ABCB4, and ABCB19. ABCBs were first implicated in auxin transport when ABCB1 was shown to localize to the PM and that antisense and overexpression lines exhibited reduced and enhanced hypocotyl elongation, respectively (Sidler et al., 1998). Soon after, the *ABCB1* homolog, *ABCB19* was

identified in a screen for genes induced by the anion channel inhibitor 5-nitro-2-(3-phenylpropyl amino)-benzoic acid (NPPB) (Noh et al., 2001). *abcb19* mutants also exhibited phenotypes consistent with defects in auxin transport including epinastic cotyledons, decreased inflorescence height, loss of apical dominance, increased lateral branching, reduced lateral root formation, and reduced stamen filaments (Noh et al., 2001; Noh et al., 2003; Geisler et al., 2005; Lewis et al., 2007). These phenotypes are even more severe in *abcb1abcb19* double mutants (Noh et al., 2001; Blakeslee et al., 2007). Further studies have shown ABCB1 and ABCB19 exhibit strong and specific binding of the polar auxin transport inhibitor NPA (Noh et al., 2001; Murphy et al., 2002). A direct role for ABCB1 and ABCB19 in mediating auxin efflux was demonstrated when reduced auxin export was observed in *abcb1* and *abcb19* protoplasts, and when they were shown to mediate auxin efflux when heterologously expressed in yeast and HeLa cells (Geisler et al., 2005; Bouchard et al., 2006).

Function of ABCBs in polar auxin transport

ABCB1 and *ABCB19* are primarily expressed in meristematic tissues where auxin concentrations are high. *abcb1* and *abcb19* single mutants show ~25% and >50% reductions in rootward auxin transport, which is further reduced to ~70% in the *abcb1abcb19* double mutant (Noh et al., 2001; Blakeslee et al., 2007). *ABCB19* expression is also enhanced in the pericycle and endodermal cells that surround the central vasculature, and mutants exhibit increased leakage from the rootward stream (Bandyopadhyay et al., 2007; Blakeslee et al., 2007). This suggests ABCB19 maintains the rootward auxin movement by bounding the rootward auxin transport

stream. *ABCB1* expression is significantly lower than *ABCB19* and in more discrete regions, pointing to more tissue specific activities. Notably, loss of function mutations in *ABCB1* in maize and sorghum is the underlying basis for the agriculturally important dwarf cultivars *brachytic2 (br2)* and *dwarf3 (dw3)* (Multani et al., 2003).

Another characterized ABCB transporter, ABCB4, is primarily expressed in the root epidermis from the root cap through the differentiation zone (Cho et al., 2007; Kubeš et al., 2012). *abcb4* mutants exhibit reduced rates of shootward auxin transport from the root tip (Lewis et al., 2007; Kubeš et al., 2012). *abcb4* mutants do not exhibit any difference in rootward auxin transport from the shoot apex indicating a primary function in regulation of auxin transport in the root (Terasaka et al., 2005). Unlike ABCB1 and ABCB19, which have only been reported to exhibit export activity, ABCB4 exhibits concentration-dependent auxin transport (Terasaka et al., 2005; Yang and Murphy, 2009; Kubeš et al., 2012). ABCB4 mediates apparent auxin accumulation at low intracellular auxin levels that reverts to efflux when threshold levels are reached. An in depth review of this mechanism is detailed in Chapter 2.

In addition to ABCB1, ABCB4, and ABCB19, other ABCB transporters have been implicated in auxin transport. ABCB21, the paralog of ABCB4, was shown to have concentration-dependent auxin uptake/efflux transport activity in *Arabidopsis* protoplasts and when expressed in yeast (Kamimoto et al., 2012). *ABCB21* was shown to be expressed in leaves, lateral organ junctions in shoots, and in the root pericycle (Kamimoto et al., 2012). However, a clear role for ABCB21 in regulating auxin transport *in planta* has not been identified. Recently, *abcb14* and *abcb15* mutants were reported to have reduced auxin transport in inflorescence stems

(Kaneda et al., 2011). However, ABCB14 was originally identified as a malate/citrate transporter involved in stomata aperture regulation (Lee et al., 2008). Further, loss of ABCB14 and ABCB15 appears to disrupt proper vascular tissue formation (Kaneda et al., 2011), indicating the effects on auxin transport may be indirect.

Interaction with FKBP42/TWD1

Proper folding and trafficking of ABCB1, ABCB4, and ABCB19 require the activity of the immunophilin FK506-BINDING PROTEIN 42/TWISTED DWARF1 (FKBP42/TWD1) (Wu et al., 2010; Wang et al., 2013). Yeast-2-hybrid and BRET (bioluminescence resonance energy transfer) assays have shown direct interaction between FKBP42 and the C-terminus of these transporters (Geisler et al., 2003; Wang et al., 2013). Members of the FKBP superfamily all share sequence motifs indicative of peptidyl-prolyl-cis-trans isomerase (PPIase) folding activity (Romano et al., 2005). It was thought that FKBP42 PPIase activity mediated proper folding of the ABCBs, however, this has not been clearly demonstrated (Kamphausen et al., 2002). Instead, FKBP42, along with its co-chaperone HEAT SHOCK PROTEIN 90 (HSP90), is proposed to maintain interacting ABCBs in their correct conformation through a proposed holdase activity (Kamphausen et al., 2002).

In *twd1* mutants, ABCB1, ABCB4, and ABCB19 are mis-localized to the endoplasmic reticulum (ER) and are unable to properly traffic to and function on the PM (Wu et al., 2010; Wang et al., 2013). This is reflected in the significant overlap in severe dwarf phenotypes observed in *twd1* and *abcb1abcb19* double mutants (Noh et al., 2001; Geisler et al., 2003; Blakeslee et al., 2007). Additionally, *twd1* mutants exhibit a further reduction in rootward auxin transport (~85% reduction compared to

wild type) and more severe helical twisting of roots, inflorescences, and siliques (Geisler et al., 2003). One hypothesis is that this increase in phenotypic severity is due to contributions of other ABCB auxin transporters that interact with FKBP42. FKBP42 has also been shown to interact with proteins associated with the cytoskeleton (ACTIN7), brassinosteroid signaling (BRI1), and cell detoxification (ABCCs) (Geisler et al., 2004; Chaiwanon et al., 2016; Mao et al., 2016), suggesting the full *twd1* phenotype may not be accounted for in additional loss of ABCB transporter function. Additionally, the blue light photoreceptor, phot1, which has been shown to inhibit ABCB19 directly by phosphorylation during phototropism is proposed to disrupt the interaction between ABCB19 and FKBP42 (Christie et al., 2011).

Substrate specificity and specific activity

In contrast to the mammalian ABCBs, plant ABCB transporters exhibit a high degree of substrate specificity for small amphipathic and aliphatic organic acids. Assays across a variety of transport assay systems have shown ABCB1 and ABCB19 exhibit a high degree of specificity for IAA, with ABCB1 having a slightly broadened specificity which includes NAA and a few other auxin-like substrates (Geisler et al., 2005; Titapiwatanakun et al., 2009; Yang and Murphy, 2009). ABCB4 specificity is similar to that of ABCB1 (Santelia et al., 2005; Terasaka et al., 2005; Yang and Murphy, 2009; Kubeš et al., 2012). When expressed in *E.coli*, ABCB14 exhibits malate and citrate uptake (Lee et al., 2008), however, whether or not these are true transport substrates remains to be determined.

When expressed in yeast, ABCB1 and ABCB19 exhibit greater substrate specificity when FKBP42 is present (Bailly et al., 2013). Recently, ABCB19 was

shown to exhibit NPPB sensitive channel activity when expressed in human embryonic kidney cells (Cho et al., 2014). However, in the presence of FKBP42, channel activity was not observed. These results suggest NPPB may function as a general inhibitor of ABCB19 and that ABCB19 channel-like activity and decreased specificity only occurs when ABCB19 is not properly folded.

Several pieces of evidence suggests the plasma membrane environment contributes to the activity and specificity observed with plant ABCBs. Homology modelling and IAA docking analyses have identified two distinct sets of putative auxin binding sites in plant ABCB transporters (Yang and Murphy, 2009; Bailly et al., 2011). These studies predict ABCB1 and ABCB19 have a general binding pocket that is positioned within the membrane bilayer that corresponds to sites associated with poly-specific substrate exclusion in mammalian PGP. Another set of plant kingdom specific binding sites associated with the inner-leaflet-cytosol interface that are believed to be the sites for specific auxin binding. In either case, auxin binding sites appear to reside within the PM bilayer.

The primary auxin efflux proteins ABCB1, ABCB19, and PIN1, reside in sterol and sphingolipid-enriched plasma membrane nanodomains, while AUX1/LAX auxin uptake premeases do not. (reviewed in Tapken and Murphy, 2015). This provides a separation between areas of auxin uptake and areas of auxin efflux. When ABCB19 and PIN1 are co-expressed in heterologous systems or in cells where their expression overlaps, synergistic increases in auxin efflux activity and specificity have been reported (Blakeslee et al., 2007; Titapiwatanakun et al., 2009; Yang and Murphy, 2009). This specificity and activity is further increased with addition of

cholesterol, sitosterol, or ergosterol (Titapiwatanakun et al., 2009; Bailly et al., 2011). Taken together, these findings suggest ABCBs and PINs function in cellular auxin transport in specific membranes designated for auxin efflux. Since PIN proteins appear to mediate the direction of auxin efflux, a primary function for ABCB transporters in excluding auxin from small cells where auxin biosynthesis occurs and preventing reuptake following PIN-mediated transport would be predicted.

Research Objectives

Of the 21 full-length ABCB transporters encoded within the *Arabidopsis* genome only ABCB1, ABCB4, and ABCB19 have sufficient evidence to support their roles in mediating auxin transport. Several others, including ABCB14, ABCB15, and ABCB21 have been implicated (Kaneda et al., 2011; Kamimoto et al., 2012), but their specific contributions to auxin transport *in planta* remain unknown.

The main objective of this dissertation was to better establish the role ABCB transporters play in mediating polar auxin transport during plant growth and development. The specific objectives were 1.) to analyze how ABCB transporters mediate auxin transport through an exclusionary mechanism, 2.) to further understand the roles ABCB1 and ABCB19 play during growth and development, 3.) to identify functional roles for uncharacterized or partially-characterized ABCB transporters that contribute to auxin transport, 4.) to develop systems and tools used to study the structure and function of ABCB transporters and auxin transport in plants, and 5.) to determine how ABCB transporters function at the molecular level.

Chapter 2. Evolution of transport directionality in ABCBs

Mark K. Jenness¹ and Angus S. Murphy^{1,*}

¹Department of Plant Science and Landscape Architecture, University of Maryland,
College Park, MD, USA

*Corresponding author, email: asmurphy@umd.edu

This work was published as a book chapter in:

Plant ABC Transporters ed. Geisler M. (Springer, Switzerland), pp 271-285.

Headings and figure numbers were changed for consistency within this dissertation.

Summary

Plant ATP-binding cassette subfamily B/P-glycoprotein/multidrug resistance (ABCB/PGP/MDR) proteins mediate the transport of a variety of aliphatic and amphipathic substrates across the plasma membrane. An unexpected characteristic of some plant ABCBs that is not seen in animal homologs is uptake transport activity. However, in the best studied example of this phenomenon, the ABCB4 auxin transporter is associated with uptake only when intracellular auxin concentrations are low, and exhibits canonical efflux activity when internal auxin concentrations increase. Physiological and biochemical characterizations of ABCB4 indicate that the protein serves as a homeostatic regulator and suggest evolutionary origins of the phenomenon. In this chapter we will review early transport studies and the discovery of putative uptake transporters in plants, the functional and structural evolution of these transporters, and what is known about the mechanisms of uptake and

conditional uptake/efflux. Further, we will explore issues with homologous or heterologous unicellular systems and how these studies may have led to a mischaracterization of uptake transporters. A re-evaluation of current transport data and new ABCB mediated transport model will also be discussed.

Introduction

ATP binding cassette (ABC) transporters form a ubiquitous super-family of proteins that utilize the energy from ATP hydrolysis to drive the transport of a variety of substrates across membrane bilayers. Found throughout the bacterial, animal and plant kingdoms, ABC transporters function in cellular detoxification (Martinoia et al., 2002), nutrient uptake (Singh and Röhm, 2008), secretion of extracellular coating components (Qin et al., 2013), and transport of lipids and hormones (reviewed in Kang et al., 2011). The B-subclass of ABCs has been extensively characterized due to the association of P-glycoprotein (ABCB1/MDR1) and related ABCBs with poly-specific export of hydrophobic drug/xenobiotic efflux in animals. ABCB transporters can function either as full-length transporters or as homo- or hetero-dimers of transporters associated with antigen processing (TAPs) type half transporters. All full-length ABCB transporters described to date are plasma membrane (PM) localized and are oriented with their twelve transmembrane helices (TMHs) spanning the PM and two nucleotide binding domains (NBDs) extending into the cytosol. Solutions of crystal structures and functional analyses have shown that ABCB transporters can exist in either an inward/cytoplasmic facing or an outward/extracellular/apoplast facing state (Dawson and Locher, 2006; Aller et al., 2009). An alternating access model of ABCB transport states that ATP hydrolysis causes conformation changes

that shift transporters between these orientations, allowing for substrate binding and release across the PM (Zou and Mchaourab, 2009).

In plants, ABC transporters have been shown to function in the accumulation of secondary metabolites (Shitan et al., 2003; Stukkens et al., 2005; Shitan et al., 2013), xenobiotic detoxification (Martinoia et al., 2002; Lee et al., 2005; Frelet-Barrand et al., 2008), transport of lipids to the cuticle (Pighin et al., 2004; Luo et al., 2007; Panikashvili et al., 2007), stomata aperture regulation (Lee et al., 2008), and transport of the phytohormones auxin (reviewed in Peer *et al.*, 2011), abscisic acid (Kuromori et al., 2010), and cytokinin (Zhang et al., 2014). ABCB transporters were initially discovered in deduced amino acid sequence comparisons of mammalian ABCB1, under the premise that plant ABCBs would exhibit functions similar to mammalian ABCB1 in cellular detoxification (Dudler and Hertig, 1992). However, subsequent biochemical studies have shown that plant ABCBs exhibit a much narrower substrate specificity compared to their mammalian homologs, and their roles in detoxification are minimal (Conte and Lloyd, 2011). Instead, detoxification involving ABCs primarily involves ABCC/MRPs located at the tonoplast and a subset of ABCG/PDRs.

The best characterized plant ABCBs are the *Arabidopsis* auxin efflux transporters ABCB1 and ABCB19, which mobilize the primary auxin indole-3-acetic acid (IAA) and contribute to the long distance polar transport of auxin from the shoot apex to the roots. ABCB1 is primarily localized apolarly in the shoot and root meristems (Sidler et al., 1998; Geisler et al., 2005; Mravec et al., 2009) and basally (top) in the cortex and endodermis in the boundary between the elongation and

maturation zones of the root (Geisler et al., 2005). ABCB19 is primarily localized apolarly in the shoot apex, bundle sheath cells in shoots, cortical and stellar cells in the root, epidermal cells near the root apex, and also in cotyledons and anther filaments (Blakeslee et al., 2007; Lewis et al., 2007; Lewis et al., 2009; Titapiwatanakun et al., 2009). *abcb1* and *abcb19* single mutants show ~25% and >50% reductions in rootward auxin transport (Noh et al., 2001; Blakeslee et al., 2007), and double mutants are reduced by ~70% (Blakeslee et al., 2007). Phenotypes consistent with this reduction in long distance rootward auxin transport include epinastic cotyledons, decreased inflorescence height, loss of apical dominance, increased lateral branching, reduced lateral root formation, and reduced stamen filaments (Noh et al., 2001; Noh et al., 2003; Geisler and Murphy, 2006; Lewis et al., 2007).

Another well-characterized *Arabidopsis* ABCB auxin transporter is ABCB4, which exhibits efflux activity similar to ABCB1 and 19 at higher intracellular auxin concentrations, but mediates auxin uptake activity when internal auxin levels are very low (Terasaka et al., 2005; Yang and Murphy, 2009; Kubeš et al., 2012). A highly similar paralog, ABCB21, appears to exhibit similar activities (Kamimoto et al., 2012). Plant ABCB uptake activity is not limited to auxin transporters, as alkaloid uptake has been associated with *Coptis japonica* ABCB1/MDR1 (Shitan et al., 2003), and *Arabidopsis* ABCB14 has been shown to function in malate/citrate uptake (Lee et al., 2008). This chapter will review the discoveries of plant ABCB transporters with uptake activity, their apparent functional divergence from exporters, structural features that are unique in putative uptake transporters, and the currently accepted

mechanism of uptake and conditional transport directionality. Additionally, uptake transporter data will be re-evaluated and a new model of controlled ABCB mediated efflux will be discussed.

Discovery of plant ABCB uptake transporters

***Coptis japonica* ABCB1.** The first reported putative ABCB uptake transporter was ABCB1/MDR1 from *Coptis japonica* (Shitan et al., 2003). Berberine, an alkaloid with strong antimicrobial properties and medicinal uses, is synthesized in the *C. japonica* root and accumulates in the rhizomes. In cultured *C. japonica* cells and xenopus oocytes expressing CjABCB1, endogenous and exogenous berberine were shown to be actively taken up by cells via a mechanism that is ATP-dependent and sensitive to inhibitors of mammalian ABCB1. Further, oocytes and *Saccharomyces cerevisiae* expressing CjABCB1 accumulated the berberine precursor reticuline and showed increased sensitivity to the mutagen 4-nitroquinoline N-oxide respectively. These results suggest that CjABCB1 mediates berberine uptake from the root into the rhizome and appears to exhibit a preference for berberine-like alkaloids. A study by the same group has recently shown that another ABCB isoform from *Coptis japonica* (CjABCB2) has nearly identical characteristics (Shitan et al., 2013).

***Arabidopsis thaliana* ABCB4.** A second plant ABCB transporter with apparent uptake activity was subsequently described by several groups (Santelia et al., 2005; Terasaka et al., 2005). ABCB4 was reported to function primarily in the lateral root cap, root epidermis, and mature root cortical cells (Santelia et al., 2005; Terasaka et al., 2005). ABCB4 was reported to be apolarly localized in the root cap and basally (top) localized in the epidermis (Terasaka et al., 2005). Analysis of *abcb4*

mutants showed light and sucrose-dependent root phenotypes. On 0.5-1% sucrose and under moderate light (100-120 uE), *abcb4* mutants exhibited reductions in primary root length and lateral root number (Terasaka et al., 2005). When grown under high light or on >1.5% sucrose *abcb4* mutants showed an increase in primary root length, lateral root number and root hair length (Santelia et al., 2005; Terasaka et al., 2005). Auxin transport assays and free IAA quantitations revealed that *abcb4* mutants had reduced basipetal auxin movement from the root tip (Santelia et al., 2005; Terasaka et al., 2005). Rootward auxin transport from the shoot apex in *abcb4* mutants was not different from wild-type however overexpression increased auxin transport (Terasaka et al., 2005). Expression of ABCB4 in *Saccharomyces cerevisiae* resulted in hypersensitivity to IAA and the toxic auxin analog 5-fluoroindole, suggesting a role in auxin uptake (Santelia et al., 2005). Consistent with this result, expression in mammalian HeLa cells resulted in a net increase in auxin accumulation and, surprisingly, treatment with NPA reverted apparent uptake to efflux (Terasaka et al., 2005). This reversion correlated to an increase in intracellular IAA and was the first report of substrate concentration-dependent regulation of ABCB activity.

A subsequent study of ABCB4 (Lewis et al., 2007) confirmed previous reports that *abcb4* mutant roots exhibit reduced shootward auxin transport, but no changes in rootward auxin transport activity. It was expected that this reduction in shootward auxin transport from the root tip would result in a reduction in gravitropic bending, as is the case in mutants of the auxin efflux carrier PIN2 (Chen et al., 1998). However, consistent with the earlier report from Terasaka *et al.* (2005), no reduction in gravitropic bending was observed and, instead, a small enhancement of gravitropic

bending was reported. Visualization of *DR5::GFP* revealed auxin distributions in the *abcb4* root apex and elongation zone were less discrete than wild-type.

The elongated root hair phenotype of *abcb4* mutants was further examined in Cho *et al.* (2007). This study showed that overexpression of ABCB4 under the control of a root hair-specific promoter (PE7) caused a decrease in root hair elongation similar to what was observed with overexpression of PIN efflux carriers in root hairs. Further, overexpression of the AUX1 auxin uptake transporter enhanced root hair length. Although subsequent work has shown that PE7 is not exclusive to root hairs (Kubeš *et al.*, 2012), these results indicated that the primary function of ABCB4 in roots hairs is auxin efflux. The same study corroborated ABCB4-mediated efflux of the artificial auxin 1-naphtalene acetic acid (NAA) when ABCB4 was overexpressed in tobacco BY-2 cells (Cho *et al.*, 2007).

Yang & Murphy (2009) provided a detailed characterization of the transport activity of ABCB4 expressed in *Schizosaccharomyces pombe*. *S. pombe* cells expressing ABCB4 showed initial IAA accumulation followed by IAA export, confirming the substrate-dependent switch to efflux observed in Terasaka *et al.* (2005). Doubling the amount of exogenous IAA doubled the initial amount of IAA accumulation and decreased the time for reversion to export. This result was consistent with reports of variability in *abcb4* phenotypes under conditions that alter auxin homeostasis and auxin transport (Gray *et al.*, 1998; Geisler *et al.*, 2005; Santelia *et al.*, 2005; Terasaka *et al.*, 2005; Cho *et al.*, 2007; Lewis *et al.*, 2007). This same study also showed that 2,4-dichlorophenoxyacetic acid (2,4-D) inhibits ABCB4-mediated uptake activity. This observation raised questions about assays of ABCB4

conducted in BY-2, as BY-2 cells are regularly grown in media containing the synthetic auxin 2,4-D. The presence of 2,4-D in the assays reported by Cho *et al.* (2007) may have obscured uptake activity by elevating the intracellular auxin to levels where reversion to export would have already occurred.

In the most recent report of ABCB4, Kubeš *et al.* (2012) reported that auxin uptake into the root tip and that basipetal auxin transport in *abcb4* mutants is reduced, which is consistent with previous findings (Santelia *et al.*, 2005; Terasaka *et al.*, 2005; Lewis *et al.*, 2007). Additionally, roots of *abcb4* mutants accumulate less auxin than wild-type initially and switch to net accumulation after incubation with IAA. Consistent with Santelia *et al.* (2005) and Cho *et al.* (2007), root hairs in *abcb4* mutants are longer and addition of increasing exogenous auxin increases root hair length (Fig. 2.1). Further investigation of root hair phenotypes was not pursued as expression of ABCB4 under the root hair specific promoter PE7 and auxin quantitation in root hairs were not successful. Expression in BY-2 suggests ABCB4 exhibits weak uptake activity. However, this result could not be investigated further, as lipophilic and AUX1/LAX-mediated 2,4-D uptake could not be inhibited, even after inhibition of AUX1 by 2-naphthoxyacetic acid (2-NOA). Expression of ABCB4 in *S. pombe* and HeLa cells produced similar concentration-dependent kinetics to those reported previously (Terasaka *et al.*, 2005; Yang and Murphy, 2009) and verified 2,4-D as a substrate for ABCB4 mediated uptake and inhibition of efflux activity.

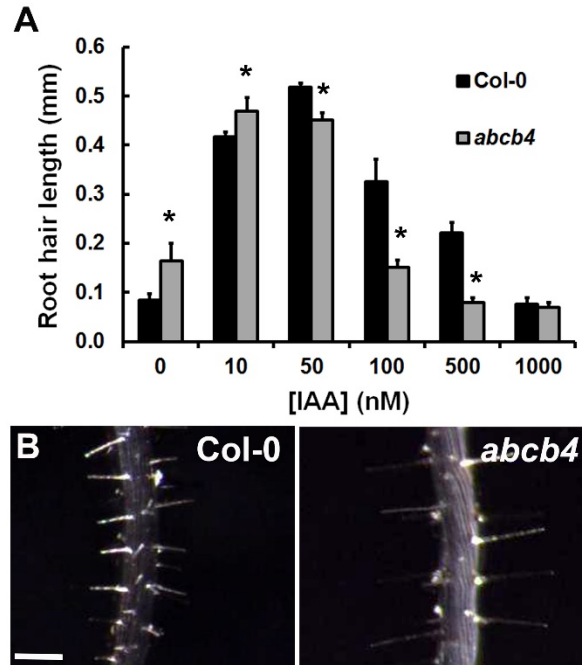


Figure 2.1. ABCB4 regulates root hair elongation in *Arabidopsis* (5-day-old *Arabidopsis* seedlings). (a) Treatment with increasing indole-3-acetic-acid (IAA) concentrations inhibits root hair elongation. Mean lengths and SD from the first 10 root hairs measured starting 1.5 mm from the root apex (10 seedling pools, n = 3). *p < 0.05. (b) Root hairs in a region 1.5 mm above the *abcb4* root apex are consistently longer than in the wild type. Bar = 100 μ m. (c) Visualisation of ABCB4pro:ABCB4-GFP shows a signal at the plasma membrane in atrichoblast (a) and trichoblast (t) cells in light-grown seedlings acclimated to dim light. Bar = 10 μ m. Figure taken from Kubeš *et al.* (2012).

From these combined results, it is evident that ABCB4 regulates cellular auxin levels primarily in the root epidermis by mediating auxin uptake when intracellular auxin levels are low and reverts to efflux when auxin concentration is increased.

***Arabidopsis thaliana* ABCB14 and ABCB21.** Only two other ABCB transporters have been described to exhibit uptake activity. ABCB14 is expressed primarily in guard cells, where it regulates stomata closing in response to increased levels of CO₂ and exogenously applied malate (Lee et al., 2008). ABCB14 expressed in *S. cerevisiae* and HeLa cells suggest that malate is taken up into the cells and that uptake activity is sensitive to the ABCB transporter inhibitors vanadate, verapamil, and cyclosporine A. Malate uptake was competed for by fumarate, and to a lesser extent succinate and citrate, suggesting a decrease in specificity compared to ABCB19. ABCB21, the closest homolog to ABCB4, is expressed on the abaxial side of leaves, in lateral organ junctions in shoots, and in root pericycle cells (Kamimoto et al., 2012). Expression in *Arabidopsis* protoplasts shows IAA and NAA export, though IAA appears to be the preferred substrate. ABCB21, like ABCB4, shows increased 5-FI sensitivity when expressed in *S. cerevisiae*. Assays in yeast expressing ABCB21 showed apparent IAA uptake when external IAA levels are high, and pre-loading with IAA returned IAA accumulation back down to control levels. Further, assays conducted with pre-loaded yeast cells and low external IAA showed net efflux activity. These results suggest that ABCB21 functions like ABCB4 in an intracellular auxin concentration dependent manner.

Phylogeny of putative uptake transporters and functional divergence

The *Arabidopsis* genome contains 21 full-length ABCB transporters. Phylogenetic analysis of these transporters reveals that they cluster into five clades (Fig. 2.2; Knöller *et al.*, 2010). The auxin exporters ABCB1 and ABCB19 are found within clade II and are the only *Arabidopsis* transporters within this group. Clade I

contains the malate/citrate uptake transporter ABCB14 along with ABCB13, ABCB2, and ABCB10. The function of the latter three transporters remains unknown, however, expression of ABCB2 in *S. pombe* suggests it is not a primary auxin transporter (Yang and Murphy, 2009). Although grouped within the same clade, ABCB14 is clearly distinct from ABCB1 and ABCB19. No data for clade III or clade IV, which contain ABCB6, ABCB20, and ABCB15-18, have been published to date. Preliminary studies of RNAi knockdowns of ABCB15-18 reveal that they may play roles in auxin transport and/or transport regulation (unpublished), but high sequence similarity of these genes due to duplication has made isolation and analysis of mutants difficult. The concentration dependent uptake/efflux auxin transporters ABCB4 and ABCB21 group together within clade V. The paralogous sets of ABCB3/5, ABCB11/12 and ABCB7/9 also group within clade V. ABCB11 has been shown to function in rootward auxin transport (Kaneda et al., 2011), however, the kinetics of ABCB11-mediated transport remain unknown. This data, along with biochemical and structure/function analyses, suggest a functional divergence of some ABCB transporters that cannot be predicted by sequence comparison alone (Yang and Murphy, 2009; Knöllner et al., 2010; Bailly et al., 2011).

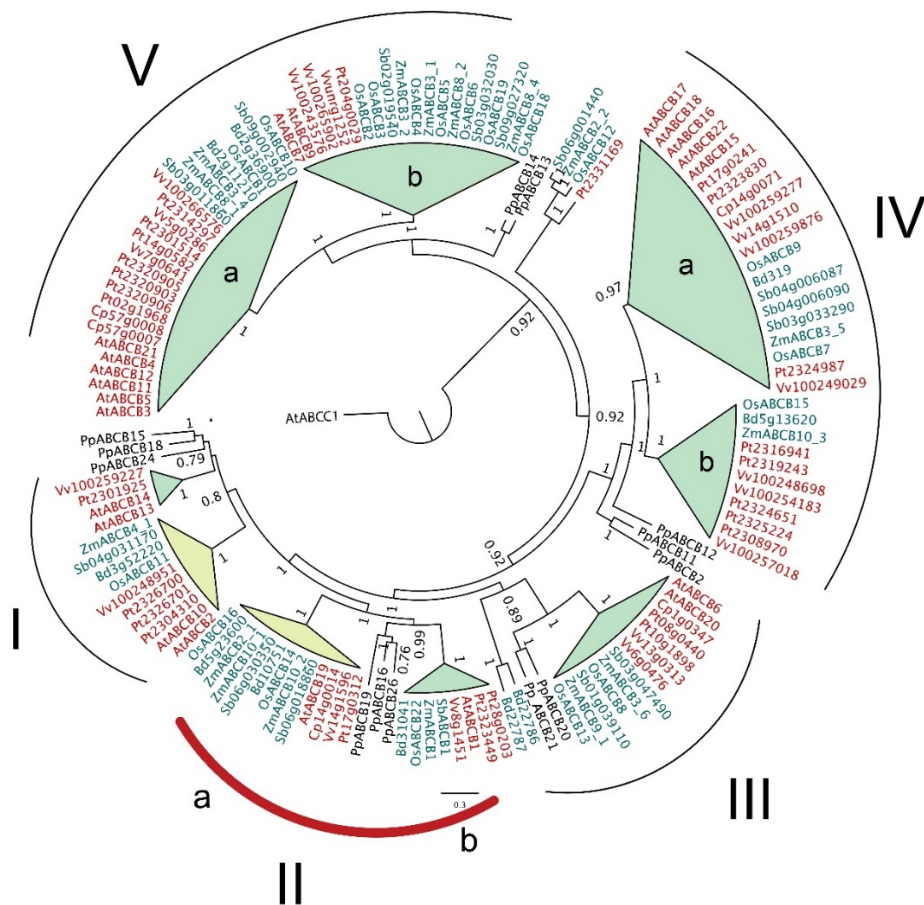


Figure 2.2. Phylogenetic tree of plant ABCB transporters, including sequences from *Arabidopsis*, *Vitis*, *Populus*, *Carica*, *Sorghum*, *Zea*, *Oryza*, *Brachypodium*, and *Physcomitrella*. The phylogenetic tree can be divided into five clades (I–V). Branch numbers represent bootstrap values. Species names are colour coded for monocots (green) and dicots (red). Subclade Ib and Iia lie outside the *Physcomitrella* root (yellow shaded subclades). Figure taken from Knöller et al. (2010).

Structural features unique to putative uptake transporters

Crystal structures of a number of ABCB transporters have been elucidated, including *Staphylococcus aureus* Sav1866 and murine ABCB1 (Dawson and Locher, 2006; Aller et al., 2009). These multidrug efflux transporters represent what are

generally accepted as the resting states of efflux transporters (MmABCB1) and putative uptake transporters, or the substrate release state of exporters (Sav1866). No crystal structures have been determined for any plant ABCB transporter, however, homology modeling has provided valuable insight into unique structural features found in putative uptake transporters that are missing in the efflux specific transporters ABCB1 and ABCB19.

Structural models threaded on Sav1866 and MmABCB1 reveal that plant ABCB transporters share a common architecture (Yang and Murphy, 2009; Bailly et al., 2011). Further, putative uptake ABCB transporters share better sequence alignments with crystal structures of exporters than prokaryotic importers, which suggest an exporter-like overall architecture. A predicted N-terminal coiled-coil domain is found in the structures of ABCB4, ABCB14, ABCB21 and CjABCB1, but not seen in the exporters ABCB1 or ABCB19. More detailed analysis of ABCB4 reveals that the hydrophobic region of transmembrane helix 4 (TMH4) is shifted inward, likely imbedding the apoplastic end of TM3 and TM4 within the PM. Additionally, this shift could change the distance between intracellular loop 2 (ILC2) and NBD2, which may rearrange the TMDs enough to alter transport directionality. Another coiled-coil domain is found in ABCB4 within the linker region connecting NBD1 and TMD2. This feature is not seen in the putative importers CjABCB1, ABCB14, and ABCB21 nor in the exporters ABCB1 or ABCB19. This suggests a specific role in regulating ABCB4 activity and not a general transport directionality mechanism. The function of these domains is unknown, but may play a role in protein interactions and/or regulating transport properties. Obviously, the function of these

features needs to be biochemically analyzed and is of utmost importance for understanding ABCB transporter function and regulation.

In addition to these structural features, analysis of substrate docking reveals kingdom-specific putative substrate binding sites within the TMDs. Docking of IAA to ABCB19, ABCB1, and ABCB4 in their outward facing states identified two putative substrate binding sites within the TMDs and associated with the inner leaflet of the PM (Yang and Murphy, 2009; Bailly et al., 2011). ABCB4, however, had an additional binding site formed by TMH5 and 8 at the PM inner leaflet-cytosol interface not present in ABCB19. The proposed role of this additional site, which would explain the apparent “transport direction reversibility” seen with ABCB4 and ABCB21 will be discussed below.

Mechanism of uptake and conditional “reversibility”

To date, no ABCB transporters with uptake activity have been reported in animals. Bacterial ABC transporters mediate the uptake of a number of primary metabolites, including maltose, vitamin B12, and histidine (reviewed in Linton & Higgins, 2007). However, prokaryotic ABC uptake transporters are structurally and mechanistically dissimilar to eukaryotic transporters. In general, prokaryotic importers, such as the maltose importer MalFGK2, have an associated periplasmic or cell-surface-associated substrate binding protein required for uptake activity (George and Jones, 2014). These binding proteins have high affinity and allow for substrate-specific and unidirectional transport.

Plant ABCB transporters probably do not have associated binding proteins and their specificities lie within the binding sites found within the TMDs. Substrate

docking simulations of IAA with ABCB1, ABCB19 and ABCB4 reveal binding sites associated with the outer and inner leaflets of the PM. Detailed analyses of mammalian ABCB1 propose that a general hydrophobic binding pocket associated primarily with the outer leaflet of the PM is responsible for the polyspecific exclusion of hydrophobic chemotherapy drugs. Similar binding positions are found in the exporters ABCB1 and ABCB19, however, surface electrostatic potentials at these positions differ (Bailly et al., 2011). This may explain the increased specificity in plant transporters compared to mammalian homologs. Docking simulations with outward facing models of ABCB4 and 14 also predict binding sites at these positions that may play roles in substrate binding and uptake. However, these sites have yet to be tested biochemically. Simulations have also identified two substrate binding sites associated with the inner leaflet of the PM for exporters and putative uptake transporters. These sites are not present in mammalian ABCB1 and likely also contribute to substrate specificity.

In addition to these sites the putative uptake transporter ABCB4 also contains a third inner-leaflet-associated binding site not found in exporters (Yang and Murphy, 2009). This site is predicted to function as a regulatory site that can control the switch between apparent uptake and efflux activity. In this model, at low intracellular auxin concentrations, the regulatory binding site is unoccupied and ABCB4 is open to the apoplast. In this state ABCB4 has been predicted to mediate auxin uptake. Upon increased intracellular auxin levels, via putative transporter-mediated or endogenous uptake, and/or passive diffusion, the site is predicted to become occupied by auxin, inducing a conformation change in ABCB4 to inward/cytosol facing and allowing for

export activity to occur. This concentration-dependent regulation or efflux activation appears to be unique to ABCB4, as ABCB1 and ABCB19 actually show increased efflux activity when auxin levels decrease (Geisler et al., 2005; Bouchard et al., 2006).

Re-Evaluation of the Data: Truly Reversible or Simply Control of Efflux?

While only a handful of ABCB transporters have been characterized to date, enough data has been produced to force us to ask a critical question: do ABCB transporters actually function in substrate uptake? While it is impossible to know for certain at this time a number of key concepts from ABCB4 suggest that this is not the case.

Increased free IAA levels in the root apex of *abcb4* mutants and apolar localization of ABCB4 in the root tip is consistent with a role in auxin export out of the root tip to the epidermis (Santelia et al., 2005; Terasaka et al., 2005). In gravitropism assays *abcb4* mutants show enhanced gravitropic bending and more diffuse auxin accumulations in the epidermis (Lewis et al., 2007), while *pin2* exhibits reduced bending and auxin accumulation at the root tip (Chen et al., 1998). This, along with the basal localization of ABCB4 in the elongation zone of the epidermis (Terasaka et al., 2005), is consistent with a role in restricting auxin to the elongation zone until it is no longer needed for cell elongation. Basipetal auxin transport from the root tip is reduced in *abcb4* mutants (Terasaka et al., 2005; Lewis et al., 2007; Kubeš et al., 2012), also supporting a role in efflux. In trichoblast-forming epidermal cells, ABCB4 on the PM increases as the root hair elongates and decreases after elongation stops, and *abcb4* mutants exhibit longer root hairs than wild-type (Kubeš

et al., 2012). This suggests that ABCB4 is involved in efflux and removal of auxin from root hairs when root hair elongation is complete.

Studies in *Arabidopsis* roots reveal that uptake into the root tip is reduced in *abcb4* mutants (Santelia et al., 2005; Kubeš et al., 2012) and that overexpression is not different than wild-type (Kubeš et al., 2012). Further, auxin uptake into the epidermis distal to the root tip, where auxin levels are decreased and ABCB4 would be expected to function as an uptake transporter, is not different in *abcb4* mutants (Santelia et al., 2005). These results suggest that the difference in apparent ABCB4-mediated uptake into the root apex is a consequence of an altered auxin gradient between the root tip and elongation zone.

Measuring transport directionality at the cellular level (i.e. uptake or efflux) in planta is not yet possible with modern techniques. Instead, transport assays using homologous or heterologous unicellular systems are performed. The issue here lies with what is actually measured in these systems: when apparent uptake is observed in assays, what is actually being measured is total cellular accumulation; a combination of endogenous and putative transporter mediated uptake, substrate embedded within the PM, and substrate bound to the transporter. In no case can we specifically separate uptake transport activity. If ABCB4 is initially open toward the apoplast, as current models suggest, then binding of substrates to the transporter and/or collection of extracellular substrate and partitioning into the PM without actual active substrate uptake may occur. This would support findings that putative uptake is less specific than export activity, and that uptake activity is low (Yang and Murphy, 2009; Kubeš et al., 2012).

This suggests that, rather than ABCB4 being a conditionally reversible transporter, ABCB4 export activity is regulated by intracellular auxin concentrations (Fig. 2.3). In this model ABCB4 would remain in its outward facing “resting state” at low intracellular auxin concentrations. ABCB4 would not actively uptake auxin, however, auxin could accumulate within the cell via lipophilic diffusion and endogenous auxin transport. Collection of auxin from the apoplast by binding to ABCB4 exposed to the apoplast and partitioning into the PM may increase diffusion rates and cellular accumulation, hence the apparent uptake activity observed. When threshold levels of intracellular auxin are reached, the third inner leaflet binding site becomes occupied and conformational changes in ABCB4 allow for export activity to begin. This controlled efflux would allow for the formation of auxin maxima and downstream auxin signaling events to occur and hold off export until auxin is no longer needed for physiological responses. Additionally, this regulation would also conserve energy, as ATP utilization would only occur when needed. This model likely applies to ABCB21 as well. Homologous and heterologous expression data show that ABCB4 and ABCB21 behave in a very similar manner. The lack of characterization in plants, however, makes the interpretation and physiological relevance of this data difficult to interpret.

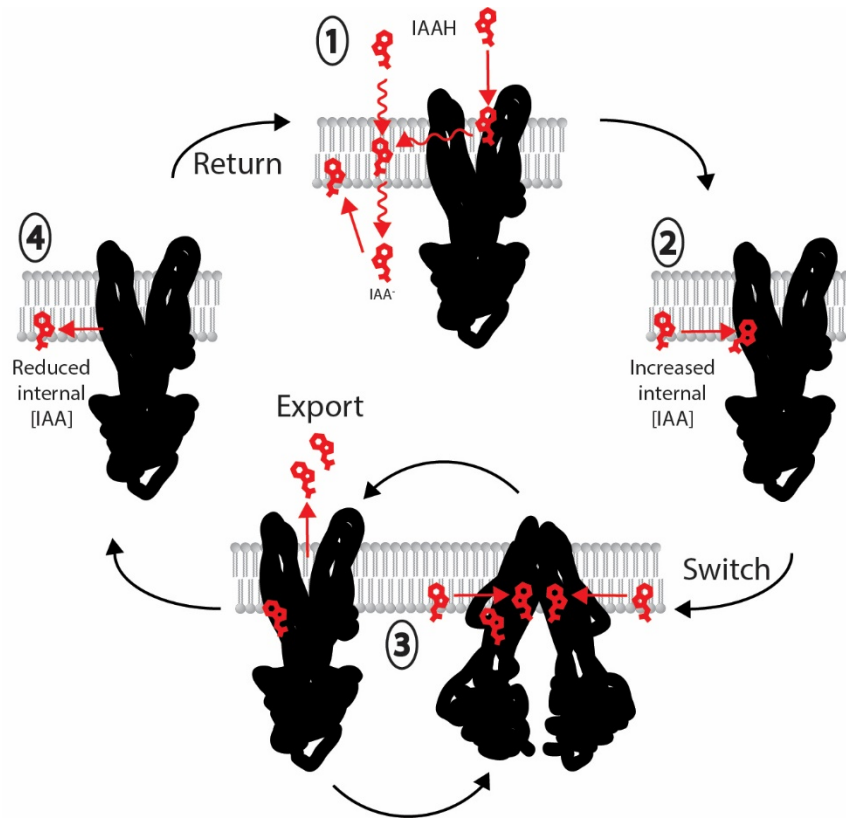


Figure 2.3. Proposed model for ABCB4 mediated accumulation and activation of efflux. (1) ABCB4 is in its outward facing conformation when intracellular auxin concentrations are low. Protonated IAA can enter the cell by lipophilic diffusion or by binding to ABCB4, which collects IAA from the apoplast and accelerates diffusional uptake. (2) Once threshold intracellular auxin levels are reached, IAA binds to the regulatory binding site in ABCB4, (3) which causes a conformation change from outward/apoplast facing to inward/cytoplasm facing and allows export to occur. The export cycle continues until (4) intracellular auxin drops below the threshold level. When this occurs the regulatory site becomes unoccupied and ABCB4 returns to its outward facing “resting state” conformation.

While studies have only shown apparent uptake activity, it is suspected that CjABCB1 functions in a similar concentration dependent manner as ABCB4. Studies characterizing berberine uptake activity in CjABCB1 has been conducted in *C. japonica* cell cultures, xenopus oocytes and yeast (Shitan et al., 2003). Berberine, however, is toxic to *S. cerevisiae* and, like what is seen with ABCB4, this toxicity may obscure efflux activity. Assays of xenopus oocytes incubated in the presence of berberine or preloaded with berberine showed cells expressing CjABCB1 accumulated and retained more berberine than controls. In both of these cases levels of intracellular berberine may not have reached the threshold needed to activate export activity.

The model proposed for accumulation and controlled export of amphipathic substrates by *Arabidopsis* ABCB4 and ABCB21 may not be applicable to simple organic acids such as malate and citrate that are associated with *Arabidopsis* ABCB14 (Lee et al., 2008). Malate and citrate are highly soluble and not expected to interact with binding sites associated with the models of substrate accumulation proposed herein. Ongoing structural and mutational analyses are required to develop testable models of ABCB14 activity.

Conclusion

ABCB transporters with apparent uptake activity are, thus far, unique to the plant kingdom and serve vital roles in regulating plant growth and development. High sequence similarity and shared overall architecture throughout the ABCB protein family suggest a functional divergence from export specific transporters. Several structural features are unique to these transporters and may function in regulating

protein-protein interactions, substrate specificity, and transport activity. In particular, models identify a putative regulatory substrate binding site that may alter transporter conformation and control the concentration dependent shift from apparent uptake to efflux.

Data suggests that some ABCB transporters have apparent uptake activity, however, experimental limitations of plant and non-plant based systems make this observation less than conclusive. The example provided by ABCB4 suggests that the uptake activity seen in homologous and heterologous unicellular systems may be an increase in accumulation by transporter-assisted diffusion or simply substrate bound to the outward facing and overexpressed transporter. This suggests that, rather than having “reversible” uptake and efflux activity, ABCB4 export is regulated by intracellular auxin concentrations and may contribute to ATP-independent auxin accumulation. Characterization of additional transporters with differing substrates, as well as in depth structural modelling and mutational analyses are needed to provide a better understanding of the mechanisms and regulation of substrate transport in ABCB transporters.

Chapter 3. *Arabidopsis ABCB21* contributes to rootward auxin streams by regulating auxin levels in the seedling pericycle

Jenness et al., manuscript in preparation

Summary

Rootward transport of the phytohormone auxin is essential for polar growth in seedlings. The ATP-binding cassette transporters ABCB1 and ABCB19 function coordinately mediate loading of auxin in excluding auxin from the shoot apex where auxin is synthesized and maintaining the rootward transport stream by restriction to the central vasculature. High levels of *ABCB19* and compensatory expression in *abcb1* suggests ABCB19 is the primary ABCB auxin transporter. Several lines of evidence suggests one or more ABCB transporter supplements the roles of ABCB19 and ABCB1 in seedlings. In this study, ABCB-RNAi knockdown and *abcb* mutants were screened for auxin related phenotypes and defects in auxin transport. From these analyses, a role for ABCB21 in retaining auxin to within the rootward auxin transport stream by preventing leakage into the pericycle was identified.

Introduction

The generation and maintenance of local and global gradients of the phytohormone auxin (indole-3-acetic acid; IAA) play fundamental roles in embryogenesis, germination, and seedling establishment (Zazimalová et al., 2010). In early seedling growth, a central rootward auxin stream is necessary for processes including hypocotyl and root elongation, cotyledon expansion, lateral root

development and outgrowth, and tropic responses to light and gravity (Reviewed in Peer et al., 2011). In more mature stages of plant growth, phloem transport makes a contribution to auxin movement (Swarup et al., 2001; Marchant et al., 2002). However, in young *Arabidopsis* seedlings, the rootward polar auxin transport stream can be primarily attributed to a fundamental cell to cell process. With apoplastic pH (~5.5), ~15% of IAA (pKa 4.75) is protonated and can enter cells through lipophilic diffusion (Parry et al., 2001). The remaining anionic IAA (~85%) enters cells via AUXIN RESISTANT1/LIKE AUX1 (AUX1/LAX) uptake permeases (Bennett et al., 1996). Anionic IAA then exits cells via PIN-FORMED (PIN) efflux carriers and ATP-Binding Cassette subfamily B (ABCB) efflux transporters (Reviewed in Zazimalová et al., 2010). Polarized localization of some PIN proteins, particularly PIN1, provides a cellular vector for efflux and, thus, the direction of the overall polar stream.

In 5-7 day *Arabidopsis* seedlings, a new pulse of auxin production at the shoot apex is transported directionally to the root tip (Peer et al., 2014). This occurs after the seedling has undergone vascular differentiation (Busse and Evert, 1999) but before the root system gains the competence to synthesize auxin at 9-10 days (Bhalerao et al., 2002). Excision experiments have shown this pulse of auxin drives lateral root emergence and outgrowth during early seedling establishment (Bhalerao et al., 2002).

Analysis of expression and transport in wild type and mutant *Arabidopsis* seedlings indicates that isotropically-localized ABCB1 and ABCB19 function in loading of auxin into the rootward auxin transport stream by exclusion from the shoot

apex and restriction of auxin to the vasculature in distal regions. Loss of ABCB1 and ABCB19 results in ~25% and >50% reductions in rootward transport, respectively, compared to a reduction of ~30% in *pin1* (Blakeslee et al., 2007). Rootward auxin transport is reduced ~60-75% in the severely dwarfed *abcb1abcb19* double mutant (Blakeslee et al., 2007). Despite these severe reductions, *abcb* mutants do not show the defects in embryo- or organogenesis that are observed in many *pin* mutants (Benková et al., 2003; Friml et al., 2003). Instead, *abcb* mutants exhibit morphogenic phenotypes that can be attributed to mis-regulation of cell elongation and expansion (Noh et al., 2001).

FK506-BINDING PROTEIN 42/TWISTED-DWARF1 (FKBP42/TWD1) is required for trafficking of ABCB1 and ABCB19 from the endoplasmic reticulum and subsequent functionality at the plasma membrane (Geisler et al., 2003; Wu et al., 2010). Auxin transport in *twd1* is reduced an additional ~10-15% compared to *abcb1abcb19*, which is reflected in its more severely stunted growth (Geisler et al., 2003; Pérez-Pérez et al., 2004). FKBP42 is also required for proper trafficking and functionality of ABCB4 (Wu et al., 2010), a conditional auxin transporter that exhibits auxin uptake activity at low intracellular auxin levels and efflux at increased internal auxin concentrations (Santelia et al., 2005; Terasaka et al., 2005; Cho et al., 2007; Lewis et al., 2007; Yang and Murphy, 2009; Kubeš et al., 2012). ABCB4, however, is primarily localized to the root epidermis and *abcb4* mutants exhibit only slight reductions in rootward auxin transport in hypocotyls or roots (Terasaka et al., 2005).

As no interaction between FKBP42 and PIN or AUX1/LAX transporters has been observed (Bouchard et al., 2006; Wu et al., 2010) and the partial reversibility of the *twd1* ‘super-twisting’ phenotype by the auxin transport inhibitor 1-naphthylphthalamic acid (NPA) (Wu et al., 2010; Wang et al., 2013), it has been hypothesized that the observed difference between *abcb1abcb19* and *twd1* is the result of at least one additional unidentified ABCB transporter that functions in rootward auxin transport. The *Arabidopsis* genome encodes 22 full-length ABCB transporters, including one pseudogene *ABCB8* (Verrier et al., 2008). Structural modelling and sequence analyses (Knoeller et al 2010; Bailly et al., 2011) identify ABCB2, 6, 10, 20, and 21 as possible candidates for this function. However, ABCB2 does not appear to transport auxin (Yang and Murphy, 2009) and both ABCB2 and 10 showed no interaction with TWD1/FKBP42 in yeast two-hybrid assays (Geisler et al, 2003).

ABCB21, the closest homolog of ABCB4, has been shown to function as a conditional auxin transporter in protoplasts and budding yeast and is expressed in the root vasculature, cotyledons, leaves and organ junctions and (Kamimoto et al., 2012). However, in that study, no obvious phenotypes were observed in RNAi or T-DNA insertion lines and auxin transport *in planta* was not investigated. Expression and direct auxin transport analyses have also been implicated ABCB11, ABCB14 and ABCB15 in rootward auxin transport in mature inflorescences (Kaneda et al., 2011). However, disorganization of the vascular bundles in mutants lacking the guard cell malate/citrate importer ABCB14 suggests an underlying structural defect not directly related to transport processes as been described in other mutants with disrupted

vasculature (Surpin et al., 2003). Rootward auxin transport in *abcb11* was not significantly reduced, however, and an examination of the *abcb11* allele (Salk_094249) described in that study indicates that the T-DNA insertion is actually located in the highly similar *ABCB11* paralog *ABCB12*.

Here, the 21 ABCB Arabidopsis transporters were analyzed to determine if they contribute to seedling rootward auxin transport. Previous reports and analyses of expression datasets were used for initial categorization. ABCB-RNAi knockdown and *abcb* mutants were then analyzed for reduced auxin transport in seedlings. From these analyses ABCB21 could be clearly identified as an auxin transporter involved in maintaining the rootward auxin transport stream in seedling roots during seedling establishment.

Results

Exclusion of auxin mediated by ABCBs at the plasma membrane

ABCB1 and ABCB19 function coordinately in loading of IAA into the rootward stream at the shoot apex and restriction of IAA to the vasculature in distal regions (Blakeslee et al., 2007; Mravec et al., 2008). Structural modelling identifies two distinct sets of auxin binding sites in these transporters: plant kingdom specific binding sites associated with the inner-leaflet-cytosol interface that are believed to mediate specific auxin efflux; and sites situated within the membrane bilayer that correspond to sites associated with polyspecific substrate exclusion in mammalian ABCB1/MDR1/PGP (Bailly et al., 2011). The closest mammalian homolog of *Arabidopsis* ABCB1 and ABCB19, P-glycoprotein (PGP1/MDR1/ABCB1), is

proposed to function as a “hydrophobic vacuum cleaner”, continuously pumping substrates from within the membrane bilayer to prevent uptake into cells (Higgins and Gottesman, 1992; Gottesman and Pastan, 1993). It has been hypothesized that ABCB1 and ABCB19 also function in this manner to prevent reuptake into source cells where auxin biosynthesis is high and to restrict IAA to within transport streams by preventing entry into neighboring cell files. This function is consistent with high levels of expression in shoot apex and leaf primordia (Fig. 3.1 A and B), and cells bounding the central cylinder in the hypocotyl and root (Fig. 3.1 A and C).

When expressed in *S. pombe*, ABCB19 exhibits greater efflux activity than PIN1 if ^3H -IAA is kept in the cell suspension during transport assays (Yang and Murphy, 2009). However, if ^3H -IAA is preloaded into cells and the radioactive substrate washed out of the external media, ABCB19 activity is less than that of PIN1 (Fig. 3.1D). This suggests that when external auxin is high, ABCB19 exhibits a combination of efflux and exclusion activity, but when external auxin levels low (cells preloaded and washed) ABCB19 exclusion activity is reduced. This exclusionary role becomes more apparent with the synthetic auxin 2,4-dichlorophenoxyacetic acid (2,4-D), which is poorly transported *in planta* (Jacobs et al., 1966; Brown and Phillips, 1982; Ito, 2006) or by ABCB19 heterologously expressed in HeLa cells (Titapiwatanakun et al., 2009). When ^3H -2,4-D is added to cold *S. pombe* cells, no ABCB19 mediated efflux is observed (Fig. 1E). However, when ^3H -2,4-D is added to cells kept at room temperature, ABCB19 reduces ^3H -2,4-D accumulation ~30%, indicating ABCB19 exclusion of 2,4-D is predominant under these conditions. These results support preventative reuptake in auxin producing cells

in the shoot apex and retention of auxin from the rootward transport stream by ABCB19 bounding the seedling central cylinder (Blakeslee et al., 2007; Mravec et al., 2008).

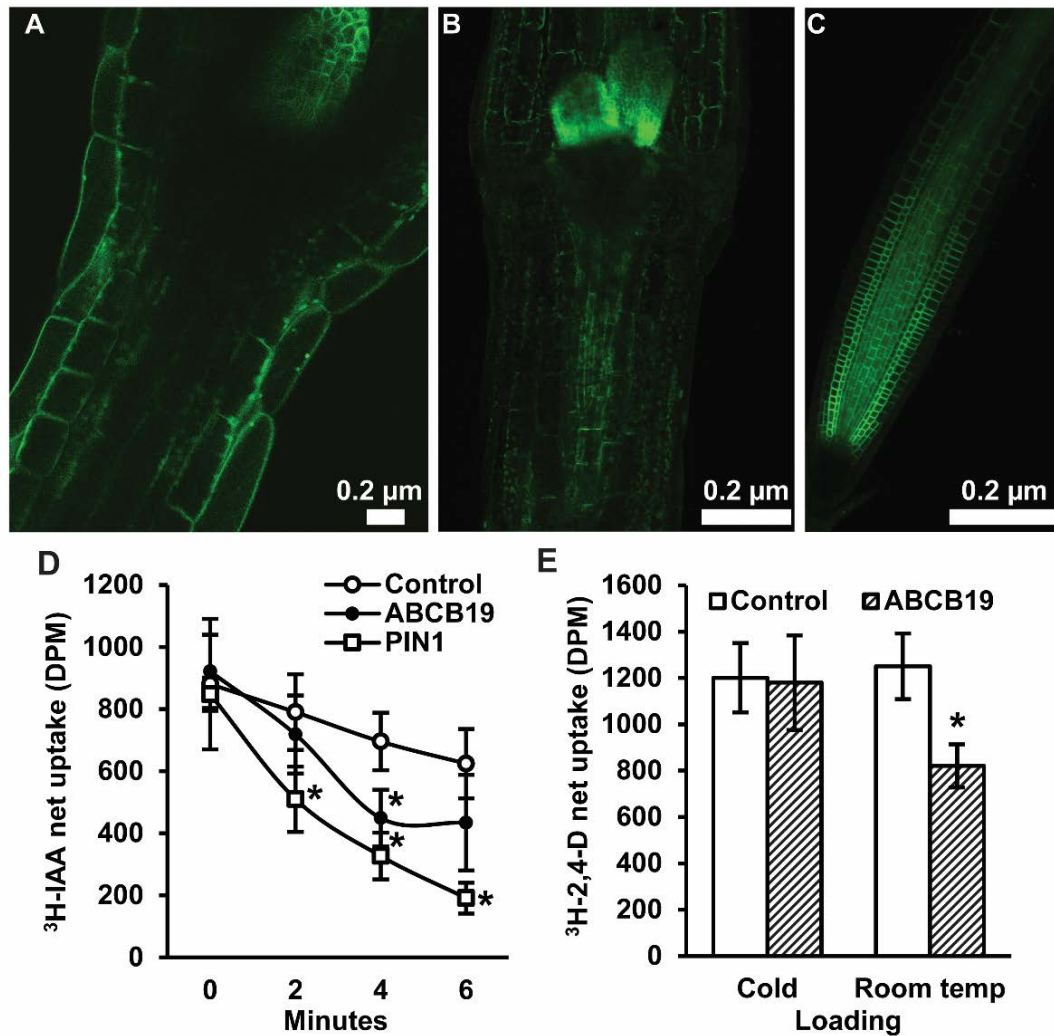


Figure 3.1. Cellular exclusion is a primary function of ABCB19. (A) In shoots, ABCB19-GFP is expressed primarily in leaf primordia and tissue layers bounding the central cylinder. (B) Hand sections through the apical region show ABCB19-GFP associated with the vasculature in regions below the shoot apical meristem. (C) In roots, ABCB10-GFP is observed in cells bounding the rootward auxin transport. (D)

³H-IAA transport assay of ABCB19 and PIN1 in *S. pombe*. Data shown are means \pm SD (n = 4-5). * indicate statistical difference by Student's *t* test (p < 0.05). (E) ³H-2,4-D transport assay of ABCB19 in *S. pombe*. Data shown are means \pm SD (n = 6). * indicate statistical difference by Student's *t* test (p < 0.05).

ABCB21 maintains auxin transport streams by restricting auxin to within the vasculature

ABCB21, the paralog to *ABCB4*, was previously shown to function as a conditional uptake/efflux auxin transporter and to be expressed primarily in the root pericycle in seedlings (Kamimoto et al., 2012). Analysis of RNAi and T-DNA insertion lines, however, did not lead to a conclusive function *in planta*. Since *ABCB21* bounds the central cylinder it was hypothesized to function similarly to *ABCB19* in keeping auxin within the rootward transport stream. *ABCB21* was therefore investigated for a role in auxin transport during seedling growth.

ABCB21 was shown to exhibit conditional uptake/efflux activity in *Arabidopsis* mesophyll protoplasts and when expressed in *S. cerevisiae* (Kamimoto et al., 2012). This activity was validated by expressing *ABCB21* in *S. pombe* (Fig. 3.2 A). Cells expressing *ABCB21* accumulated ~25% more ³H-IAA after 6 minutes than control lines. However, after 10 minutes cells expressing *ABCB21* accumulated ~23% less ³H-IAA than controls. These results suggest that, like *ABCB4*, *ABCB21* exhibits initial IAA uptake activity and efflux is activated by reaching a threshold intracellular IAA concentration. The timing of the switch between uptake and efflux

is very similar between ABCB21 and ABCB4 (Yang and Murphy, 2009), suggesting they may share similar transport and/or regulatory mechanisms.

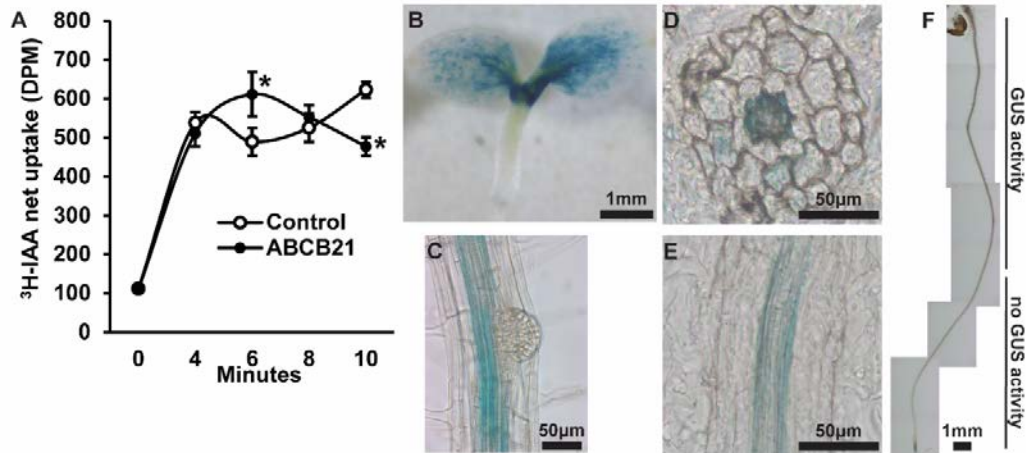


Figure 3.2. Activity and expression of *ABCB21*. (A) ABCB21 exhibits conditional auxin uptake/efflux in *S. pombe* similar to ABCB4. Data shown are means \pm SD (n = 4). * indicate statistical difference by Student's *t* test ($p < 0.05$). In shoots, *proABCB21:GUS* expression is observed in the (B) cotyledonary node, petioles and cotyledons. In roots, *proABCB21:GUS* is observed in the (C) central cylinder. (D) Cross sections and (E) longitudinal sections confirm expression is primarily associated with the root pericycle. (F) *proABCB21:GUS* expression is observed in the upper two-thirds of the root.

ABCB21 expression was previously analyzed using a promoter sequence 0.75 kb upstream of the *ABCB21* start codon fused to the β -glucuronidase (GUS) reporter (Kamimoto et al., 2012). This promoter, however, included 122 nucleotides of the 3' UTR of the upstream gene (At3g62160). To see if this fragment had any effect on expression a shorter 0.625 kb promoter was fused to GUS and transformed into Col-0. Overall, no observable expression differences were seen between the two promoters. Consistent with the previous report, *ABCB21* is expressed on the abaxial side of cotyledons, the petioles, the cotyledonary node and the vasculature of 5-10 day seedlings (Fig. 3.2 B and C). Cross and longitudinal sections show that expression is primarily within the pericycle (Fig. 3.2 D and E). Expression in the pericycle is continuous throughout the top two-thirds of the root, but absent in lateral root primordia and emerging lateral roots (Fig. 3.2C and F). Prior to 5 days and after 10 days expression in the pericycle is mostly absent and the GUS signal that is present is highly variable and discontinuous.

The previously described allele of *ABCB21*, *abcb21-1* (WiscDsLox1C2), forms a partial transcript and, potentially, a partially functional transporter (Fig. S3.1 A and B) (Kamimoto et al., 2012). Therefore, a new allele, *abcb21-2* (Gabi_954H06) was obtained. *abcb21-2* also forms a partial transcript, however, the T-DNA insertion is further upstream and would be expected to further reduce any potential ATPase/transport activity (Fig. S3.1 A and B).

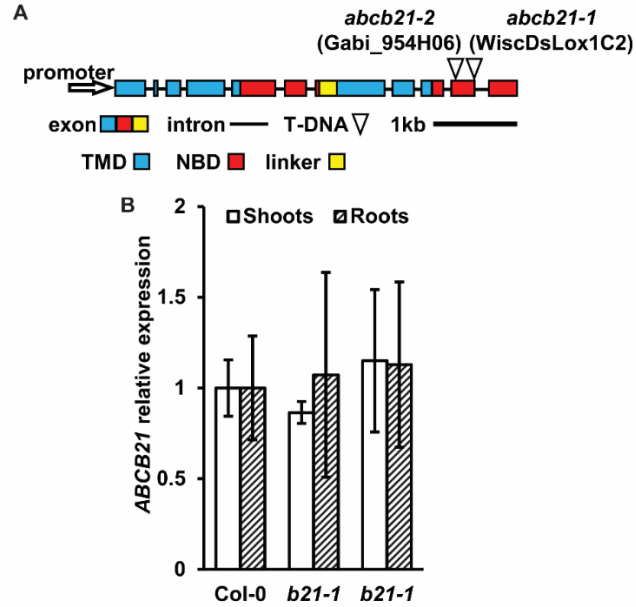


Figure S3.1. Isolation of *abcb21-2*. (A) *ABCB21* gene model indicating T-DNA insertion positions. (B) *ABCB21* expression in *abcb21-1* and *abcb21-2*. Data shown are means \pm SD (n = 3).

To identify a functional role for *ABCB21*, *abcb21-1* and *abcb21-2* were analyzed for root phenotypes. *abcb21-2* 5-day primary roots are shorter than Col-0 but slightly longer at 10 and 14 days (Fig. 3.3 A). *abcb21-1* showed an intermediate phenotype consistent with the hypothesis that it may be a partially functional transporter. In 7-day seedlings the number of lateral root primordia (stage I-IV) in both *abcb21* mutants is not different from Col-0, but the number of unemerged and emerged (stage V-VIII) lateral roots is reduced in *abcb21-2* (Fig. 3.3 B). Neither *abcb21* allele show differences in lateral root primordia formation or lateral root emergence in 10-day seedlings (Fig. S3.2), which is consistent with the previous report (Kamimoto et al., 2012).

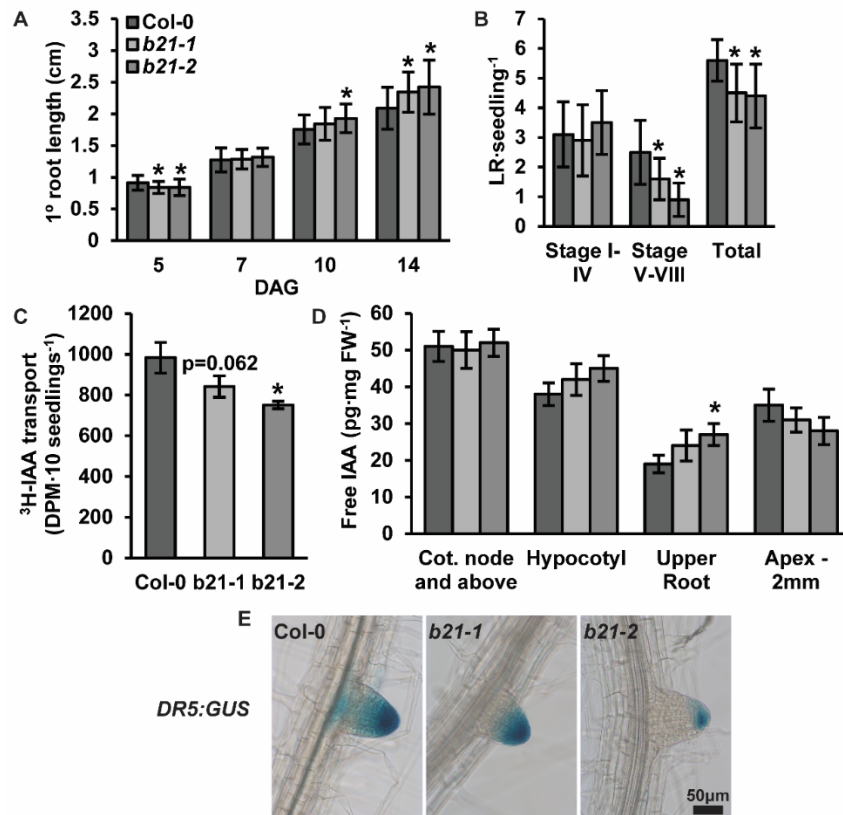


Figure 3.3. Loss of ABCB21 reduces the supply of auxin to emerging lateral roots. (A) *abcb21* seedlings have shorter primary roots are shorter after 5 days and longer after 14 days. Data shown are means \pm SD (n = 40-50), * Student's *t* test $p < 0.05$ vs Col-0. (B) *abcb21* seedlings have fewer Stage V-VIII lateral root. Data shown are means \pm SD (n = 10). * indicate statistical difference by Student's *t* test ($p < 0.05$). (C) Auxin transport from the RSTZ to the root apex is reduced in *abcb21*. Data shown are means \pm SD (n = 3 pools of 10). * indicate statistical difference by Student's *t* test vs Col-0 ($p < 0.05$). (D) Quantification of free IAA levels in 5.5 day light grown *abcb21* mutants. Data shown are means \pm SD (n = 3 pools of 10). * indicate statistical difference vs Col-0 by Student's *t* test ($p < 0.05$). (E) *DR5:GUS* is reduced in *abcb21* lateral root tips.

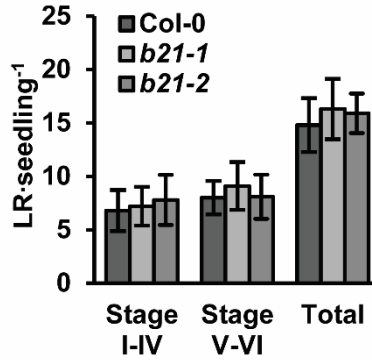


Figure S3.2. Lateral root number in 10-day seedlings. Data shown are means \pm SD (n = 10).

The timing of expression in the pericycle, and defects in primary root elongation and lateral root development are indicative of an ABCB21 role in regulating rootward auxin transport in seedlings. To test this, transport of ^3H -IAA was measured in 5.5-day *abcb21* seedlings. Rootward transport of ^3H -IAA from the RSTZ to the root tip is reduced by ~14% and ~24% in *abcb21-1* and *abcb21-2*, respectively (Fig. 3.3 C). No difference in transport of ^3H -IAA from the shoot apex to the RSTZ was detected (data not shown). Quantification of free IAA levels in *abcb21* indicate auxin is increased in the hypocotyl and upper root, and reduced in the root apex (Fig. 3.3 D). This suggests the reduction in rootward auxin transport in *abcb21* causes auxin to back up and pool in the upper root and hypocotyl. This pooling was not enough to activate the *DR5:GUS* auxin reporter in either *abcb21* background. However, *DR5:GUS* signals are reduced in emerging and newly emerged indicating defect in lateral root outgrowth is due to lower auxin levels (Fig. 3.3 E).

In addition to expression in the root, *ABCB21* expression is highest at the base of the cotyledons, the petioles and the cotyledonary node (Fig. 3.2 B). Due to this expression *abcb21* mutants were tested to see if ABCB21 mediates transport of auxin from the cotyledons into the rootward transport stream. ³H-IAA was placed in the center of one cotyledon and the hypocotyl and root were collected after 2 hours (Fig 3.4 A). ³H-IAA transport in *abcb21-2* is reduced by > 50%. Transport in *abcb21-1* is reduced by ~25% but is not statistically different due to a high amount of variability. Removal of the cotyledons alone, or cotyledons and petioles in light grown seedlings reduces phototropic bending ~20% and ~40%, respectively (data not shown). No difference in phototropic bending was observed in post-photomorphogenic *abcb21* seedlings (Fig. 3.4 B). Although the cotyledons have been shown to have only a minor role in supplying auxin to the rootward auxin transport stream, these results suggest ABCB21 contributes to this process to some extent.

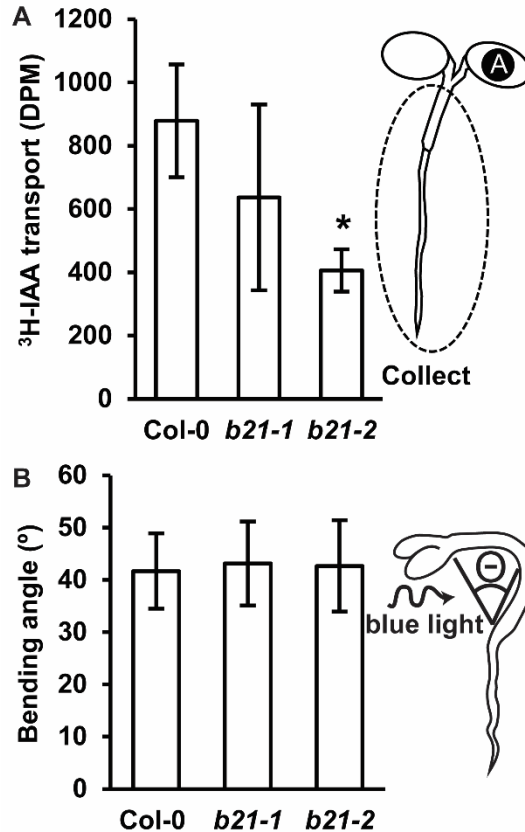


Figure 3.4. Cotyledon-hypocotyl auxin transport and phototropic bending in *abcb21*. (A) Cotyledon-to-hypocotyl auxin transport is reduced in *abcb21*. Data shown are means \pm SD (n = 3 pools of 12). * indicate statistical difference by Student's *t* test (p<0.05). (B) Phototropic bending is not different from Col-0 in *abcb21*. Data are means \pm SD for 2 independent replicates (n > 20 for 2 replicates).

One of the hallmark phenotypes of *twd1* is the 'super-twisting' of the root (Wang *et al.*, 2013). Reports of epidermal root twisting in *abcb1abcb19* double mutants are variable (Wu *et al.*, 2010; Wang *et al.*, 2013). In an *abcb1-labcb19-101* (Col-0) background, primary roots exhibit increased waving and twisting compared to Col-0 but evidence of *twd1*-like 'super-twisting' is not observed (Fig. 3.5 A). To see

if additional loss of *abcb21* would increase root twisting, *abcb1abcb19abcb21-2* triple mutants were generated. Additionally, since ABCB4 has also been shown to interact with FKBP42, triple *abcb1abcb19abcb4-1* mutants were also made. No *twd1*-like 'super-twisting' was observed in either triple mutant (Fig. 3.5 A). Triple *abcb21* and *abcb4* mutants had a partial reversion of the enhanced primary root elongation observed with *abcb1abcb19* but the reduction was not as great as in *twd1* (Fig. S3.3). This supported the idea that *ABCB4*, and possibly *ABCB21*, contributes to the *twd1* phenotypes but also suggested that there were other ABCB transporters involved in rootward auxin transport in seedlings.

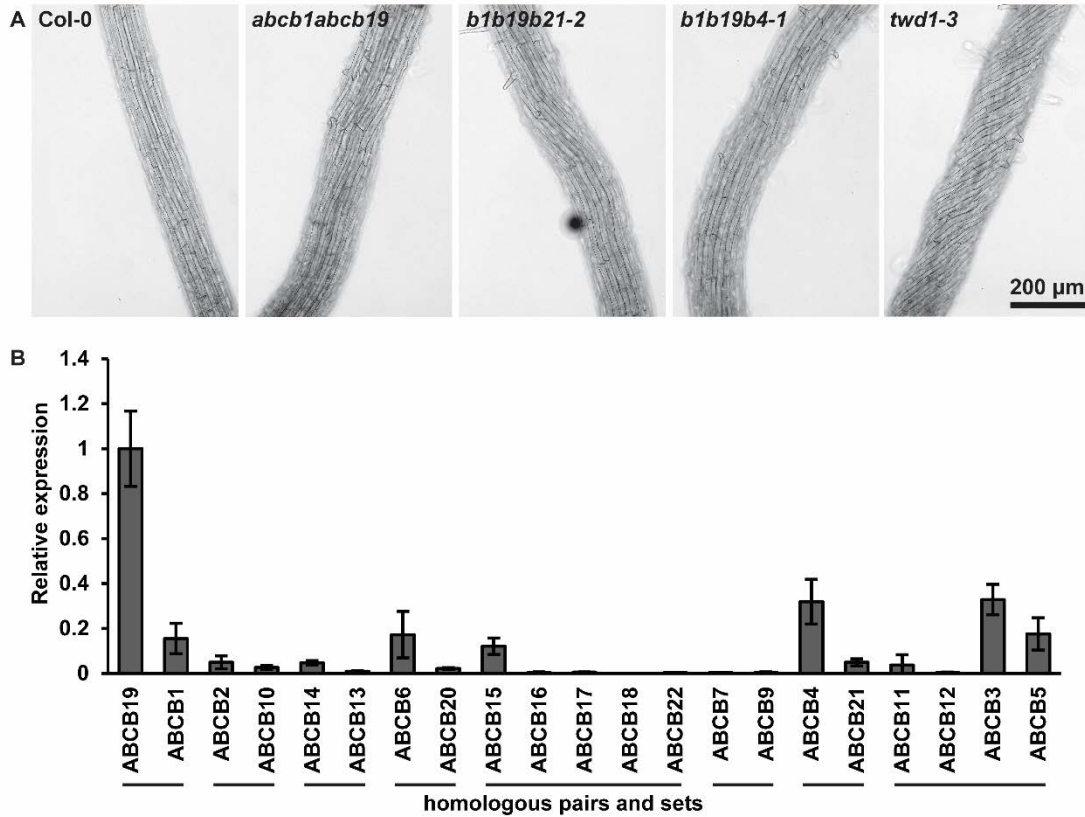


Figure 3.5. Root twisting in *b1b19b21* and expression of ABCB transporters in seedlings. (A) Bright field images showing root twisting in Col-0, *abcb1abcb19*, *b1b19b21-2*, *b1b19b4-2*, and *twd1-3* seedlings. Contrast and brightness were adjusted using Photoshop. (B) qRT-PCR of ABCB transporters in 7-day Col-0 seedlings. Data shown are means \pm SD (n = 3).

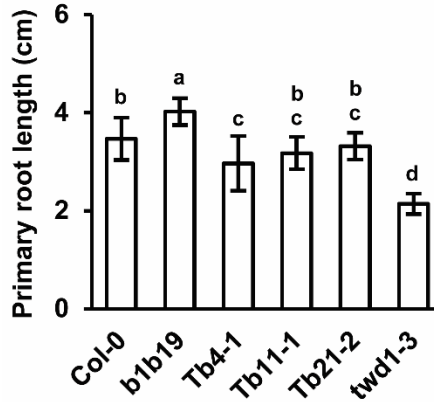


Figure S3.3. Primary root growth in *abcb* triple mutants is *twd1*-like. 7-day primary root lengths. Data shown are means \pm SD (n = 12-14). Letters represent statistical difference by ANOVA $p < 0.001$, Tukey's post-hoc $p < 0.05$.

ABCB transporter expression

Phylogenetic analysis reveals ABCB transporters cluster into homologous pairs and sets (Geisler and Murphy, 2006; Knöllner et al., 2010). Expression by qRT-PCR and analysis of the TraVA RNA-seq database reveal that within these sets one transporter is generally expressed to higher levels than the others (Fig. 3.5 B; Fig. S3.3 A and B). This difference in expression explains the reduction in phenotypic severity observed in *abcb1* compared to *abcb19* (Noh et al., 2001; Blakeslee et al., 2007). The relative expression levels of both *ABCB1* and *ABCB19* compared to all others validate their roles in auxin transport and help to explain why the functions of the other ABCB transporters remain elusive.

From the expression data, *ABCB2*, *ABCB14*, *ABCB6*, *ABCB15* and *ABCB11* are expressed to levels that merit further investigation (Fig. 3.5 B; Fig S3.4 A and B). Although *ABCB3* and *ABCB5* showed moderate expression by qRT-PCR, melting

curve analysis and visualization of the PCR products suggest non-specific amplification. RNA-seq and microarray data both support that *ABCB3* and *ABCB5* are not expressed in seedlings. A previous study reported reduced auxin transport in *abc12* (SALK_094249 annotated as *abc11*) inflorescence stems (Kaneda et al., 2011). While *ABCB12* does not appear to be expressed to any appreciable level, single mutants of *ABCB12* was included in a subsequent analysis. *ABCB2* does not transport auxin in *S. pombe* (Yang and Murphy, 2009) and expression of *ABCB2* and *ABCB10* are relatively low. However, since *ABCB2* and *ABCB10* are closely related to *ABCB1* and *ABCB19* (Knöller et al., 2010) both were analyzed. *abc14* and *abc15* were also reported to have reduced auxin transport in inflorescences but function in seedlings was not examined (Kaneda et al., 2011).

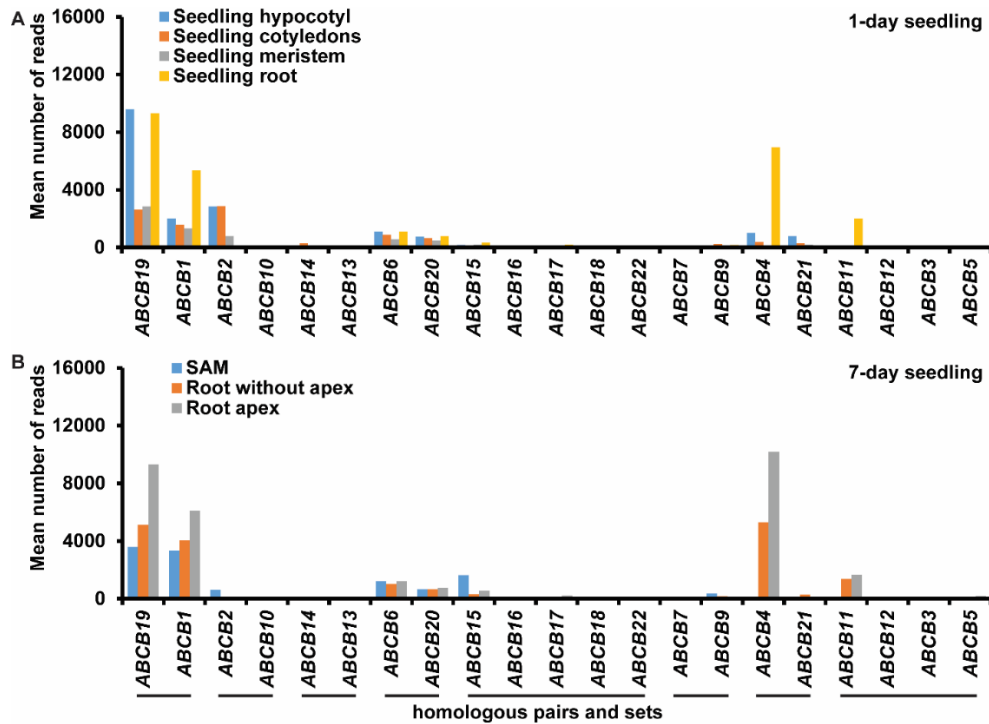


Figure S3.4. ABCB transporter expression in seedlings from the TraVA RNA-seq database. Expression data from the TraVA RNA-seq database for (A) 1-day and (B) 7-day seedlings.

Auxin transport in cluster specific ABCB-RNAi lines

Due to possible functional redundancy and compensatory expression, RNAi lines were generated to target the sets of ABCB transporter paralogs. Two independent homozygous lines were analyzed for each *ABCB2/10RNAi*, *ABCB3/5/11/12RNAi*, *ABCB13/14RNAi*, and *ABCB15/16/17/18RNAi* construct. qRT-PCR was performed to verify knockdown of each target gene. Since *ABCB19* plays a significant role in mediating rootward auxin transport, its expression was also monitored. *ABCB6/20RNAi* lines showed effects on several off target genes and was

not included. Reduced expression of the target genes was confirmed without a major effect on *ABCB19* for *ABCB2/10-*, *ABCB3/5/11/12-*, and *ABCB13/14RNAi* (Fig. 3.6 A-C). Expression of the target genes in *ABCB15/16/17/18RNAi* was variably reduced and *ABCB19* expression was also negatively regulated (Fig. 3.6 D). The greatest reduction in ³H-IAA transport was observed in *ABCB3/5/11/12RNAi* from the shoot apex to the root-shoot transition zone (RSTZ) (Fig. 3.6 F). Transport was reduced to a lesser extent in *ABCB2/10RNAi* (Fig. 3.6 E), but was not different from vector controls in *ABCB13/14RNAi* (Fig. 3.6 G). Transport to the RSTZ and root apex in *ABCB15/16/17/18RNAi* was also variably reduced (Fig. 3.6 H), however, these may be an effect of reduced *ABCB19* expression. Further efforts to reduce *ABCB15/16/17/18* expression via 21-mer RNAi yielded similar results.

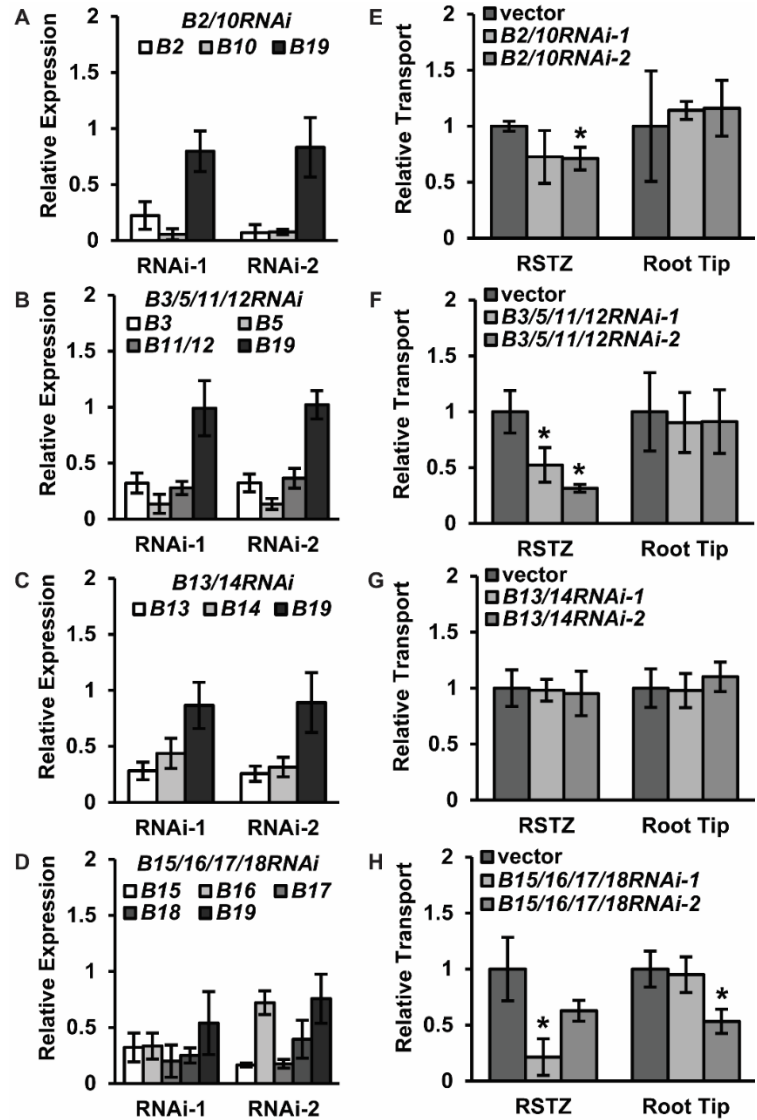


Figure 3.6. Expression and transport in *ABCB-RNAi* lines. (A-D) qRT-PCR of *ABCB-RNAi* lines. Data shown are means \pm SD (n = 3). (E-H) Auxin transport in *ABCB-RNAi* lines. Data shown are means \pm SD (n = 3 pools of 10). * indicate statistical difference from vector controls by Student's *t* test (p < 0.05).

Since transport was reduced in *ABCB2/10-* and *ABCB3/5/11/12RNAi* lines and *ABCB2*, *ABCB10* and *ABCB11* are expressed in seedlings, single mutants of these transporters were further analyzed. Of the *ABCB15/16/17/18* cluster only *ABCB15* is expressed in seedlings, therefore, *abcb15* was included. *abcb12*, *abcb14* were also analyzed due to previous report of reduced transport in *abcb12* and *abcb14* inflorescence stems (Kaneda et al., 2011).

Phenotypes and transport in ABCB single mutant lines

abcb single mutants were then screened for differences in auxin related phenotypes including hypocotyl elongation under low light (50-60 uE), primary root elongation, and lateral root density (Table 1). Overall phenotypic differences from Col-0 were minor. *abcb2* mutants exhibit slightly longer 5-day primary root length but are not different from Col-0 at 7 or 10 days. *abcb10* mutants exhibit increased hypocotyl elongation and decreased 5-day primary root length compared to Col-0. The most dramatic phenotype was observed was reduced primary root elongation in *abcb11*. *abcb6*, *abcb12*, *abcb14*, and *abcb15* mutants were not different from Col-0 in any of the phenotypes.

Table 1. Single mutant phenotypes.

	Light grown hypocotyl length	5 day root length	7 day root length	10 day root length	10 day LR density
<i>abcb2</i>	n.d.	111.8 ± 14.5%	n.d.	n.d.	n.d.
<i>abcb6</i>	n.d.	n.d.	n.d.	n.d.	n.d.
<i>abcb10</i>	111.8 ± 3.6%	89.8 ± 3.5%	n.d.	n.d.	n.d.
<i>abcb11</i>	n.d.	87.6 ± 12.1%	86.1 ± 16.5%	88.4 ± 9.7%	n.d.
<i>abcb12</i>	n.d.	n.d.	n.d.	n.d.	n.d.
<i>abcb14</i>	n.d.	n.d.	n.d.	n.d.	n.d.
<i>abcb15</i>	n.d.	n.d.	n.d.	n.d.	n.d.

% of Col-0 ± SD, only % significantly different from Col-0 (<0.05) by Student's t test are shown. n.d. = not different

To assess if the candidate ABCB transporters contribute to rootward auxin movement, transport of ³H-IAA in 5.5-day seedlings was measured. ³H-IAA transport from the shoot apex to the RSTZ was significantly reduced in *abcb11* and *abcb14* compared to Col-0, but to a much lesser extent than in *abcb19* (Fig. 3.7A). No reduction was observed in *abcb1*, *abcb2*, *abcb6*, *abcb10*, or *abcb12*. The lack of reduction in *abcb1* can be attributed to compensation by *ABCB19*, as expression is increased ~4.5 times in the *abcb1* background (Fig. S3.5). *ABCB14*, however, was originally identified as a malate/citrate transporter in guard cells (Lee et al., 2008). Competition with malate (5:1 molar ratio) reduced rootward ³H-IAA transport in Col-0, *abcb1*, *abcb6*, *abcb10*, *abcb11*, *abcb12*, and *abcb19* to a similar extent (Fig. 3.7 A). No reduction was observed in *abcb14*, suggesting that transport of malate, and not auxin, is its primary function of *ABCB14*. Malate competition is also observed in *abcb2*, suggesting *ABCB2* may be able to transport malate as well. ³H-IAA transport from the RSTZ to the root tip was not different from Col-0 for any mutants except

abcb19 (Fig. 3.7 B). *abcb19* showed a very slight decrease in ^3H -IAA in the root tip and increased levels in above sections.

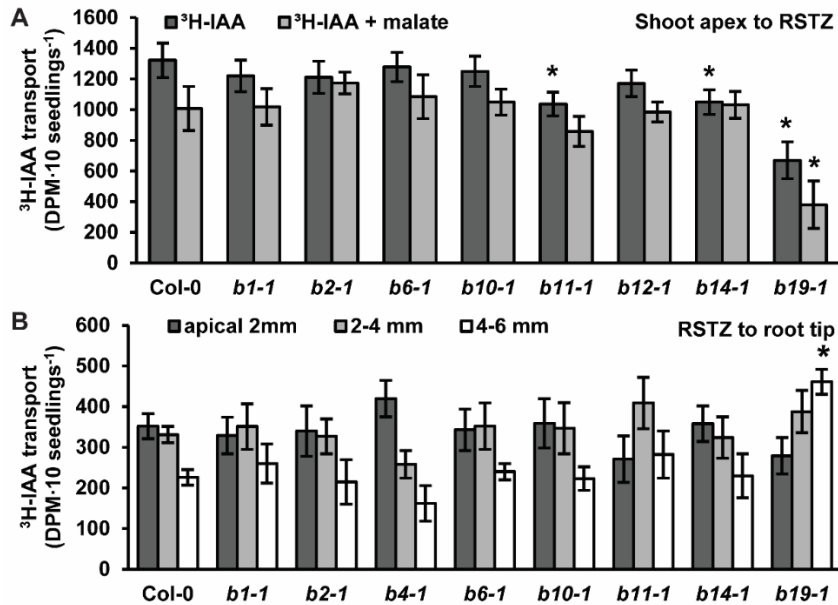


Figure 3.7. Auxin transport assays in *abcb* mutant seedlings. (A) ^3H -IAA transport from the shoot apex to the root-shoot transition zone (RSTZ). Means \pm SD (n = 3 pools of 10). * indicate statistical difference from Col-0 by ANOVA $p < 0.001$, Dunnett's post-hoc $p < 0.05$. (B) ^3H -IAA transport from the RSTZ to the root tip. Means \pm SD (n = 3 pools of 10). * indicate statistical difference by ANOVA $p < 0.001$, Dunnett's post-hoc $p < 0.05$.

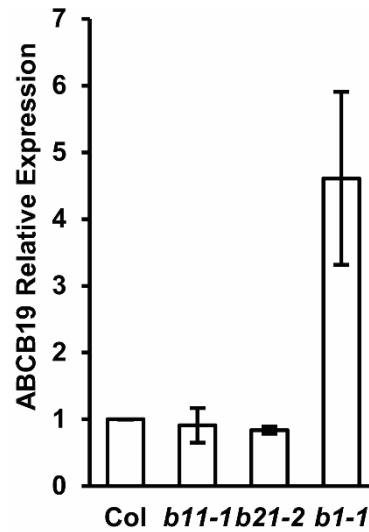


Figure S3.5. Compensatory expression of *ABCB19* in *abcb1* but not *abcb11* or *abcb21*. Data shown are means \pm SD (n = 3 biological replicates, 2 technical replicates).

From analysis of expression, FKBP42 interaction, and transport in RNAi lines and single mutants, only *ABCB11* showed consistent characteristics of an auxin transporter.

Characterization of ABCB11

Previously, *ABCB11* was reported to be expressed in the root vasculature in seedlings, however, the promoter used in the study did not include the two nucleotides (AT) directly upstream of the ATG start codon (Kaneda et al., 2011). To confirm this expression, the 2.104 kb fragment of *ABCB11* upstream of the ATG, including the AT, was fused to GUS and transformed into Col-0. Contrary to the previous report, GUS activity was not observed within the vasculature (Fig. 3.8 A and B). Strong GUS staining is observed in the meristematic, transition and elongation

zones of the root (Fig. 3.8 A) and diffuse GUS signal is observed in the upper portions of the root (Fig. 3.8 B). This result agrees with the microarray data that shows expression in the maturation zone, elongation zone and root tip are each ~5X greater than the level of expression in the stele (Genevestigator). No staining could be detected in the cotyledons, shoot apex, or hypocotyl (Fig. 3.8 C and D).

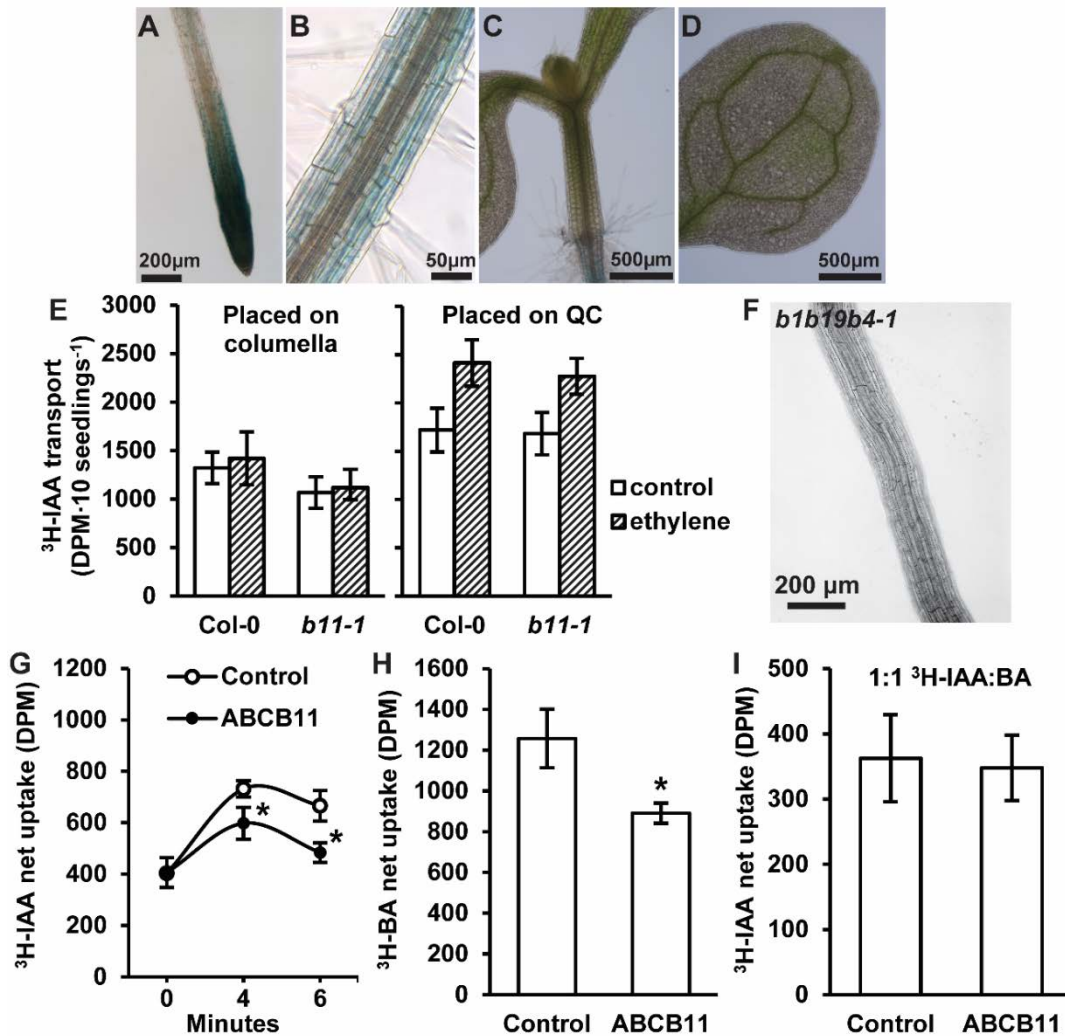


Figure 3.8. Expression and activity of ABCB11. (A) Strong *proABCB11:GUS* expression is observed in the root tip. (B) Diffuse expression is observed throughout the rest of the root but not associated with the vasculature. No *proABCB11:GUS*

expression is observed in the (C) hypocotyl or (D) cotyledons. (E) No difference in shootward auxin transport from the root tip is observed in *abcb11* seedlings). Assays were conducted as in Kubes et al. (2012). Data shown are means \pm SD (n = 3 pools of 10). (F) Bright field images showing root twisting an *abcb1abcb19abcb11* triple mutant. Contrast and brightness was adjusted using Photoshop. (G) ABCB11 mediates export of ^3H -IAA when expressed in *S. pombe*. Data shown are means \pm SD (n = 4). * indicate statistical difference by Student's *t* test (p < 0.05). (H) ABCB11 mediates export of ^3H -benzoic acid when expressed in *S. pombe*. Data shown are means \pm SD (n = 4). * indicate statistical difference by Student's *t* test (p < 0.05). (I) Competition of ^3H -IAA with cold benzoic acid (1:1 molar ratio) reduces auxin transport to control levels. Means \pm SD (n = 4).

Since *ABCB11* expression is highest in the root it was hypothesized that the reduction in transport in the hypocotyl may be due to disruption of the auxin sink at the root tip. Shootward auxin transport from the root tip was therefore measured in *abcb11-1* (Fig. 3.8 E). Assays were conducted as in Kubes et al. (2012). No difference in shootward auxin transport could be detected in *abcb11* with auxin placed overlaying the columella or the quiescent center. *abcb19* was previously shown to have a greater decrease in shootward auxin transport compared to Col-0 when ethylene was added to the system. Ethylene reduced shootward auxin transport to a similar extent in Col-0 and *abcb11*. Like with *abcb21* and *abcb4*, generation of an *abcb1abcb19abcb11-1* triple mutant slightly reduced primary root elongation compared to *abcb1abcb19* but no *twd1*-like root twisting was observed (Fig. 3.8 F).

Mutant phenotypes can be masked by upregulation of genetically or functionally redundant paralogs (Rensing, 2014). For example, *ABCB19* is upregulated 4-5 times in *abcb1* (Fig. S3.5; Blakeslee *et al.*, 2007). *ABCB12* is only 1,090 bp downstream of the *ABCB11* stop codon. While little *ABCB12* expression could be detected in Col-0 seedlings (Fig 3.5 B; Fig. S3.4), *ABCB12* was measured for elevated expression in *abcb11*. *ABCB11* transcript levels were below the detection limit in *abcb11* roots (Fig. S6 A). *ABCB12* does not appear to compensate for loss of *ABCB11* function, as *ABCB12* expression is slightly reduced in *abcb11* mutants (Fig. S3.6 B). Additionally, no compensation by *ABCB19* could be detected (Fig. S3.5). This suggests that *ABCB12* and *ABCB19* do not compensate for loss of *ABCB11* and that *ABCB11* may even promote expression of *ABCB12*.

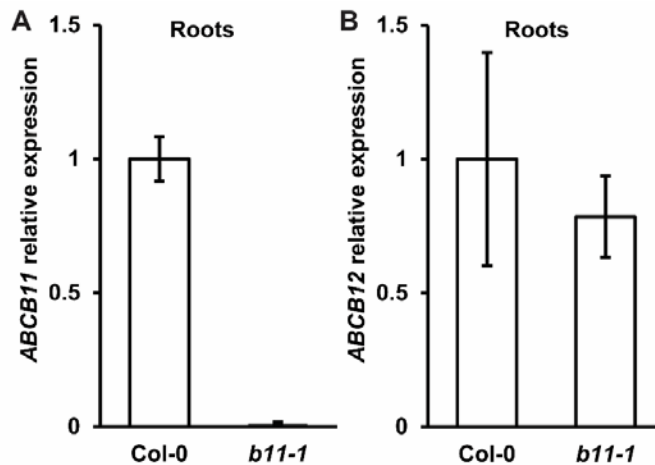


Figure S3.6. ABCB12 does not compensate for loss of ABCB11. Data shown are means \pm SD (n = 3 biological replicates, 2 technical replicates).

To verify that ABCB11 has the capacity to transport auxin ^3H -IAA transport assays with ABCB11 expressed in *S. pombe* were performed. Cells expressing ABCB11 accumulated ~18% less ^3H -IAA after 4 minutes and ~27% less after 6 minutes, which is comparable to the efflux activity of ABCB19 (Fig. 8G). Transport of ^3H -benzoic acid was analyzed as a control for specificity. Cells expressing ABCB11 accumulated less ^3H -benzoic acid, suggesting decreased specificity for IAA compared to ABCB19 (Fig. 8H). Competition with benzoic acid (1:1 molar ratio) reduced ^3H -IAA transport to control levels indicating ABCB11 preferentially transports benzoic acid over IAA (Fig. 8I). These results suggest that, like ABCB14, ABCB11 has the capacity to transport auxin but may transport alternate substrates *in vivo*.

Discussion

The best characterized ABCB transporters, ABCB1, ABCB19 and ABCB4, have been shown to function in auxin transport with a possible additional function in auxin-activated small anion movement (Noh et al., 2001; Geisler et al., 2005; Kubeš et al., 2012). In seedlings, ABCB1 and ABCB19 function coordinately in loading of auxin into the rootward transport stream in the shoot apex and restricting auxin to within the central cylinder in the hypocotyl and root (Noh et al., 2001; Blakeslee et al., 2007; Mravec et al., 2008). ABCB4 is expressed primarily in the root epidermis where it regulates shootward auxin transport from the root tip (Terasaka et al., 2005; Santelia et al., 2005; Lewis et al., 2007; Kubeš et al., 2012).

Quantification of expression by qRT-PCR (Fig. 3.5 B) and RNA-seq (Fig. S3.4 A and B) reveals ABCB19 is the most abundant transporter in seedlings,

followed by ABCB4 and ABCB1. ABCB19 is expressed throughout all tissue layers but is highest in the small auxin producing cells in the shoot apical meristem and in young leaf primordia, and in cell layers bounding the central cylinder in the hypocotyl and root (Fig. 3.1 A-C). In the shoot apex and leaf primordia, where auxin biosynthesis is high, PIN proteins mediate the direction of auxin flux (Benková et al., 2003) while ABCB19 maintains the auxin flow by preventing reuptake. In the hypocotyl and root, ABCB19 bounds the central cylinder (Blakeslee et al., 2007; Titapiwatanakun et al., 2009), preventing leakage of auxin from the rootward transport stream by continuously pumping it back into the stele. This exclusionary activity is not trivial as loss of ABCB19 reduces auxin transport by > 50% while loss of directional transport by PIN1 is reduced by ~30% (Blakeslee et al., 2007).

FKBP42/TWD1 interacts directly with ABCB1 and ABCB19 and is required for their proper trafficking to and activity on the plasma membrane, and auxin transport is reduced ~10-15% more in *twd1* than *abcb1abcb19*. One hypothesis to reconcile this difference is that at least one other unidentified ABCB transporter mediates rootward auxin transport and interacts with FKBP42. However, interaction does not necessarily indicate a function in auxin transport as FKBP42 has also been shown to interact with the arsenic and glutathione S-conjugate transporters ABCC1 and ABCC2 (Geisler et al., 2004).

Function of ABCB21. Lateral root primordia initiation in young seedlings is dependent on auxin synthesized in the root tip, however, lateral root emergence is dependent on auxin produced in the shoot apical meristem and first true leaves, and to

a lesser extent cotyledons, up to 10 days after germination (Bhalerao et al., 2002). At this point auxin biosynthesis in the root increases 10-fold and root derived auxin regulates both lateral root primordia initiation and lateral emergence (Bhalerao et al., 2002). ABCB21 is expressed in the root pericycle of 5 to 10 day seedlings, coinciding with the pulse of shoot derived auxin transported to the root. Loss of ABCB21 leads to a reduction in rootward transport from the RSTZ to the root tip and causes an increase in auxin levels in the upper root and hypocotyl. These results are consistent with a role for ABCB21 in preventing leakage from the rootward transport stream by excluding auxin from entering the pericycle (Fig. 3.9 A). This role is further supported by the observation that ABCB21 expression is absent in lateral roots where an auxin accumulation is necessary for lateral root primordia formation and lateral root outgrowth (Fig. 3.9 B). ABCB21 exhibits conditional auxin uptake and efflux when expressed in *S. pombe*. This suggests ABCB21 may help to initiate a localized auxin accumulation for early lateral root development, but is then down-regulated to prevent reloading of auxin into the rootward stream. *abcb21* mutants show only differences in the timing of lateral root emergence, possibly due to an overlap in function with ABCB19. ABCB21 also regulates movement of auxin from the cotyledons to the hypocotyl (Fig. 3.4 B). Expression of ABCB21 at organ junctions in inflorescence stems, leaves, and flowers (Kamimoto et al., 2012) suggests ABCB21 may have a similar role in mature tissues. It remains unknown whether ABCB21 is exclusively an auxin transporter or if specificity extends to other substrates.

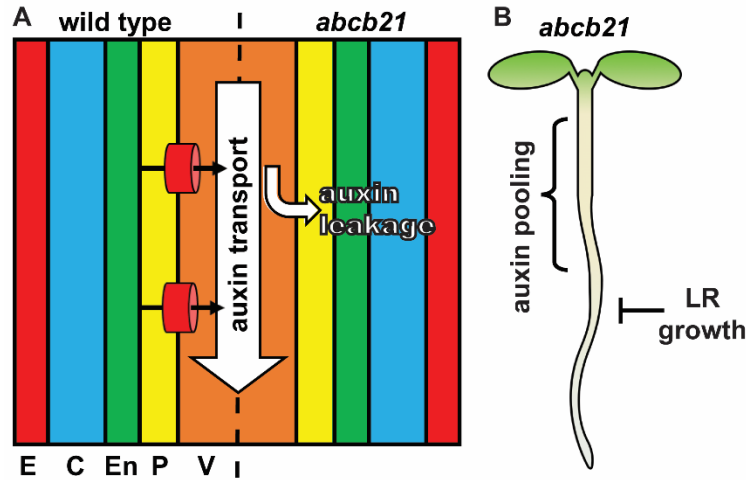


Figure 3.9. Model for ABCB21 function in the root. (A) ABCB21 appears to function primarily in restricting auxin to within the rootward auxin transport stream. Loss of ABCB21 leads to leaking of auxin from the central cylinder, resulting in reduced rootward auxin transport. E, epidermis; C, cortex; En, endodermis; P, pericycle; V, vasculature. (B) The reduction in auxin transport in the root causes pooling of auxin in the upper root and lower hypocotyl, reducing the supply of needed for lateral root outgrowth.

Screening of other ABCB transporters. Characterization of single ABCB transporter mutants can be complicated due to compensation by paralogous genes. The high level of sequence homology between transporters allowed for the use of RNAi to knock-down multiple transporters with a single construct. Using this method RNAi lines to target the pairs/sets of transporters *ABCB2/10*, *ABCB3/5/11/12*, *ABCB13/14* and *ABCB15/16/17/18* were generated. *ABCB2/10* and *ABCB3/5/11/12RNAi* lines exhibited reductions in rootward auxin transport suggesting at least one transport in each group could function as an auxin transporter (Fig. 3.6 E and F).

Phenotypic analysis of *abcb* single mutants showed only minor effects on growth and development (Table 3.1). Rootward transport in *abcb2*, *abcb6*, *abcb10*, and *abcb12* is not different from Col-0 (Fig. 3.7 A and B), suggesting they are not auxin transporters and/or don't mediate rootward transport in seedlings. While isolating *abcb6* lines a modest decrease in inflorescence height was noted. This, along with increased expression of ABCB6 and ABCB20 in mature plants, points to a more predominant role for these transporters in mature tissues than in seedlings. Rootward auxin transport was only reduced in *abcb11* and *abcb14* single mutants. Competition with malate, however, showed that ABCB14 has higher specificity for malate than auxin (Fig. 3.7 A). This result is consistent with a previous study that reported ABCB14 as a malate and citrate transporter (Lee et al., 2008). Since cellular concentrations of malate are over 1,000-fold greater than IAA, ABCB14 mediated auxin transport is expected to be minimal *in vivo*. A more detailed analysis revealed ABCB11 is primarily expressed in the root tip and in cell layers outside of the central cylinder of the root (Fig. 3.8 A and B). It was hypothesized that the reduction in rootward transport in *abcb11* hypocotyls was due to defects in the auxin sink in the root tip. This does not appear to be the case, as shootward transport is not altered (Fig. 3.8 E). ABCB11 is able to transport auxin in *S. pombe* but benzoic acid is able to outcompete auxin (Fig. 3.8 G-I). This suggests ABCB11 may have specificity for other substrates *in planta*.

Conclusions and Outlook. The lack of obvious phenotypes and defects in auxin transport are not unexpected as all *ABCB* transporters are expressed to levels several

fold lower than that of ABCB19. This points to the majority of these transporters having little to no role in growth and development in the seedling stage. Since seedlings lack the complex organs and transport systems that appear to have driven the diversification and expansion of the ABCB subfamily, analysis of *abcb* transporter mutants in mature tissues may provide more answers.

Biochemical characterization of ABCB transporters remains a challenging task. While several ABCB transporters have the ability to transport auxin, the mechanisms of substrate specificity and the range of substrates for each transporter remain largely unknown. Analysis of the mechanisms of specificity and ATPase activity will require development of isolated proteoliposome or membrane vesicle systems.

Materials and Methods

Plant material and growth conditions. Seeds were surface sterilized and sown on ¼ MS medium (RPI Corp.) containing 0.5% sucrose and 0.8% agar, pH 5.5. Seeds were stratified at 4 °C for 2 days then grown under continuous 100 $\mu\text{mol m}^{-2} \text{s}^{-1}$ light at 22°C for the times indicated. Lines used are listed in Appendix B.

Confocal Microscopy. Confocal microscopy was performed using an LSM 710 Laser Spectral Scanning Confocal Microscope (Zeiss) with either a 20x or 40x lens. The master gain was always set to less than 800, with a digital gain of 1.9. For ABCB19-GFP, 488-nm (5% laser for hypocotyl, 20% for root) was used for excitation and emission collected from 493- to 598-nm. For DII-VENUS, 514-nm

(20% laser) was used for excitation and emission was collected from 515- to 562-nm. All images were processed with ZEN (Zeiss) and Illustrator (Adobe).

Yeast transport assays. Yeast assays were conducted as described in Yang and Murphy, 2009. The ABCB21 expression construct was created by amplifying ABCB21 with Gateway BP primers (Table S2) and recombining the product into pDONRzeo by BP reaction (Thermo Fisher). ABCB21 CDS was then transferred into pREP41GW by LR reaction (Thermo Fisher). The ABCB11 expression construct was created by amplifying ABCB11 using primers containing NcoI and XmaI restriction sites (Table S2). The digested ABCB11 product was ligated into the pREP41 vector digested with NcoI and XmaI. Expression vectors were transformed into *S. pombe* by electroporation.

Histochemical staining. The 0.625 kb fragment of ABCB21 and the 1.650 kb fragment of ABCB11 upstream of the start codon was cloned into pENTR-D-TOPO (Thermo Fisher) then transferred into the Gateway compatible vector pGWB3 (Nakagawa et al., 2007) by LR reaction (Thermo Fisher). Constructs were transformed into Col-0 by floral dip. For GUS staining, tissues were incubated in 90% acetone for 20 mins on ice, then immersed in staining solution (50 mM sodium phosphate buffer, pH 7.0, 0.1% triton X-100, 0.5 mM potassium ferrocyanide, 0.5 mM potassium ferricyanide, and 1 mM X-gluc) and incubated in the dark at 37°C for 5-6 hours. Stained samples were cleared with 70% ethanol before imaging. For sectioning tissue was dehydrated in a series of tert-butanol (TBA) and embedded in

Paraplast Plus. 20 µm sections were prepared using a Leica Reichert-Jung 2030 rotary microtome.

Seedling transport assays. Rootward seedling transport assays were conducted as described in Blakeslee et al., 2007. Shootward transport assays from the root tip were conducted as described in Kubeš et al., 2012.

IAA quantification. Free IAA quantification for *abcb21* was conducted as described in Novák et al., 2012. Free IAA quantifications for *abcb1*, *abcb19*, and *abcb1abcb19* were conducted as described in Zhang et al., 2016.

Cotyledon-hypocotyl transport assays. 5-day seedlings were placed on filter paper (Whatman 3MM) saturated with ¼ MS with the hypocotyl and cotyledons not touching any surface. Seedlings were allowed to equilibrate vertically in light for 1 hour. A 6% agarose bead (Collodial Science Solutions, AMB-0601-0010) incubated in solution containing 2 µM IAA (1:1 3H-IAA (25 Ci/mmol, ARC) : cold IAA) was placed in the middle of one cotyledon per seedling. After 2 hours both cotyledons were removed by cutting just below the cotyledonary node using a surgical blade. 3H-IAA transported from the cotyledons to the hypocotyl and root was measured by liquid scintillation counting.

Phototropism assays. Seeds were surface sterilized, sown on ¼ MS medium (RPI Corp.) containing 0.5% sucrose and 1% phytigel (Sigma, P8169), then stratified at

4°C for 2 days. Plates were placed under 65 $\mu\text{mol m}^{-2} \text{s}^{-1}$ white light for 24 hours, then moved to dark. After seedlings reached 0.3 cm tall they were light treated for 12h to undergo photomorphogenesis. Seedlings were then returned to dark to undergo dark acclimation until they reached approximately 0.7 cm (at least 12h to allow for the reset of phot1). For bending assays seedlings were placed in unilateral 0.6-0.9 $\mu\text{mol m}^{-2} \text{s}^{-1}$ blue light (Manufacturer) for 8h. Bending angles were measured made using ImageJ.

RNA isolation and quantitative real-time PCR (qRT-PCR). For qRT-PCR total RNA was extracted using ZR Plant RNA Mini Prep kit (Zymo Research) followed by treatment with DNaseI (New England Biolabs). Total RNA (1.5 μg) was used for first-strand synthesis using SuperScript III reverse transcriptase (ThermoFisher). Real-time PCR was performed on a CFX Connect (Bio-Rad Laboratories) using EvaGreen qPCR master mix (Biotium). Primers used are listed in Appendix C. Transcript levels normalized against PP2A or ACT2 produced similar results.

Construction of RNAi lines. In order to knock down multiple ABCB genes with one RNAi construct, a fragment of 350-470 bp in length was designed to target a unique region within the transmembrane domains of all target genes within a given cluster. RNAi fragments were obtained through reverse transcription PCR using the primers in Table S1 and then cloned into pENTR-D-TOPO (Thermo Fisher). RNAi fragments were then transferred into the inducible pOpOff Gateway-compatible system (Wielopolska et al., 2005) by LR reaction (Thermo Fisher). All four ABCB-RNAi

constructs were transformed into Col-0. For RNAi induction plants were grown on media containing 10 μ M dexamethasone.

Statistical analysis. All statistical analyses were performed using SigmaStat or JMP PRO 13.

Chapter 4. ABCB regulation of auxin transport in *Arabidopsis* stems, leaves and flowers

Jenness et al., manuscript in preparation

Summary

Local and global gradients of the phytohormone auxin control plant growth and development from seed through maturity. These gradients are generated primarily through cellular auxin efflux mediated by PIN efflux carriers and ABCB transporters. However, much of what we understand about auxin transport in mature tissues is extrapolated from transport studies in seedlings. Analysis of *abcb* mutants suggests like in seedlings, ABCB1 and ABCB19 primarily function in the shoot apex where auxin biosynthesis occurs. Investigation of the remaining ABCB transporters identified ABCB6 as a contributor to rootward auxin transport in inflorescence stems, ABCB21 in leaves, and ABCB11 in flowers.

Introduction

Plant height, leaf area, and leaf angle are important agronomic traits that are controlled by the phytohormone auxin (indole-3-acetic acid, IAA). Reduced polar auxin transport caused by loss of the ATP-BINDING CASSETTE TRANSPORTER B1 (ABCB1) in maize *brachytic2* (*br2*) and sorghum *dwarf3* (*dw3*) lead to decreases in internode length, and increases in leaf inclination angle (Multani et al., 2003; Pilu et al., 2007; Truong et al., 2015). While mutations in brassinosteroid (BR) and gibberellic acid (GA) synthesis / perception can also reduce plant height, these

mutants are often associated with other developmental defects such as pollen infertility that impact overall production (Hartwig et al., 2011; Vriet et al., 2013; West and Golenberg, 2018).

Polar auxin streams are maintained by coordinated cellular transport activities. The polarity of these flows is directed by anisotropic distribution of PINFORMED (PIN) anion efflux carrier proteins (Benková et al., 2003; Friml et al., 2003). Lipophilic diffusive uptake of protonated auxin (IAAH) is amplified in some cells by AUXIN /LIKE AUXIN 1 (AUX1/LAX) H^+ / IAA^- symporters. ATP Binding Cassette subclass B (ABCB) transporters are isotropically – distributed PM proteins that are concentrated in small cells and appear to prevent cellular reuptake and bound primary auxin flows (Blakeslee et al., 2007; Titapiwatanakun et al., 2009).

Structural, biochemical, and mutational analyses suggest that ABCBs mobilize auxin associated with the inner leaflet of the plasma membrane, with additional exclusion of auxin from within the membrane bilayer (Bailly et al., 2010). ABCB1, 4, and 19, and PIN1 and 2 all reside in ordered sterol and sphingolipid-enriched plasma membrane nanodomains (reviewed in Tapken and Murphy, 2015) and synergistic increases in the amount and specificity of auxin efflux have been reported when ABCB19 and PIN1 co-occur (Blakeslee et al., 2007; Titapiwatanakun et al., 2009; Yang and Murphy, 2009). This specificity and activity is further enhanced by addition of sterols like cholesterol, sitosterol, or ergosterol (Titapiwatanakun et al., 2009; Bailly et al., 2011). *In silico* docking of sitosterol with ABCB19 suggests sterols preferentially interact with the transmembrane domain regions associated with IAA binding (Yang and Murphy, 2009; Bailly et al., 2011;

Yang et al., 2013). Evidence of how membrane interactions control PIN1-auxin binding and specificity remain unknown as no PIN structure has been determined. In contrast, AUX1 resides in less ordered domains, providing a spacial separation of auxin uptake and efflux mechanisms. Additional modulation of ABCB1 and ABCB19 activity is controled by phosphorylation (Christie et al., 2011; Henrichs et al., 2012) and is though to be coordianted with regulation of other auxin transporters (Titapiwatanakun and Murphy, 2009).

The best characterized ABCB transporters in *Arabidopsis* are ABCB1 and 19 (Noh et al., 2001; Geisler et al., 2005; Blakeslee et al., 2007). ABCB1 and 19 function coordinately in loading of auxin into the basipetal stream in apical regions and maintain long-distance transport streams by preventing entry into bounding tissues (Blakeslee et al., 2007; Mravec et al., 2008). Polar auxin transport is reduced by ~25% and >50% in single *abcb1* or *abcb19* mutants, and is reduced by ~75% in the severely dwarfed *abcb1abcb19* double mutant (Blakeslee et al., 2007).

Other members of the *Arabidopsis* ABCB subfamily have been implicated in long distance auxin transport in vegetative tissues and may contribute to the primary auxin transport activities of ABCB1 and 19. ABCB2, 6, 10, and 20 exhibit structural similarities with ABCB1/19 that suggest possible auxin transport function (Knöllner et al., 2010; Bailly et al., 2011). *ABCB11* is reportedly expressed in inflorescence stems, and *abcb14* exhibits defects in inflorescence auxin conductance (Kaneda et al., 2011). *ABCB21* has recently been shown to function loading of auxin from cotyledons and hypocotyls into the rootward transport stream as well as auxin retention within the vascular cylinder (Jeness et al., in preparation).

Loss of directional auxin transport in *pin* mutants leads to severe defects in embryogenesis and organogenesis (reviewed in Zazimalová et al., 2010). However, mutations in *PINI*, the primary PIN involved in long distance auxin transport, reduces polar auxin transport in hypocotyls only about 30% (Blakeslee et al., 2007), suggesting that the long distance auxin transport stream is less important to overall development than localized auxin vectors. On the other hand, *abcb* mutants exhibit reduced long-distance auxin transport and defects in cell/plant size and shape, but have only minor defects in embryogenesis and organogenesis (Noh et al., 2001; Geisler et al., 2003; Blakeslee et al., 2007). Mutations in AUX1/LAX permeases do not contribute to any significant reductions in plant size or morphology (Bainbridge et al., 2008).

To better understand the contribution of ABCB1 and ABCB19 to long distance auxin transport, *aux1/lax*, *pin* and *abcb* mutants were analyzed for defects in auxin transport in inflorescence stems using an assay similar to those conducted in pea stems (Beveridge, 2000; Morris et al., 2005). Phenotypic variations in *abcb1* and *abcb19* mutants related to light levels and ecotypic background have been reported in the literature (Noh et al., 2001; Geisler et al., 2003; Blakeslee et al., 2007; Yang et al., 2013; Zhao et al., 2013). Here, these have been evaluated in terms of proposed ABCB function in auxin transport. Finally, the contributions of additional candidate *ABCB* transporters is assessed with physiological and phenotypic analyses in stems, leaves and flowers from single and higher order mutants.

Results

ABCB1 and ABCB19 function by excluding auxin from the shoot apex in inflorescences

To further investigate the roles of the primary auxin transporters in inflorescence stems, *aux1lax1lax2lax3* (Bainbridge et al., 2008), *pin1* (*pin1-7*), *pin3* (*pin3-4*), and *abcb1abcb19* (*abcb1-1abcb19-1* in Col-0) for altered rootward transport (Fig. 4.1). A 0.2 μ l droplet of 10 μ M 3 H-IAA was applied to the shoot apex of intact inflorescence stems. After the time points indicated, stems were cut into 2.5 mm segments starting 5 mm from the apex, then segments were measured for radioactivity. In Col-0 inflorescences rootward auxin transport occurs in a pulse (Fig. 4.1 A), similar to what is observed in seedlings (Peer et al., 2014). In *aux1lax1lax2lax3* and *pin1* the initial amount of 3 H-IAA loaded into the system was reduced by ~36% and ~22% (Fig. 4.1 B and C), respectively, while no difference in loading was observed in *pin3* or *abcb1abcb19* (Fig. 4.1 D and E). After 4 hours, however, the total amount of 3 H-IAA within *aux1lax1lax2lax3* inflorescences was 25% more than the wild type. In *aux1lax1lax2lax3* the majority of the IAA remained in the very upper portion of the inflorescence and the rate of rootward auxin transport that was able to enter the long-distance stream was slightly reduced (Fig. 4.1 B). No difference in the rate of transport was observed in *pin1* or *pin3* (Fig. 4.1 C and D). Loss of PIN3 resulted spreading of the 3 H-IAA peak presumably due to leakage of from the rootward stream (Fig. 4.1 D). This supports a role for PIN3 in restricting auxin to within the vasculature in mature tissues as well as in seedlings (Friml et al., 2002). In *abcb1abcb19* the majority of 3 H-IAA pooled in the upper inflorescence and

very little was loaded into the rootward stream. As a result the rootward pulse of auxin could not be detected. Treatment with the auxin transport inhibitor N-1-naphthylphthalamic acid (NPA) resulted in auxin distribution similar to that observed in *abcb1abcb19* after 4 hours (Fig. 4.1 F). This indicates NPA acts on ABCB1 and ABCB19 upstream of PIN1 or PIN3. These results suggest ABCB1 and ABCB19 are the primary drivers of auxin out of the shoot apex by excluding auxin from small auxin producing cells in the inflorescence apex, which is consistent with their role in seedlings (Jenness, et. al., in review).

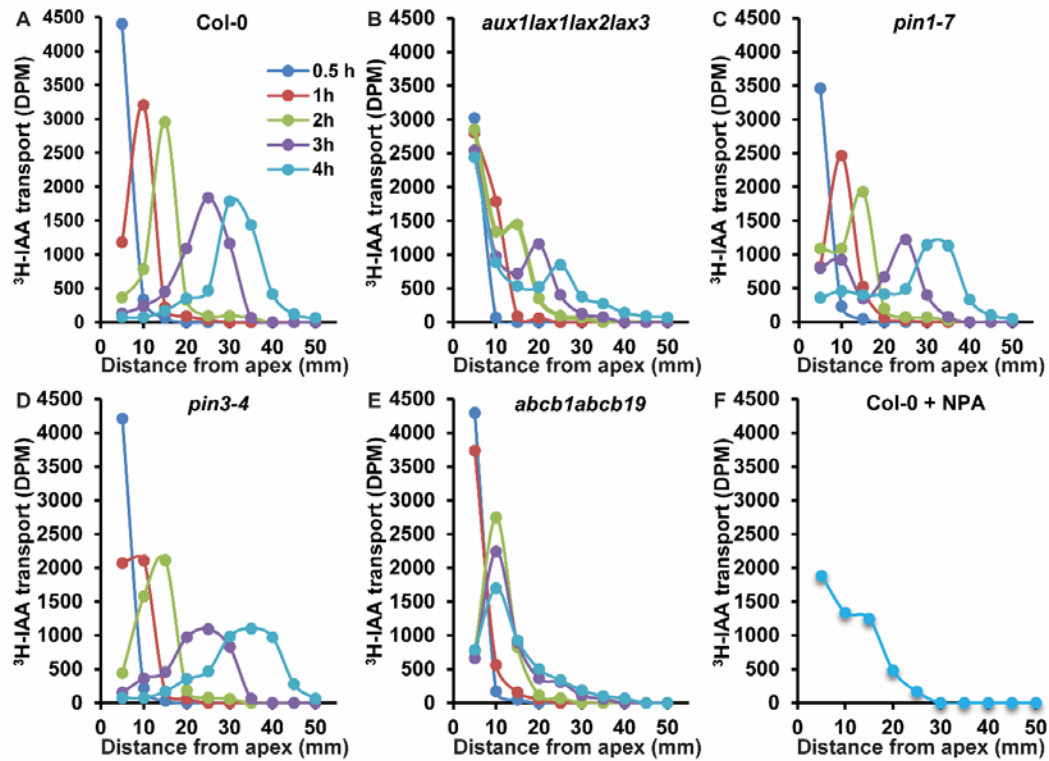


Figure 4.1. ABCB1 and ABCB19 exclude auxin out of the shoot apex in inflorescences. Rootward transport of ³H-IAA placed at the shoot apex with intact inflorescence stems of four week old plants. Data shown are means (n = 3 pools of 5).

Light dependent phenotypes in *abcb1* and *abcb19* mutants

Several reports have analyzed phenotypes of *abcb1* and *abcb19* (Noh et al., 2001; Yang et al., 2013; Zhao et al., 2013), however, differences in ecotypic background and growth conditions make phenotypic comparisons and assessments difficult. To investigate how light intensity affects the phenotypes of *abcb1* (*abcb1-100*), *abcb19* (*mdr1-101*) and *abcb1abcb19* (*abcb1-100mdr1-101*) double mutant, plants were grown under varying fluence (60, 100, and 120 $\mu\text{mol m}^{-2} \text{s}^{-1}$). In the late seedling stage, first true leaf petiole angles decrease with increasing light (Fig. 4.2 A and B). Under all light conditions *abcb19* petiole angles are greater than Col-0 and *abcb1*. Due to the leaf and petiole curling *abcb1abcb19* was not able to be measured, however, angles appeared to greater than Col-0 and *abcb1*, but less than *abcb19*. In the mid- rosette-growth stage, total rosette area increased with increased light (Fig. 4.2 C and D). Under low (60 $\mu\text{mol m}^{-2} \text{s}^{-1}$) to moderate (100 $\mu\text{mol m}^{-2} \text{s}^{-1}$) light, *abcb19* rosettes are smaller than Col-0 and *abcb1*. However, under the high light condition (120 $\mu\text{mol m}^{-2} \text{s}^{-1}$) no difference is observed between Col-0 and either single mutant. While *abcb1abcb19* rosette areas appear much smaller, total rosette area from overhead does not reflect leaf area due to the curled nature of the double mutant rosette leaves.

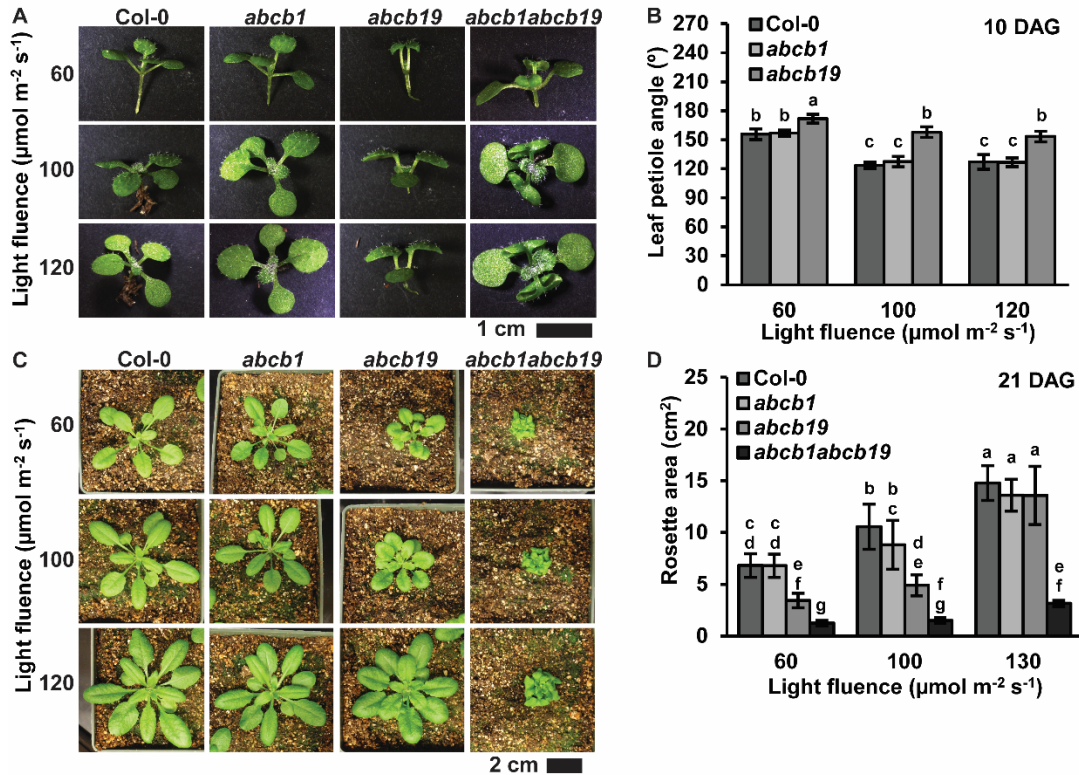


Figure 4.2. Leaf angles and areas in *abcbl* and *abcb19* mutants with varying light. (A) Images of 10 day seedlings removed from soil. Some cotyledons were removed to so true leaves could be viewed. (B) Measurement of true leaf petiole angles in 10 day plants. Data shown are means \pm SD (n = 17-20). Letters indicate statistical differences by ANOVA $p < 0.001$, Tukey's post-hoc $p < 0.05$. (C) Images of 21 day rosettes. (D) Measurement of rosette leaf area in 21 day plants. Data shown are means \pm SD (n = 10-14). Letters indicate statistical differences by ANOVA $p < 0.001$, Tukey's post-hoc $p < 0.05$.

In mature plants, inflorescence length increases with increasing light fluence in Col-0, *abcbl*, and *abcb19* (Fig. 4.3 A and B). Internode length is not different

between Col-0 and single mutants under low fluence condition (Fig. 4.3 C). Under high light *abcb1* internodes are significantly shorter than Col-0 suggesting compensation by ABCB19 does not rescue this phenotype. Single mutants show slightly reduced secondary inflorescence number under $100 \mu\text{mol m}^{-2} \text{s}^{-1}$ light but are not different from Col-0 under low or high fluence (Fig. 4.3 D). Previously *abcb19* has been shown to have more secondary inflorescences compared to Col-0 (Yang et al., 2013). However, the plants grown in this analysis were either under natural Midwestern (USA) summer sunlight or HID lights ($150 \mu\text{mol m}^{-2} \text{s}^{-1}$).

abcb1abcb19 is not different from Col-0 or the single mutants under low light but has less secondary inflorescences under mid to high light conditions. Changes in branching from the primary inflorescence are nominal and difficult to interpret (Fig. 4.3 E). Like what is observed in true leaf petiole angles, silique angles become more upright decrease with decreasing light, and is most pronounced in *abcb19* (Fig. 4.3 F). *abcb1abcb19* mutants remained unchanged for all phenotypes and light conditions analyzed. Any changes in statistical difference are due shifts in Col-0 and the single mutants.

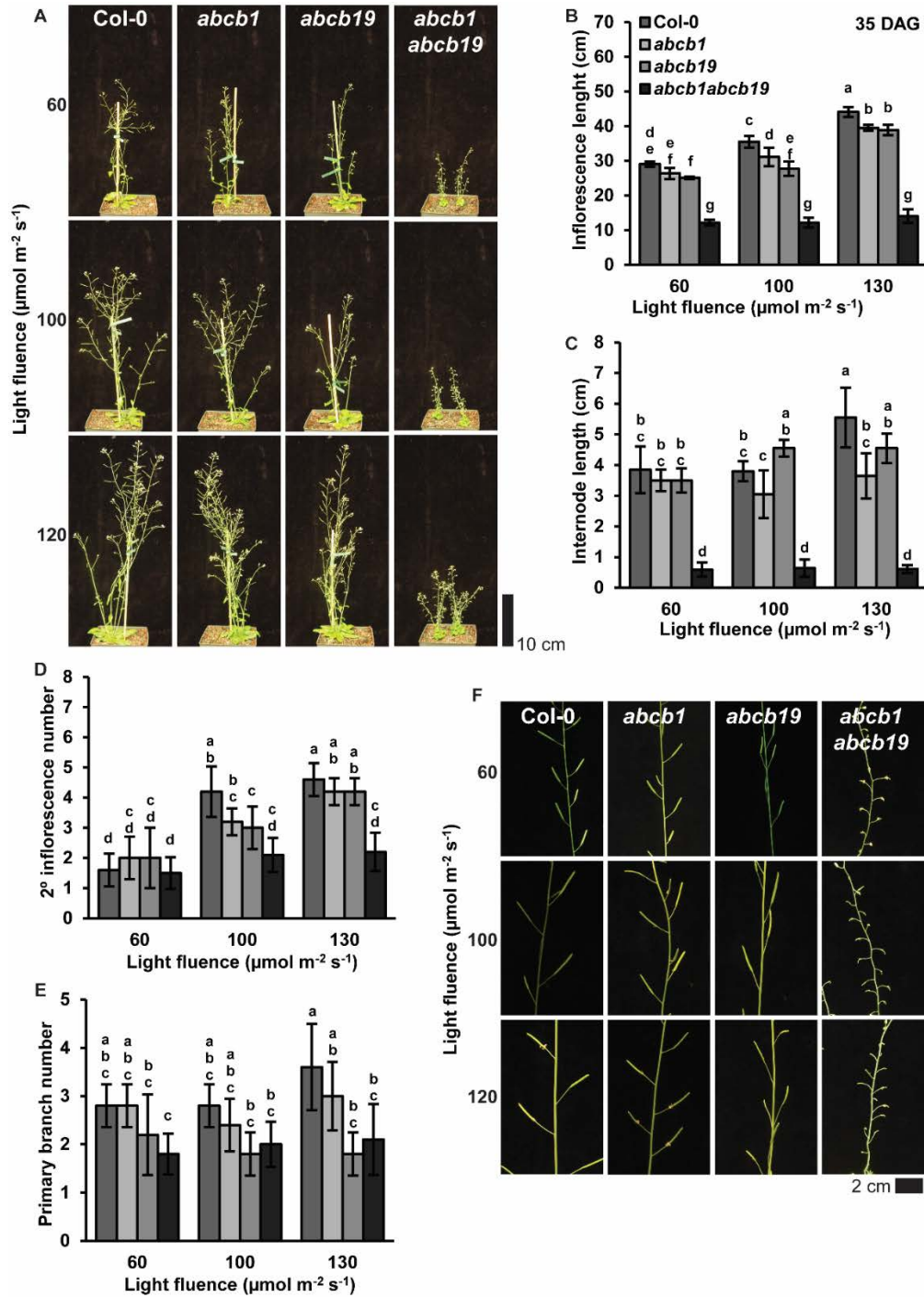


Figure 4.3. Inflorescences of *abcb1* and *abcb19* mutants with varying light. (A) Mature Col-0, *abcb1*, *abcb19*, and *abcb1abcb19* mature plants. **(B)** Measurement of inflorescence length. **(C)** Measurement of internode length. **(D)** Measurement of secondary (2°) inflorescence number. **(E)** Branching from the primary inflorescence.

(F) Inflorescences showing silique angles. Data shown are means \pm SD (n = 5-10). Letters indicate statistical differences by ANOVA $p < 0.001$, Tukey's post-hoc $p < 0.05$.

Generally the phenotypic plasticity is consistent with higher auxin biosynthesis levels with increasing light fluence. These results phenotypically reflect a primary role for *ABCB19*, with additional contribution from *ABCB1*, in regulating morphology but not organogenesis. The maize and sorghum *abcb1* mutants *brachytic2 (br2)* and *dwarf3 (dw3)* also exhibit upright leaf angles and dwarf statures (Multani et al., 2003), indicating monocots and dicots share conserved mechanisms of ABCB-mediated auxin transport.

ABCB6 mediates auxin transport in inflorescence stems

Based on phenotype, expression, and activity, *ABCB19* appears to be the primary ABCB involved in bulk movement of auxin. Proper folding and trafficking of ABCB1 and ABCB19 depend on interaction with TWD1/FKBP42. Since *twd1* mutants exhibit more severe organ twisting than *abcb1abcb19* double mutants (Fig. S4.1) it is believed other FKBP42-interacting ABCB transporters supplement the activities of ABCB1 and ABCB19. To identify other ABCB transport that could supplement their activities in inflorescence stems expression by quantitative real-time PCR (qRT-PCR) was performed and in the TRAvA RNAseq database was analyzed. qRT-PCR was performed using the apical 0-2 cm of ~15 cm Col-0 inflorescences. Expression by qRT-PCR are comparable to RNA-seq data. Expression of *ABCB19* is

10-fold higher than ABCB1 (Fig. 4.4 A). *ABCB12* expression levels are near that of *ABCB1*. This explains the reduction in rootward transport in *abcb12* stems observed in Kaneda et al., (2011). Recent evidence that the C-terminus of ABCB11/12 interacts with FKBP42/TWD1 (Jenness et al., in preparation) suggests loss of *ABCB12* may contribute to the *twd1* phenotypes. The only other transporter expressed to detectable levels are *ABCB6* and *ABCB13*. Since the *ABCB13* paralog, *ABCB14*, exhibits specificity for malate over auxin it was assumed *ABCB13* would act in a similar manner.



Figure S4.1. Comparison of *abcb1abcb19* and *twd1*.

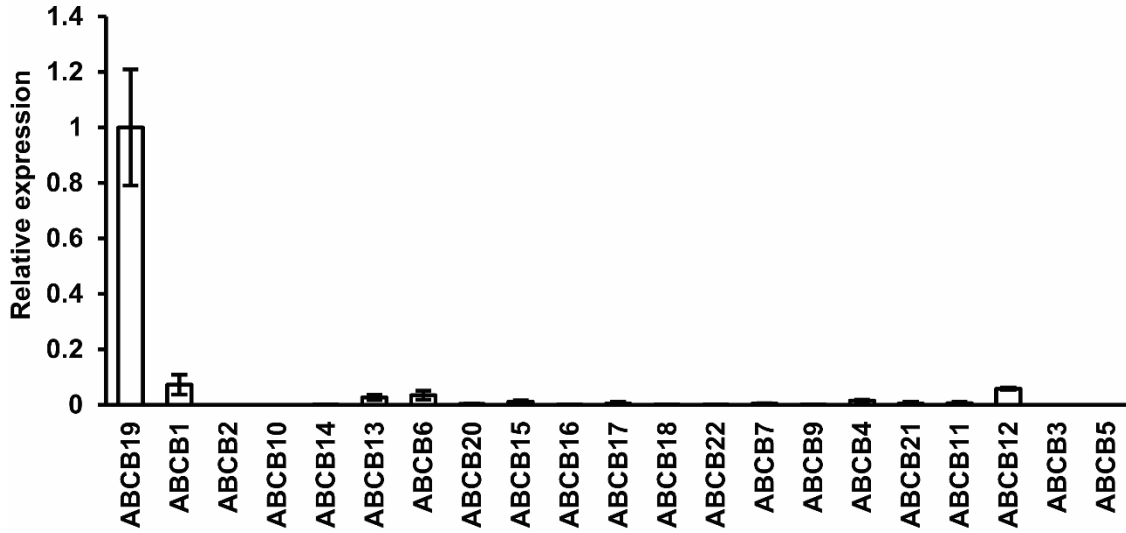


Figure 4.4. *ABCB* transporter expression in inflorescence stems. qRT-PCR of ABCBs from the top 0-2 cm of ~15 cm Col-0 inflorescence stems (n = 3).

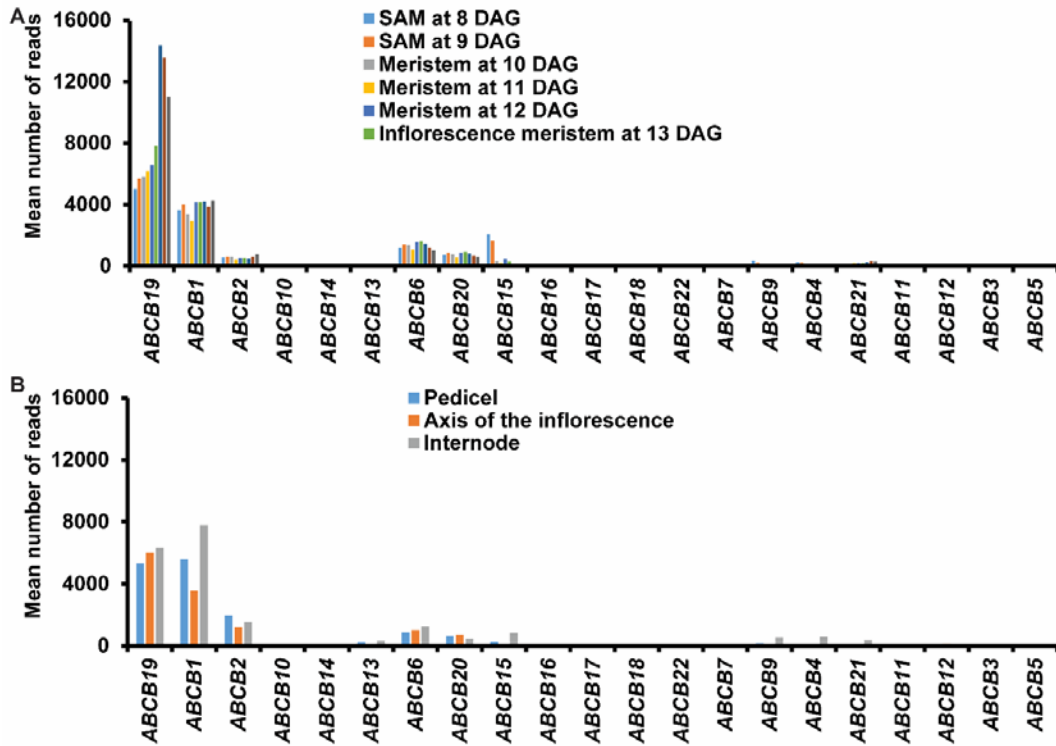


Figure S4.2. *ABCB* transporter expression in inflorescence stems from the TraVA RNA-seq database.

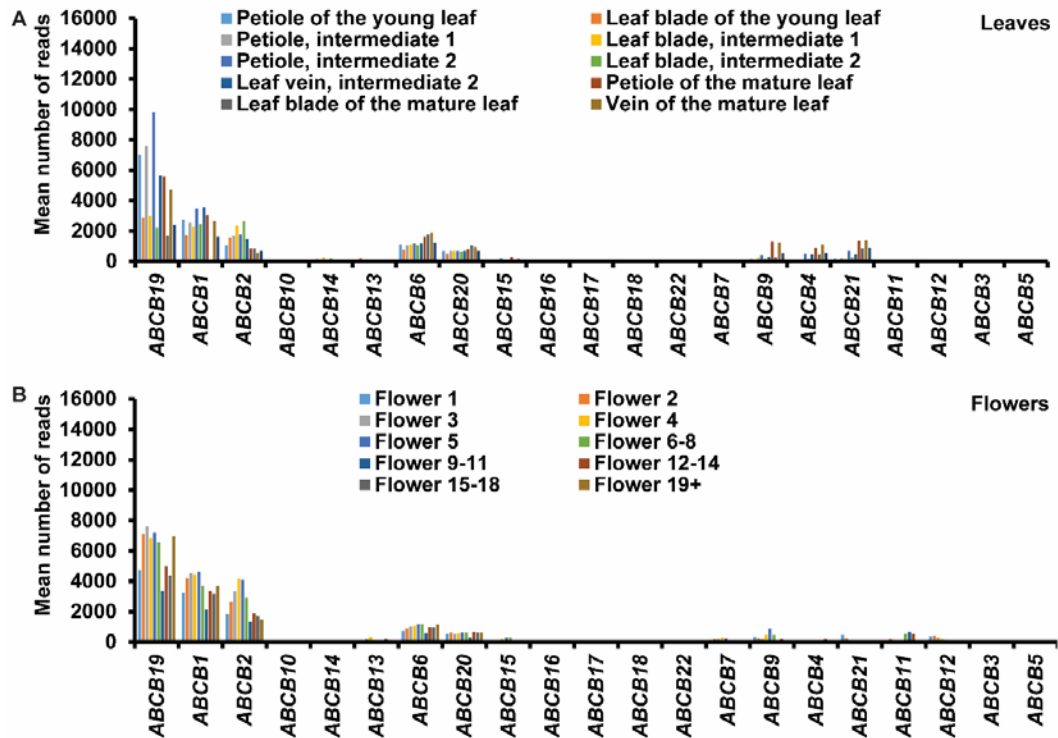


Figure S4.3. ABCB transporter expression in leaves and flowers from the TraVA RNA-seq database.

Rootward auxin transport is not altered in *abcb6* seedlings (Jenness et al., in preparation). However, since it is expressed in inflorescence stems (Fig. 4.4, Fig. S4.2 A and B) *abcb6* (Sail_7_C04.v1) mutants were tested for reduced auxin transport. Due to previous reports (Kaneda et al., 2011), *abcb11* (*abcb11-1*) and *abcb14* (*abcb14-1*) were also included. Additionally *abcb1* (*abcb1-1* in Col-0), *abcb19* (*abcb19-1* in Col-0), and *pin1* (*pin1-7*) were included as controls. Assays were conducted as in Kaneda et al. (2011) with some modifications. Apical 2 cm inflorescence segments were placed inverted (or upright) in ^3H -IAA solution for 1

hour, then washed and incubated in blank buffer for an additional 12 hours. The distal 2 mm were then collected and measured for radioactivity. In the apical 2 cm segments of *abcb6*, *abcb19* and *pin1* auxin transport is reduced by ~16% ~52%, and ~28%, respectively (Fig. 4.5 A). In the 4-6 cm segments, transport is reduced in *abcb19* and *pin1* by ~15% and ~32% (Fig. 4.5 A). No differences are observed when stems were placed in upright in the ^3H -IAA (Fig. 4.5 B).

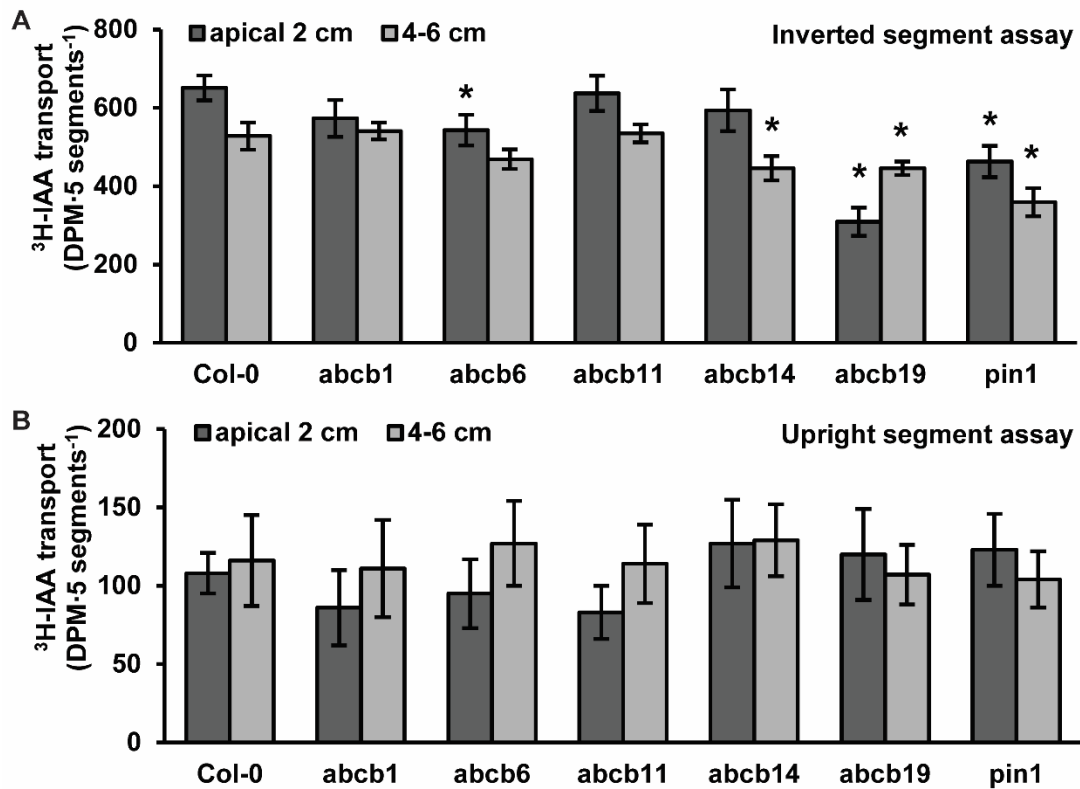


Figure 4.5. Auxin transport in inflorescence segments. (A) Inverted segment assays. **(B)** Upright segment assays. Data shown are means \pm SD ($n = 3$ pools of 5 segments). * indicate statistical difference by ANOVA $p < 0.001$, Dunnett's post-hoc $p < 0.05$.

These results support a role for *ABCB6* in mediating rootward auxin transport in inflorescence stems, but only in the apical region. Although *abcb14* did exhibit reduced auxin transport, this has been shown to be due to distorted vascular development (Kaneda et al., 2011).

Analysis of ABCB11 and ABCB21 in aerial tissues

abcb11 was previously reported to have reduced auxin transport in inflorescence stems (Kaneda et al., 2011), however, no difference in auxin transport was observed here (Fig. 4.5 A). Investigation of the mutant used in the previous study indicate the allele was actually an *abcb12* (Salk_094249) insertion line. Differences in expression between *proABCB11:GUS* constructs used in Kaneda et al. (2011) and Jenness et al. (in preparation) in seedlings were also observed. Using the promoter construct from Jenness et al., no *proABCB11:GUS* expression was detected in the upper 3-4 cm of the inflorescence (Fig. 4.6 A). This is also different from the previous report, but is supported by qRT-PCR and RNA-seq data (Fig. 4.4 A, Fig. S4.2 A and B). *proABCB11:GUS* expression was not observed in mature rosette leaves or mature flowers (Fig. 4.6 B and C) but some expression could be detected in young, unopened flowers (Fig. 4.6 C inset). *ABCB21* was recently identified as an auxin transporter that maintains the rootward auxin transport stream by regulating auxin levels in the root pericycle (Kamimoto et al., 2012, Jenness et al., in preparation). In mature plants, *proABCB21:GUS* is expressed in the abscission zone of rosette leaves, cauline leaves, and sepals (Fig. 4.5 D-F), and associated with the midvein of rosette leaves (Fig. 4.5 G). During *GUS* staining it was noted that *proABCB21:GUS* expression is observed where inflorescences were cut off.

Wounding of inflorescence stems with a razor blade induced expression in *proABCB21:GUS* that is not observed in Col-0 or *DR5:GUS* stems (Fig S4.4).

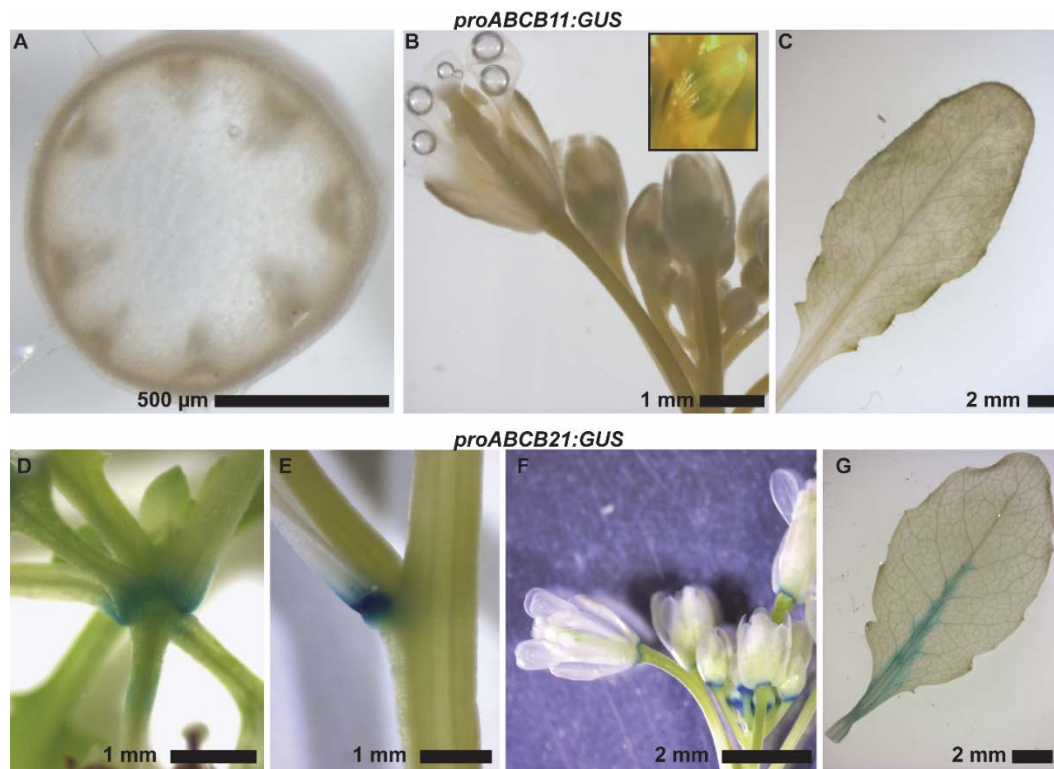


Figure 4.6. Expression of *ABCB11* and *ABCB21*. (A-C) *proABCB11:GUS* expression in (A) hand sections of the upper 3-4 cm of the inflorescence stem, (B) flowers, and (C) mature rosette leaves. (B, inset) *proABCB11:GUS* expression in young unopened flowers. (D-G) *proABCB21:GUS* expression in (D) rosette leaf-stem junctions, (E) cauline leaf-stem junctions, (F) sepal-receptacle junctions, and (G) rosette leaves.

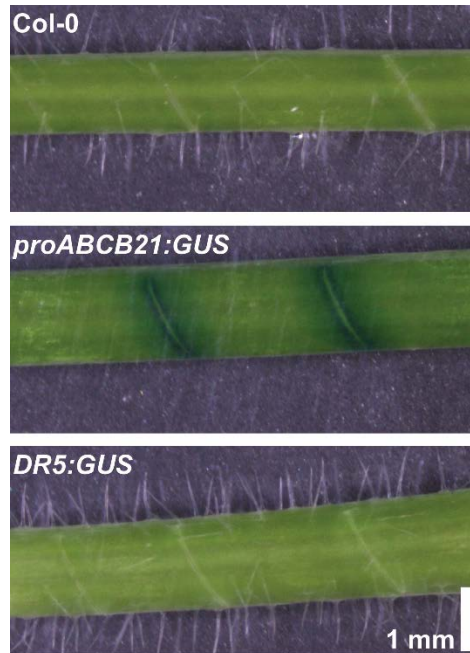


Figure S4.4. proABCB21:GUS is expressed after wounding.

Single *abcb11* and *abcb21* mutants have no obvious phenotypic differences in mature plants. This is not surprising as expression of *ABCB11* and *ABCB21* are quite low in nearly all tissues (Fig. 4.4 A, Fig. S4.2 A and B, Fig. S4.3 A) with the exception of *ABCB21* in leaves and leaf junctions (Fig. 4.6 D-G, Fig. S4.3 A). Therefore, *abcb21* (*abcb21-2*) mutants were analyzed for defects in auxin transport in rosette leaves. *abcb1* (*abcb1-1* in Col-0), *abcb19* (*abcb19-101*) and *abcb4* (*abcb4-1*) were also included. For transport along the tip-petiole axis, ^3H -IAA soaked agarose beads were placed on the leaf tips. After 3 hours, petioles or 0.5 mm mid-leaf punches were collected and measured for radioactivity. For centro-lateral transport, ^3H -IAA soaked agarose beads were placed on the leaf midvein. After 3 hours, 0.5 mm punches were collected from the leaf margin and measured for radioactivity. Transport of ^3H -IAA from the tip to the mid-leaf and petiole was significantly

reduced in *abcb19* (Fig. 4.7 A and B). In contrast, *abcb21* showed a significant decrease in transport of ^3H -IAA from the midvein to the margin (Fig. 4.7 C).

Consistent with these results, IAA levels are significantly reduced near the midvein of *abcb19* (Fig. 4.7 E). IAA levels along the margin are reduced by ~30% in *abcb19* and *abcb21* but is not statistically different from Col-0. Quantification of IAA levels in whole *abcb21* leaves reveals a slight increase in young leaves and a slight decrease in mature leaves (Fig. 4.7 F).

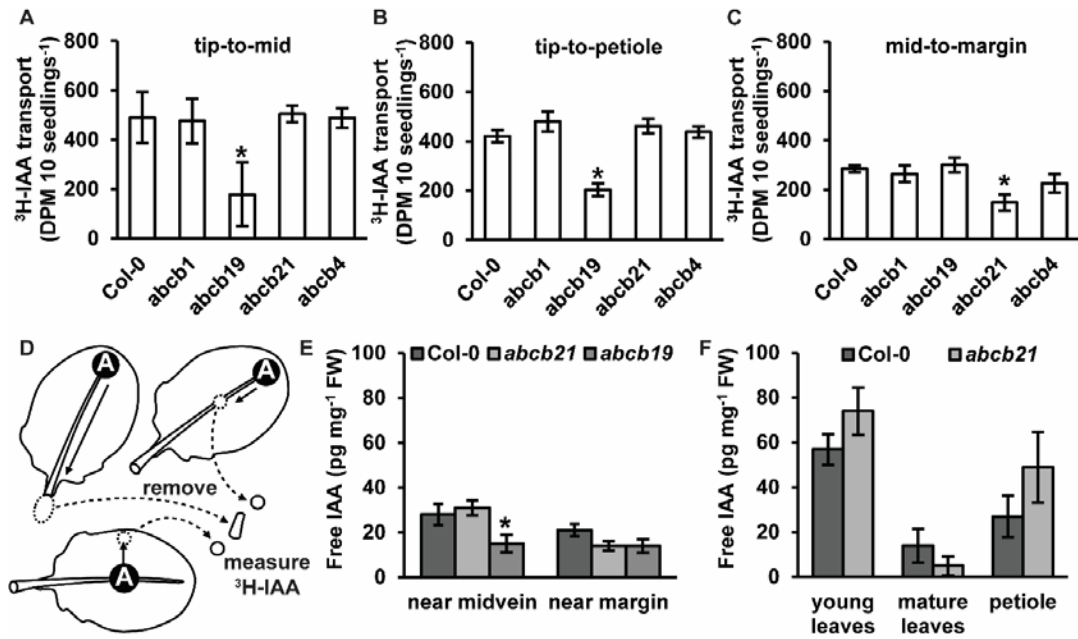


Figure 4.7. Expression of *ABCB21* and activity in leaves. (A-C) Auxin transport assays in rosette leaves. (A) Transport of ³H-IAA from the leaf tip to the leaf midpoint. (B) Transport of ³H-IAA from the leaf tip to the petiole. (C) Transport of ³H-IAA from the leaf midvein to the margin. Data shown are means ± SD (n = 3 pools of 10). * indicates statistical difference by ANOVA p < 0.001, Dunnett’s post-hoc p < 0.05. (D) Schematic showing areas of ³H-IAA placement and tissue collection in A-C. Black circles with “A” represent positions of auxin application. Dotted lines represent positions of tissue collection. (E) Free IAA levels in rosette leaves near the midvein and near the margin. (F) Free IAA levels in young leaves, mature leaves, and petioles. Data shown are means ± SD (n = 3 pools of 10). * indicates statistical difference by ANOVA p < 0.001, Dunnett’s post-hoc p < 0.05.

Interestingly, IAA levels in petioles are also elevated (Fig. 4.7 F). *abcb21* mutants were recently shown to be defective in transport of auxin from the cotyledons

to the hypocotyl (Jenness et. al., in preparation). Backup of auxin in the petioles suggests *abcb21* is also defective in transport auxin from the petiole into the stem. This supports a conserved role for *ABCB21* in mediating auxin transport between organ junctions.

Analysis of abcb11 and abcb21 triple mutants

It was hypothesized that loss of *abcb11* or *abcb21* in addition to *abcb1* and *abcb19* would reveal phenotypes not observed in the single mutants and may produce the more severe phenotypes observed in *twd1* mutants compared to *abcb1abcb19*. Crosses of *abcb11* (*abcb11-1*) and *abcb21* (*abcb21-1*) with *abcb1abcb19* were analyzed. Adaxial and abaxial epidermal cells of *twd1* leaves are significantly smaller than those of the wild type (Pérez-Pérez et al., 2002). The leaves of both *twd1* and *abcb1abcb19* develop small rosettes and more rounded, abaxially curling leaves than wild type (Fig. 4.8 A). Careful examination of leaf development revealed no defects in basic abaxial/adaxial definition, venation, or leaf margin development in *twd1* or single, double, or triple *abcb* mutants. However, in *twd1* and all higher order *abcb* mutants examined, the aberrant leaf phenotypes reflected irregular patterns of epidermal cell expansion that became more exaggerated over time, particularly on the abaxial surface.

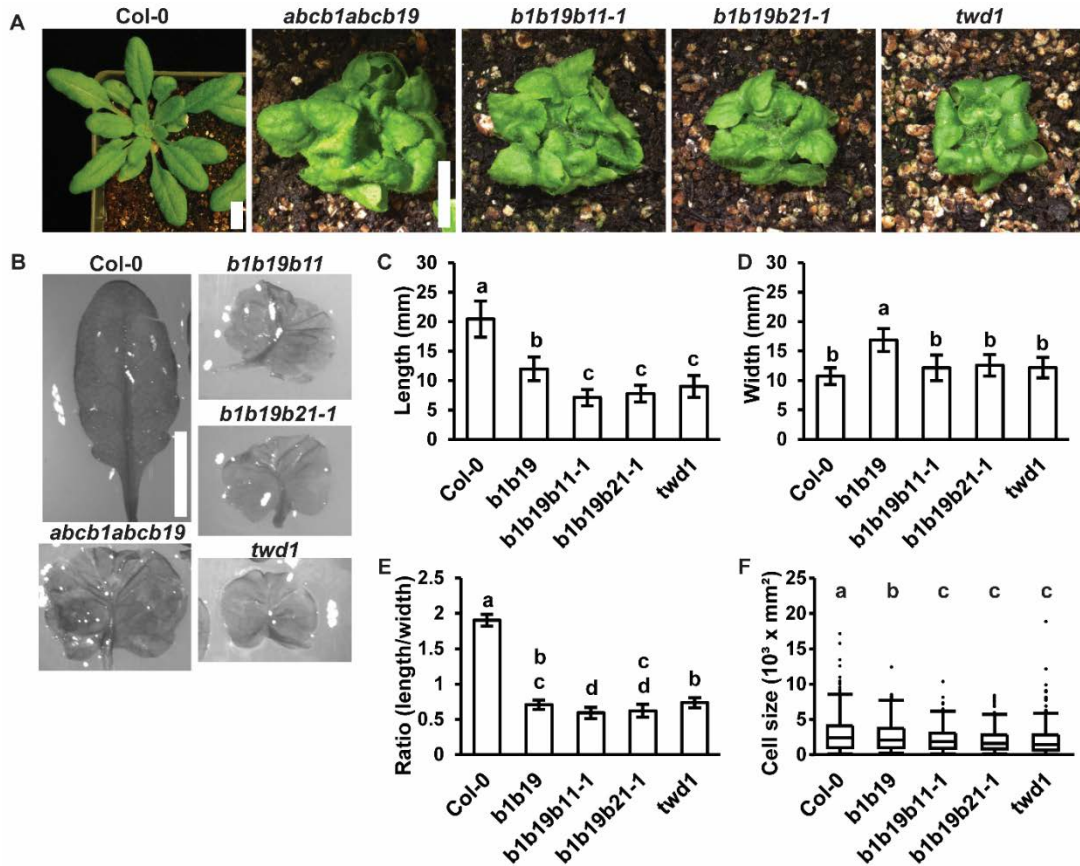


Figure 4.8. ABCB triple mutant leaf phenotypes. (A) Representative images of 4 week rosettes. (B) 5th rosette leaf removed from A. Leaves were soaked in ethanol to allow curled leaves to lay flat. (C-E) Measurement of (C) length, (D) width, and (E) length/width ratio in leaves from B. Data shown are means \pm SD ($n > 10$). Letters indicate statistical difference by ANOVA $p < 0.001$, Tukey's post-hoc $p < 0.05$. (F) Boxplot of showing 5th leaf cell size. Data shown are means \pm SD ($n > 219$ from at least 3 leaves per line). Letters indicate statistical difference by ANOVA $p < 0.001$, Tukey's post-hoc $p < 0.05$.

The leaf phenotypes of *twd1* cannot be unequivocally attributed to auxin action alone, as FKBP42 has been shown to interact with the BRI1 brassinosteroid

(BR) receptor (Wang et al., 2013; Chaiwanon et al., 2016; Zhao et al., 2016). BR treatment of *twd1-3* had no effect on leaf cell size, but did very slightly increase the size of leaves in *abcb1abcb19* and the triple mutants. However, these size differences disappeared before inflorescence bolting occurred, and BR treatment did not reduce the extent of leaf curling and differential epidermal cell sizing in the higher order *abcb* mutants.

Further examination revealed *abcb1abcb19* rosette leaf length is ~60% of Col-0 (Fig. 4.8 B and C). *b1b19b11*, *b1b19b21*, and *twd1* leaves are ~35%, ~38%, and ~44% of Col-0, respectively. *twd1-3* leaves are shorter than *abcb1abcb19* but slightly longer than the triple mutants. Rosette leaves of *abcb1abcb19* are significantly wider than Col-0, *twd1*, and triple mutants (Fig. 4.8 D). The triple mutants and *twd1* appear slightly wider than Col-0 but are not statistically different. Taken these measurements together, all mutants analyzed have a dramatically reduced length-to-width ratios compared to Col-0, with the triple mutants having a slightly greater effect than *abcb1abcb19* and *twd1* (Fig. 4.8 E). These differences can be attributed to differential cell expansion as loss of additional ABCB transporters results in progressively decreasing pavement cell size (Fig. 4.8F). Abaxial epidermal cells were measured at a midpoint from the leaf tip to the petiole and half way from the leaf margin to the center. All mutants showed a significant reduction in cell size compared to Col-0. Cell size in *b1b19b11* and *b1b19b21* are significantly smaller than Col-0 or *abcb1abcb19* but are not different from *twd1*. This indicates loss of *abcb11* and *abcb21* in addition to *abcb1* and *abcb19* does cause a more *twd1*-like leaf morphology.

Overall, inflorescences of *b1b19b11* and *b1b19b21* phenotypically resembled *abcb1abcb19* (Fig. 4.9 A). Due to the severe delay in bolting and flowering *twd1* was not analyzed. Inflorescence height is reduced >40% in *abcb1abcb19* and triple mutants (Fig. 4.9 B). Both triple mutants developed significantly more pedicels per centimeter compared to Col-0, but less than that observed in *abcb1abcb19* (Fig. 4.9 C). An apparent shift in pedicel phyllotaxis was observed in mature *abcb1abcb19* and triple mutants from the golden angle 137.5° (Fig. 4.9 C). The mean divergence angle between consecutive pedicels was quantified using previously described methods (Peaucelle et al., 2007). The distribution of divergence angles in Col-0 centers on a mean of 146° (Fig. 4.9 D), which is consistent with previous reports (Peaucelle et al., 2007). *abcb1abcb19*, *b1b19b11* and *b1b19b21* had mean angles of 129, 140, and 146 degrees, respectively (Fig. 4.9 D). Although the mean angle of deflection in the triple mutants is similar to Col-0, the distribution is much more irregular and the frequency of large and small angles is greater. Closer examination revealed that pedicel positioning was not actually altered in the double and triple mutants. Instead, the apparent change in angle is due to altered cell expansion at the stem-pedicel junctions. The recently characterized *abcb19* allele, *abcb19-5*, exhibits pedicel-inflorescence separation defects that appear to be linked to the mis-regulation of the auxin-responsive gene CUP-SHAPED COTYLEDON2 (*CUC2*), resulting from alterations in auxin distribution at the pedicel-inflorescence boundary (Zhao et al., 2013). However, since *abcb19-5* was also shown to produce a partial transcript and organ-separation phenotypes have not been observed in any other *abcb19* allele, these phenotypes may be the result of interference with other ABCB transporters.

abcb1abcb19, *b1b19b11*, and *b1b19b21* all exhibit abnormal tissue growth at the pedicel-inflorescence junctions (Fig. 4.9 E). Hand sectioning and Toluidine Blue O (TBO) staining of the pedicel-inflorescence junctions reveal separation defects reminiscent of those observed in *abcb19-5*. Additionally, epidermal swelling was observed in all double and triple mutants below the pedicel-inflorescence junction. This tissue swelling can be attributed to leakage of auxin from the vasculature and pooling at the pedicel junctions. In some cases this was enough to generate ectopic vasculature tissue (Fig. 4.9 F), a PIN mediated auxin canalization response.

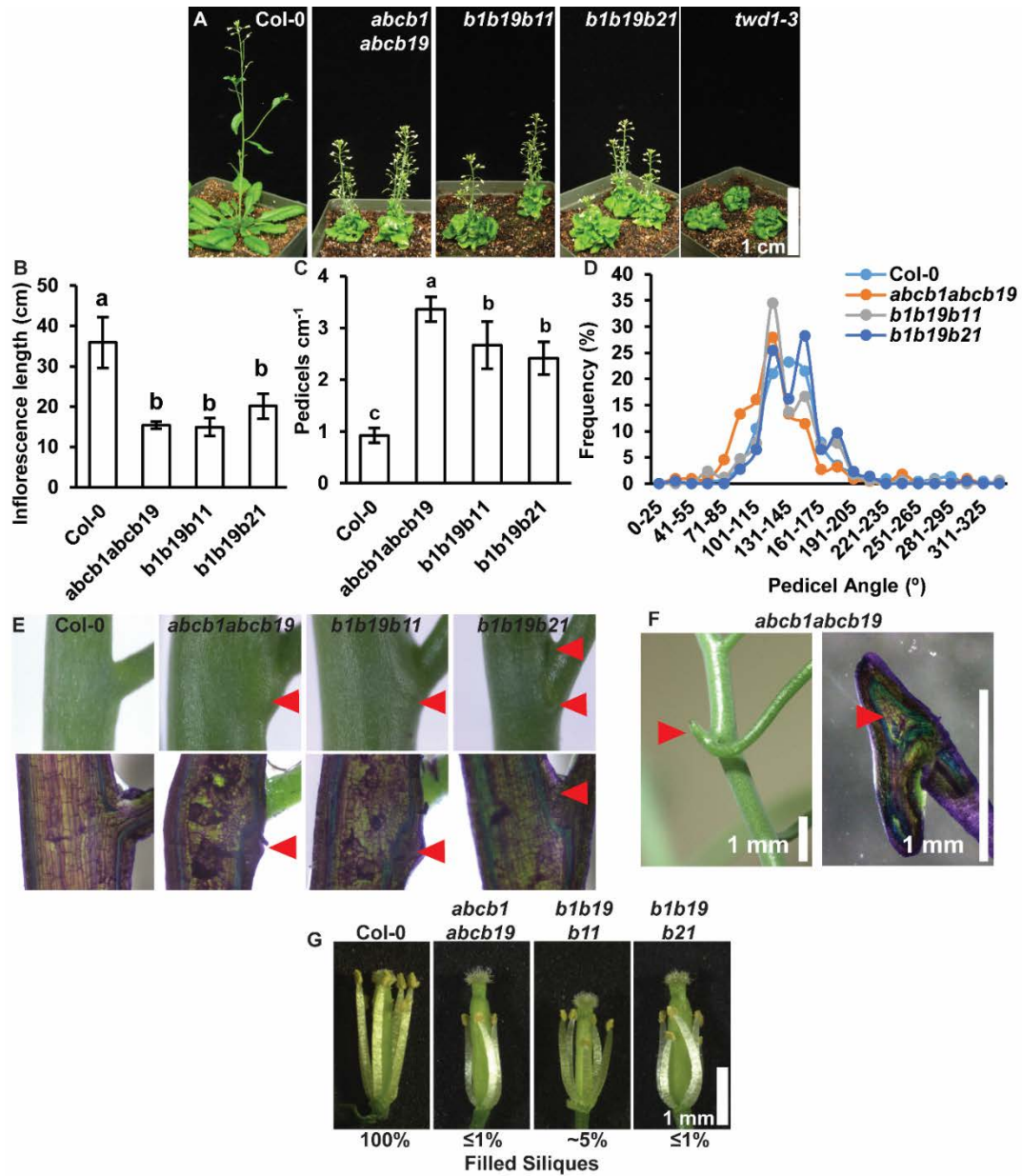


Figure 4.9. Triple mutant inflorescence phenotypes. (A) Representative images of 5 week old plants. (B) Mature primary inflorescence height. Data shown are means \pm SD (n = 5-8). Letters indicate statistical difference by ANOVA $p < 0.001$, Tukey's post-hoc $p < 0.05$. (C) Pedicel density of mature primary inflorescences. Data shown are means \pm SD (n = 5-8). Letters indicate statistical difference by ANOVA $p < 0.001$, Tukey's post-hoc $p < 0.05$. (D) Distribution of divergence angles between

consecutive pedicels. **(E)** Representative images of aberrant pedicel-stem junctions (red arrows). Lower panel shows hand-sectioned pedicel-stem junctions stained with toluidine blue O (TBO). **(F)** Ectopic vascular tissue formation at pedicel-stem junctions. **(G)** Post-anthesis flowers with petals removed to show pistil.

Single mutants *abcb1abcb19* mutants exhibit poor fertility because the anther filaments do not elongate enough to allow for self-fertilization (Fig. 4.8 B) (Noh et al., 2001; Cecchetti et al., 2015). Triple *abcb1abcb19abcb11* mutant had a noticeable increase in the amount of filled siliques of non-hand-pollinated plants. Intact *abcb1abcb19abcb11* flowers resemble flowers of *abcb1abcb19*, with petals that fail to open completely (Fig. S4.5). Removal of the flower petals revealed *abcb1abcb19abcb11* have shorter pistils which lead to partial recovery of the self-pollination defect (Fig. 4.9 G). Triple *abcb11* mutants have ~5% filled siliques, while *abcb1abcb19* mutants have $\leq 1\%$. The shortened pistils of *abcb11* triple mutants resemble wild-type NPA-treated gynoecia (Nemhauser et al., 2000) and lacked the developmental defects observed in auxin biosynthesis (*yuc1/yuc4*), transport (*pin/pid*) or signaling (*ett-3*) mutants (Hawkins and Liu, 2014). Like *abcb1abcb19* double mutants, all hand-pollinated triple mutants produced viable, normal looking seed. These results suggest *ABC11* is involved in pistil elongation, however transporters that are expressed to higher levels like *ABC6* and *ABC20* are predicted to play a greater role.

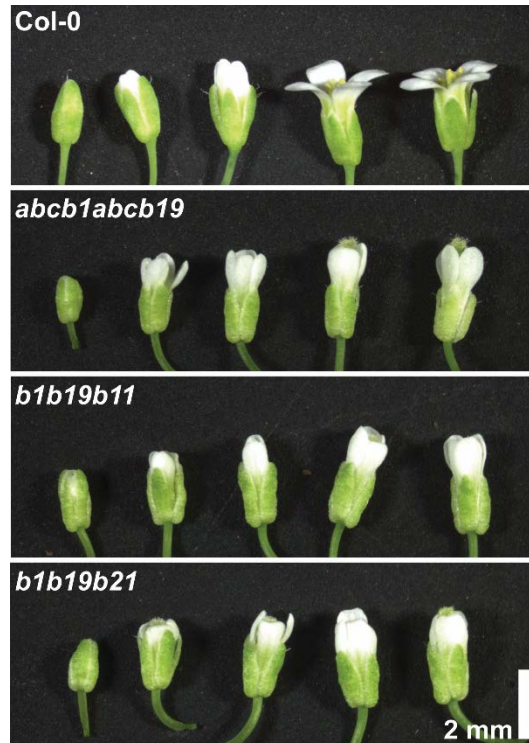


Figure S4.5. Intact triple mutant flowers.

Discussion

The results presented herein support a primary function of ABCB auxin transporters in excluding this hydrophobic anion from small cells at points of efflux. In seedlings, ABCB1 and 19 exclude auxin from small cells in the shoot apex. This activity is conserved in mature tissues as loss of ABCB1 and 19 caused a pooling of auxin in the most apical region of the inflorescence (Fig. 4.1). Since no developmental defects are observed in *abcb1abcb19* mutants (Fig. 4.2, Fig. 4.3) this supports a role for these ABCBs in exclusion of auxin from the apical region and bulk loading of auxin into the rootward stream.

Based on the phenotypic severity of *abcb19* mutants (Fig. 4.2, Fig. 4.3), high levels of *ABCB19* expression (Fig. 4.4, Fig. S4.2, Fig. S4.3), and lack of compensation by *ABCB1* (Jenness et al., in preparation, Blakeslee et al., 2007), it must be concluded that *ABCB19* is the predominant ABCB auxin transporter in *Arabidopsis*. Contributions from *ABCB1* to auxin transport are reflected in the *abcb1abcb19* double mutant, however, further reductions in auxin transport and the increase in phenotypic severity of *fkbp42/twd1* suggests other ABCB transporters may provide supplementary roles to *ABCB19*. Association of FKBP42 with ACT7, BRI1, and MRP1/2 (Geisler et al., 2004; Chaiwanon et al., 2016; Mao et al., 2016) suggests some of these phenotypes may not be tied directly to auxin or ABCB transporters.

In inflorescence stems, *abcb6* and *abcb12* mutants exhibit reduced auxin transport (Fig. 4.5 A) (Kaneda et al., 2011). This suggests that inflorescence twisting observed in *twd1* is likely additive effects of loss of *ABCB1*, 19, 6 and 12. A preliminary screen of *abcb1abcb19abcb6* triple mutants revealed an increased in silique twisting. No difference in auxin transport was observed in *abcb11* stems and *ABCB11* expression in inflorescence stems could not be detected by qRT-PCR, *proABCB11:GUS*, or RNA-seq (Fig. 4.4, Fig. 4.6 A-C, Fig. S4.2). *ABCB21* expression is strongest in leaves and at leaf-stem junctions (Fig. 4.6 D-G). Analysis of auxin transport in leaves shows that *ABCB21* mediates auxin transport outward from the midvein to the margins (Fig. 4.7), although no differences in leaf size were noticed. *ABCB21* expression at organ junctions or a sites of wounding is consistent

with a role in mediating auxin transport at programmed or induced attachment/breakage points.

abcb11 and *abcb21* showed no observable phenotypic differences in mature plants. However, *abcb21* exhibits auxin transport defects in leaves, and ABCB11 has shown the capacity to transport auxin in yeast (Jenness et. al., in preparation). Therefore, triple mutants were generated to see if loss of *abcb11* or *abcb21* in addition to *abcb1* and *abcb19* could lead to a more *twd1* like phenotype. Although, no difference in inflorescence height was observed, triple mutants did have leaves did become more *twd1*-like (Fig. 4.8). Additionally, *abcb1abcb19abcb11* exhibited a short pistil phenotype that lead to partial recovery of the fertilization defects observed *abcb1abcb19*. From the RNA-seq data and *proABCB11:GUS*, the only tissue where ABCB11 shows any expression is in flowers (Fig. 4.6 B, Fig. S4.3).

Overall these these results further establish ABCB19 as the primary ABCB auxin transporter. While, ABCB1, 6, 11, and 21 do mediate auxin transport, their contributions to long distance transport are relatively minor. Instead, increased tissue specific expression point to more discrete roles. Interestingly ABCB21, like ABCB1 and 19, has also been reported to reside in ordered membrane nanodomains (Demir et al., 2013). In silico docking of IAA with ABCB21 shows IAA binding positions and energies are equivalent to that of ABCB19. This further suggests direct links between auxin transporter activity and specificity and how transporters and auxin interact within the local membrane environment.

Materials and Methods

Plant growth conditions. All plants were grown under long-day conditions (16h:8h light:dark cycles) with $100 \mu\text{mol m}^{-2} \text{s}^{-1}$ light (unless otherwise specified) at 22°C for times specified.

Auxin transport assays. Intact inflorescences. A 0.2 nL agar droplet containing $10 \mu\text{M}$ ^3H -IAA was deposited at the shoot apex of inflorescence stems containing a single floral cluster. Plants were then incubated under $20 \mu\text{mol m}^{-2} \text{s}^{-1}$ yellow light and 55% relative humidity. After the times indicated, the top 5 cm starting 5 mm from the apex were collected. Stems were then dissected into 2.5 mm segments and individual segments were measured for radioactivity. **Inflorescence segments.**

Assays were conducted as in Kaneda et al. (2011) with some modifications. Apical 2 cm inflorescence segments were placed inverted or upright in ^3H -IAA solution for 1 hour, then washed and incubated in blank buffer for an additional 12 hours (pulse/chase). The distal 2 mm were then collected and measured for radioactivity.

Leaves. Agarose beads coated in ^3H -IAA were placed on equal size rosette leaves of ~4 week old plants at the positions indicated (Fig. 3.7 D). After bead placement plants were incubated under $20 \mu\text{mol m}^{-2} \text{s}^{-1}$ yellow light and 55% relative humidity for 3 hours. 0.5 mm punches were collected at positions indicated (Fig. 3.7 D) and measured for radioactivity.

Quantitative real-time PCR. For qRT-PCR total RNA was extracted using Trizol reagent (Invitrogen) followed by lithium chloride precipitation. Total RNA ($1.5 \mu\text{g}$) was used for first-strand synthesis using SuperScript III reverse transcriptase (Invitrogen). Real-time PCR was performed on a CFX Connect (Bio-Rad

Laboratories) using EvaGreen qPCR master mix (Biotium). Primers used are listed in Appendix C.

Histochemical staining. promoter:GUS. *proABCB11:GUS* and *proABCB21:GUS* are from Chapter 3. For GUS staining, tissues were incubated in 90% acetone for 20 mins on ice, then immersed in staining solution (50 mM sodium phosphate buffer, pH 7.0, 0.1% triton X-100, 0.5 mM potassium ferrocyanide, 0.5 mM potassium ferricyanide, and 1 mM X-gluc) and incubated in the dark at 37°C for 5-6 hours.

Stained samples were cleared with 70% ethanol before imaging. **Toluidine blue O.**

Hand-sectioned mature inflorescence stems were incubated in 0.05% toluidine blue O for ~7 minutes, rinsed briefly, then visualized.

Auxin quantifications. Free IAA quantification were conducted as described in Novák et al., 2012.

Statistical analysis. All statistical analyses were performed using SigmaStat or JMP PRO 13.

Chapter 5. Auxin transport sites are visualized in planta using fluorescent auxin analogs

Ken-ichiro Hayashi ^{a,1}, Shouichi Nakamura ^a, Shiho Fukunaga ^a, Takeshi Nishimura ^b,
Mark K. Jenness ^c, Angus S. Murphy ^c, Hiroyasu Motose ^d, Hiroshi Nozaki ^a,
Masahiko Furutani ^e, and Takashi Aoyama ^f

^a Department of Biochemistry, Okayama University of Science, Okayama 700-0005, Japan; ^b Department of Biological Sciences, Tokyo Metropolitan University, Tokyo 192-0397, Japan; ^c Department of Plant Science and Landscape Architecture, University of Maryland, College Park, MD 20742; ^d Division of Bioscience, Graduate School of Natural Science and Technology, Okayama University, Okayama 700-8530, Japan; ^e Graduate School of Biological Sciences, Nara Institute of Science and Technology, Nara 630-0192, Japan; and ^f Institute for Chemical Research, Kyoto University, Kyoto 611-0011, Japan

Author contributions: K.H., T.N., A.S.M., and H.N. designed research; K.H., S.N., S.F., **M.K.J.**, H.M., M.F., and T.A. performed research; K.H., A.S.M., H.M., M.F., and T.A. analyzed data; and K.H., S.N., **M.K.J.**, A.S.M., and T.A. wrote the paper.

¹To whom correspondence should be addressed. Email: hayashi@dbc.ous.ac.jp.

This work was published in Hayashi et al., (2014). Headings and figure numbers were changed for consistency within this dissertation. Supplementary information can be found in Appendix A.

Summary

The plant hormone auxin is a key morphogenetic signal that controls many aspects of plant growth and development. Cellular auxin levels are coordinately regulated by multiple processes, including auxin biosynthesis and the polar transport and metabolic pathways. The auxin concentration gradient determines plant organ positioning and growth responses to environmental cues. Auxin transport systems play crucial roles in the spatiotemporal regulation of the auxin gradient. This auxin gradient has been analyzed using SCF-type E3 ubiquitin-ligase complex-based auxin biosensors in synthetic auxin-responsive reporter lines. However, the contributions of auxin biosynthesis and metabolism to the auxin gradient have been largely elusive. Additionally, the available information on subcellular auxin localization is still limited.

Here we designed fluorescently labeled auxin analogs that remain active for auxin transport but are inactive for auxin signaling and metabolism. Fluorescent auxin analogs enable the selective visualization of the distribution of auxin by the auxin transport system. Together with auxin biosynthesis inhibitors and an auxin biosensor, these analogs indicated a substantial contribution of local auxin biosynthesis to the formation of auxin maxima at the root apex. Moreover, fluorescent auxin analogs mainly localized to the endoplasmic reticulum in cultured cells and roots, implying the presence of a subcellular auxin gradient in the cells. Our work not only provides a useful tool for the plant chemical biology field but also demonstrates a new strategy for imaging the distribution of small-molecule hormones.

Introduction

The plant hormone auxin plays a pivotal role in embryogenesis, vascular tissue differentiation, tropic responses to light and gravity, and the lateral branching of shoots and roots. Plants establish auxin gradients in response to light, gravity, and touch stimuli that direct tropic growth to allow plants to adapt to environmental inputs. The regulation of auxin distribution in plant tissue is coordinately determined via multiple processes involved in auxin biosynthesis, polar transport from sites of synthesis, storage as inactive precursors, and the degradation of auxin (Petrasek and Friml, 2009; Hayashi, 2012; Sauer et al., 2013). The major naturally occurring auxin, indole-3-acetic acid (IAA), is mainly biosynthesized from tryptophan by two sequential enzymatic steps involving TAA1, a tryptophan aminotransferase, and YUCCA, a flavin-monooxygenase in the indole-3-pyruvic acid (IPA) pathway (Mashiguchi et al., 2011; Won et al., 2011). Molecular genetic studies in *Arabidopsis* have demonstrated that a combination of auxin transport proteins, comprising AUX1/LAX uptake permeases, the PINFORMED (PIN) efflux carriers, and ATP-binding cassette group B (ABCB) auxin transporters, coordinately regulates auxin transport (Peer et al., 2011). These transport proteins generate auxin gradients through the expression and subcellular relocalization of transport proteins in response to environmental and developmental cues (Petrasek and Friml, 2009). These multiple complicated processes coordinately regulate intra- and intercellular auxin distribution and ultimately determine the entire architecture of a plant. Thus, analysis and visualization of auxin distribution are essential to understand plant development.

SCF-type E3 ubiquitin-ligase complex (SCF^{TIR1})-based auxin-responsive reporters, such as *DR5::GFP* and *DII-VENUS*, are widely used to monitor auxin distribution in plants (Friml et al., 2003; Brunoud et al., 2012). However, the spatiotemporal resolution of these reporter systems is limited due to the general nature of reporter protein expression and degradation. Alternatively, endogenous IAA distribution has been visualized through the direct detection of IAA molecules by means of immunostaining (Benková et al., 2003) and mass spectrometry-based IAA quantification (Petersson et al., 2009). However, these direct-detection approaches require multiple and time-consuming procedures and present an insufficient spatial resolution of the IAA distribution at the cellular level. These direct and indirect approaches have illustrated an endogenous auxin distribution profile as the final output of the local biosynthesis, inactivation, and transport of auxin.

Here we developed fluorescent auxin analogs [7-nitro-2,1,3- benzoxadiazole (NBD)-conjugated naphthalene-1-acetic acid (NAA), NBD-NAA and NBD-IAA] that can be used to generate images of auxin distribution (Fig. 5.1A). These analogs were designed to function as active auxin analogs for the auxin transport system but to be inactive for auxin signaling. The analogs would be recognized as substrates by auxin transporters and then show a distribution pattern similar to auxin. This strategy of using fluorescent auxin analogs enabled the imaging of the auxin transport site and revealed the crucial role of local auxin synthesis in the formation of auxin maxima. Furthermore, these fluorescent analogs indicated the presence of a subcellular auxin gradient in plant cells.

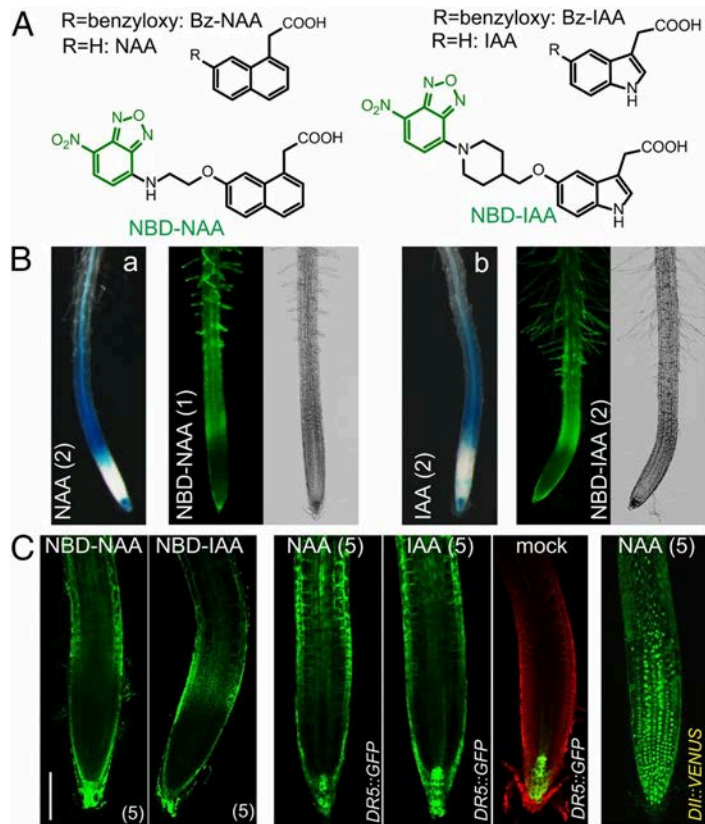


Figure 5.1. Distribution of fluorescent auxin analogs in *Arabidopsis* root. (A) Structures of the auxins NAA and IAA and their fluorescent analogs NBD-NAA and NBD-IAA. (B and C) Distribution of NBD-auxins in *Arabidopsis* roots. Six-day-old wild-type seedlings were treated with medium containing NBD-auxins for 15 min. Six-day-old *DR5::GUS* (B, a and b) and *DR5::GFP* seedlings (C) were incubated with auxins for 4 h or 6 h, respectively. Six-day-old *DII::VENUS* seedlings were treated with 10 μ M auxinole for 6 h and then incubated with NAA for 10 min. The pictures in C are confocal images. The values presented in parentheses indicate the concentration of chemicals (μ M). (Scale bar, 100 μ m.)

Results

Design and Synthesis of Fluorescently Labeled Auxin Analogs

Fluorescently labeled forms of the plant hormones gibberellin, strigolactone, and brassinosteroid were recently generated for analysis of the distribution of hormones and receptors (Bhattacharya et al., 2009; Prandi et al., 2011; Irani et al., 2012; Prandi et al., 2013; Rasmussen et al., 2013; Shani et al., 2013). These fluorescently labeled hormones were designed to retain the original hormonal activity and to activate signaling by binding to hormone receptors (Bhattacharya et al., 2009; Prandi et al., 2011; Irani et al., 2012; Prandi et al., 2013; Rasmussen et al., 2013; Shani et al., 2013). Under our strategy for design of fluorescent auxin analogs, the analogs undergo auxin transport in the same manner as native auxin molecules but are completely inactive for the signaling machinery. Auxins rapidly induce auxin-inactivating enzymes, such as *GH3*, and influence their own transport by regulating the localization of PIN proteins at the plasma membrane (Petrasek and Friml, 2009; Löffke et al., 2013). Similarly, active auxin analogs will immediately affect the localization of PIN and GH3 enzymes, and the distribution of the labeled analogs will therefore no longer reflect the native auxin gradient. According to our strategy for developing fluorescent auxin analogs, the analogs should satisfy the following criteria: First, they should be selective for auxin transporters, but not for the TIR1–Aux/IAA auxin receptor complex; and second, the overall polarity of the fluorescent auxin molecules should be as similar to that of native auxin molecules as possible. Lipophilic analogs would be free to travel across the plasma membrane and would therefore not establish a concentration gradient, thus showing a uniform distribution.

We recently reported that the alkoxy-auxin analogs Bz-IAA and Bz-NAA function as potent competitive inhibitors of the auxin transporters AUX1, PIN, and ABCBs (Fig. 5.1A) (Tsuda et al., 2011). These alkoxy-auxin analogs are inactive at auxin receptors but are recognized as auxin by auxin transporters. A structure–activity analysis revealed that auxin transporters ignore the alkoxy-chain substructure of auxin analogs (Tsuda et al., 2011). Based on our previous findings, we synthesized 5-fluorescently labeled IAAs and 7-fluorescently labeled NAAs as analogs of IAA and NAA, respectively (Fig. 5.1A, Appendix A Fig. S5.1). The artificial auxins NAA and Bz-NAA were efficiently exported by efflux transporters but were not imported by the AUX1 influx symporter, suggesting that fluorescent NAA analogs can be used to visualize efflux transport via PINs and ABCBs (Tsuda et al., 2011). The BODIPY and NBD fluorescent dyes were introduced into 5-hydroxy-IAA and 7-hydroxy-NAA using various alkyl linkers (Appendix A Fig. S5.1). Additionally, fluorescently labeled indole (NBD-indole) and benzoic acid (NBD-benzoic acid) were synthesized as negative controls to confirm the specificity of the fluorescence images of the auxin analogs (Appendix A Fig. S5.2A). The fluorescent gradient mimicking the auxin distribution should disappear when using negative control analogs if the transporters specifically recognize the auxin substructure of the fluorescent analogs. The fluorescent analogs were initially evaluated according to the fluorescence images they generated in comparison with the expression pattern of the *DR5* reporter in auxin-treated roots (Fig. 5.1B). Two of the tested fluorescent auxin analogs, NBD-IAA and NBD-NAA, represented analogs of the natural auxin IAA and synthetic auxin NAA, respectively, and produced similar fluorescence images compared with *DR5* reporter

expression. The exogenously applied NBD-NAA and IAA (NBD-auxins) were preferentially accumulated in the root cap and elongation zone but not in the meristematic zone. These fluorescence images of NBD-auxins were similar to the exogenous auxin response profile of *DII-VENUS* (Fig. 5.1C, Appendix A Fig. S5.3). In contrast to NBD-auxins, the negative controls NBD-benzoic acid and NBD-indole showed faint, uniform fluorescence in the root (Appendix A Fig. S2B), suggesting that the auxin substructure is required for the *DR5* reporter-like distribution of NBD-auxin analogs.

Fluorescent Auxin Functions as an Auxin Analog Specific for Auxin Transport

We next assessed the effects of the fluorescent auxin analogs on auxin signaling and metabolism. To examine whether the fluorescent auxins were inactive in the SCF^{TIR1} pathway, *Arabidopsis* auxin-responsive reporter lines, including the synthetic auxin-responsive *BA3::GUS* (Oono et al., 1998) and *DR5::GUS* lines and native *pIAA3::GUS* and *pIAA12::GUS* lines (Weijers et al., 2005), were incubated with NBD-auxins. Neither NBD-IAA nor NBD-NAA affected auxin-regulated reporter gene expression (Fig. 5.2, Appendix A Fig. S5.4A), indicating that the fluorescent analogs are inactive regarding the modulation of early auxin-responsive gene expression. To further confirm that the fluorescent auxins are inactive as ligands of TIR1/AFB–Aux/IAA receptor complexes, we examined the binding of NBD-auxins to the TIR1–Aux/IAA receptor complex using a yeast two-hybrid system (Arase et al., 2012). In this system, IAA promotes the interaction between TIR1-DBD and Aux/IAA (IAA7)-AD to rescue *LEU2*-deficient yeast growth (Fig. 5.2C). NBD-auxins did not affect yeast growth in the absence or presence of IAA, suggesting that

NBD-auxins do not bind to the TIR1 receptor. Calculations of molecular docking further indicated that NBD-auxins were inactive ligands for TIR1 receptor and auxin-binding protein 1 (ABP1) due to the larger molecular size of the analogs with respect to the auxin-binding cavity (Appendix A Fig. S5.4). These findings demonstrate that the fluorescent auxin analogs, NBD-auxins, are inactive in SCF^{TIR1} auxin signaling. The *Arabidopsis* early auxin-responsive gene *GH3* encodes an auxin-amino acid-conjugating enzyme that plays a central role in the modulation of endogenous auxin levels (Ludwig-Müller, 2011). GH3.6 recognizes both IAA and NAA as substrates and converts them to amino acid conjugates. To investigate whether the GH3 enzyme metabolizes the fluorescent auxins in vivo, fluorescence images of NBD-auxins were obtained in *GH3.6*-overexpressing (GH3ox) plants (Appendix A Fig. S5.5A). The fluorescence images of NBD-auxin would be expected to be altered in the GH3ox line if the analogs were rapidly converted to non-transportable amino acid conjugates. However, in GH3ox roots, the fluorescence images of the analogs were not altered, suggesting that the fluorescent auxins were not suitable substrates for the GH3 enzyme (Appendix A Fig. S5.5B). To further assess the stability of NBD-auxin, tobacco BY-2 cells were incubated with NBD-NAA and its cellular metabolites were analyzed via fluorescence HPLC. The cellular NBD-NAA level was maintained, and the resultant fluorescent chromatograms were not altered after 50 min of incubation (Appendix A Fig. S5.5C).

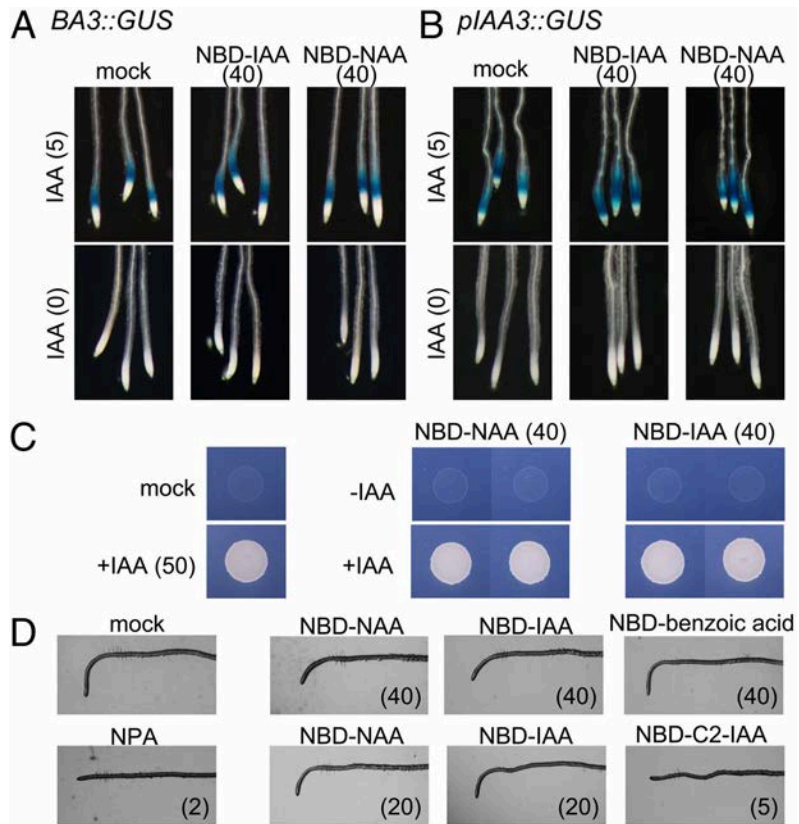


Figure 6.2. Effects of NBD-auxins on SCF^{TIR1} auxin signaling. (A and B) Effects of NBD-auxins on auxin-responsive reporter gene expression. Six-day-old *BA3::GUS* (A) and *pIAA3::GUS* (B) lines were incubated with or without IAA, together with NBD-auxins, for 5 h or 16 h, respectively. (C) Yeast two-hybrid assay in which TIR1-DBD and Aux/IAA(IAA7)-AD fusion proteins were expressed. IAA enhanced the interaction between TIR1 and Aux/IAA to rescue LEU2-deficient yeast growth. (D) Effect of NBD-labeled analogs on the root gravitropic response. Roots (6-d-old) were placed on GM agar plates containing chemicals and grown in the dark for 5 h after rotating the plates at a 90° angle against the vertical direction. The values in parentheses indicate the concentrations of chemicals (μM).

In a previous study, we found that Bz-IAA and Bz-NAA inhibited root gravitropism by competing with the transport of endogenous auxin (Tsuda et al., 2011). IAA and NAA have been reported to reduce the root gravitropic response (Ottenschlager et al., 2003). We next studied the inhibitory activity of the fluorescent analogs against root gravitropism (Fig. 5.2D). NBD-auxins inhibited root gravitropism at a concentration of 40 μ M, whereas NBD-benzoic acid did not. However, NBD-IAA and NBD-NAA were less active than the previously reported Bz-NAA and the auxin transport inhibitor 1-*N*-naphthylphthalamic acid (NPA) (Fig. 5.2D, Appendix A Fig. S5.6C). Although membrane-permeable analogs, such as Bz-NAA, are exported outside the cell, the subcellular concentration of diffusible Bz-NAA is maintained via simple diffusion. Thus, diffusible analogs would be expected to exhibit higher inhibitory activity than NBD-auxins. Accordingly, BOC-C2-NAA, a lipophilic analog of NBD-NAA, caused potent inhibition of gravitropism but was inactive to signaling, similar to Bz-NAA (Appendix A Fig. S5.6C,D). Additionally, another diffusible fluorescent auxin, NBD-C2-IAA, showed a uniform fluorescent signal in the roots and inhibited gravitropism to a greater extent than NBD-IAA, as expected (Appendix A Fig. S5.6). This evidence indicated that the fluorescent auxin analogs are recognized by the auxin transport system as active auxin analogs but are inactive regarding auxin signaling and the metabolic pathway.

Auxin Transport System Regulates the Distribution of Fluorescent Auxin

To examine whether the auxin transport system establishes an asymmetric distribution of NBD-auxin analogs, we observed the distribution profiles of the analogs in the auxin transport mutant *pin2*, PIN1-overexpression lines (*35S::PIN1*),

and wild-type plants treated with auxin transport inhibitors. Exogenous auxin strongly induced the expression of *DR5* reporters in the root elongation zone (Fig. 5.3A). Cotreatment with auxin transport inhibitor 2,3,5-triiodobenzoic acid (TIBA) blocked IAA movement, and DR5 reporters were consequently expressed throughout the root tip, including in the meristematic zone (Fig. 5.3A). NBD-NAA was uniformly distributed in the *pin2* mutant, *35S::PIN1*, and wild-type plants treated with the auxin transport inhibitors brefeldin A, TIBA, NPA, and Bz-NAA (Fig. 3B, Appendix A Figs. S6.7, S6.8). Additionally, the asymmetric distribution of NBD-NAA disappeared in the presence of excess IAA and NAA, but benzoic acid and 2-naphthoic acid did not affect the distribution of NBD-NAA. Similarly, the asymmetric distribution of NBD-IAA was abolished by excess amounts of NAA and auxin transport inhibitors. Furthermore, IAA and Bz-IAA decreased the fluorescent signal of NBD-IAA via competitive inhibition of auxin import. NBD-IAA signal was also reduced in the *aux1-7* auxin influx transport mutant (Marchant et al., 1999), but NBD-NAA signal was not affected (Appendix A Fig. S5.9). NBD-NAA was able to bypass the AUX1 importer in the same manner as NAA (Marchant et al., 1999). Consistent with the transport profile of alkoxy-auxins, these results suggest that NBD-auxins show the same transport profile as the original IAA and NAA molecules. Other mutants, for the auxin efflux transporters *abcb1*, *abcb19*, *pin3*, and *pin3 pin7* (Peer et al., 2011), did not show a dramatically altered distribution image of NBD-auxins in the roots (Appendix A Fig. S5.9). This altered distribution of NBD-auxins was observed only in the agravitropic roots in *pin2*, *35S::PIN1*, and *aux1-7* mutants. We further studied the accumulation of fluorescent auxin analogs using

Arabidopsis cultured cells. Both NBD-auxins were accumulated in the cultured cells, but NBD-benzoic acid did not (Appendix A Fig. S10). Treatment with the auxin transport inhibitor TIBA and excess NAA promoted the accumulation of NBD-auxins within the cells by repressing the export of NBD-auxins (Fig. 5.3D, Appendix A Fig. S5.10). This evidence indicates that fluorescent auxins are transported by the auxin transport system in roots.

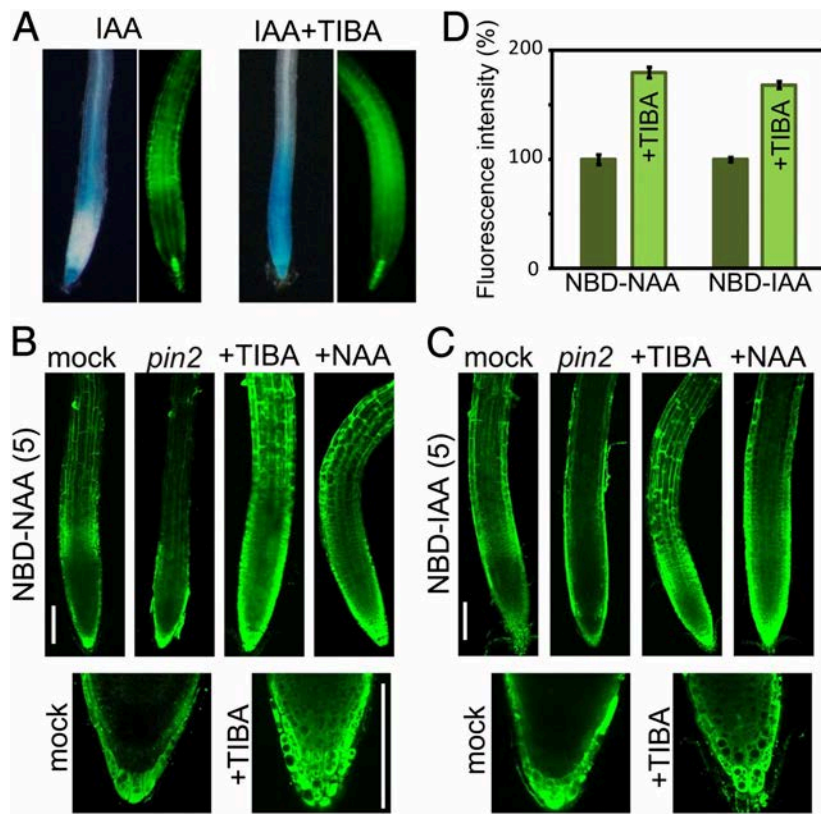


Figure 6.3. Auxin transport system affects the distribution of fluorescent auxin in roots. (A) Effects of auxin transport inhibitors on the auxin-responsive DR5 expression profile. Six-day-old *DR5::GUS* (Left) and *DR5::GFP* (Right) lines were treated with or without 20 μ M TIBA, together with 2 μ M IAA, for 5 h or 8 h, respectively. (B and C) Wild type (Columbia-0) and *pin2/eir1-1* mutants were treated

with 5 μM NBD-auxins for 15 min. Wild-type roots were pre-incubated with 20 μM TIBA or 50 μM NAA for 4 h and 30 min, respectively, and then treated with 5 μM NBD-auxins, together with TIBA and NAA, for 15 min. The values presented in parentheses indicate the concentration of chemicals (μM). (Scale bars, 100 μm .) (D) *Arabidopsis* MM1 cells were incubated with 2 μM NBD-auxins with or without 50 μM TIBA for 30 min after pre-incubation with TIBA for 3 h. NBD-auxins were extracted from the harvested cells using methanol and quantified with a fluorometer.

Error bars represent SEM; $n = 6$.

Distribution of Fluorescent Auxin at the Root Apex

Recent findings regarding auxin biosynthesis through the IPA pathway have indicated an important contribution of locally synthesized IAA to the formation of auxin maxima (Petersson et al., 2009; Chen et al., 2014). The *DR5* reporter system allows for the visualization of auxin levels as the sum of transported and locally synthesized auxin, whereas our system using NBD-auxins selectively displays the flow of auxin. To estimate the contribution of auxin transport to the formation of auxin maxima at the quiescent center (QC), we monitored the distribution of exogenously applied auxins in auxin-depleted seedlings. *DR5::GFP* reporter seedlings were grown on medium containing the auxin biosynthesis inhibitors kynurenine and yucasin to deplete endogenous auxin (Fig. 5.4) (He et al., 2011; Nishimura et al., 2014). Combined treatment with the TAA1 and YUCCA inhibitors dramatically inhibited primary root growth (Appendix A Fig. S5.11B,C), similar to the auxin-deficient phenotype observed in the *taa1 tar2* double mutant and the *yuc 3*

5 7 8 9 quintuple mutant (Stepanova et al., 2008; Won et al., 2011). The *DR5::GFP* maxima at the root apex disappeared in auxin-deficient seedlings (Fig. 5.4C, Appendix A Fig. S5.11A). This impaired root growth was completely restored by exogenous auxins supplied from the medium. However, exogenous NAA failed to recover *DR5::GFP* expression at the QC region in auxin-deficient roots (Fig. 5.4D, Appendix A Fig. S5.11), but NAA enhanced *DR5* expression at the columella and lateral root cap of auxin-deficient roots, similar to the distribution profile of NBD-NAA in wild-type roots. Additionally, exogenously applied 2,4-dichlorophenoxyacetic acid (2,4-D) was unable to form auxin maxima at the columella and lateral root cap (Appendix A Fig. S5.11A). This result is consistent with evidence showing that auxin efflux transporters effectively transport IAA and NAA but not 2,4-D (29). These findings suggest that auxin transport and local biosynthesis coordinately determine the position of auxin maxima in the root apex.

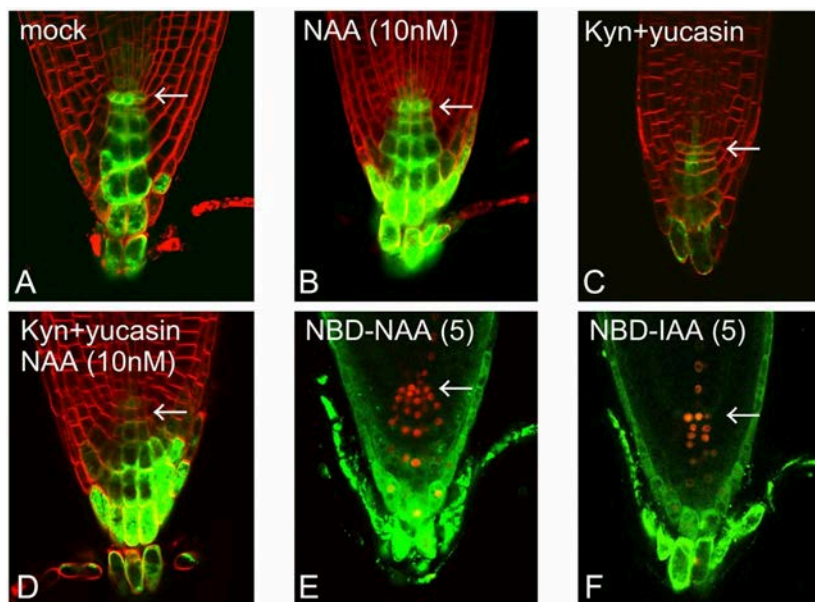


Figure 6.4. Auxin maxima in the root apex. (A–D) *DR5::GFP* maxima in auxin-deficient roots. The *DR5::GFP* line was grown for 5 d on medium containing auxin biosynthesis inhibitors [10 μ M kynurenine (Kyn) and 20 μ M yucasin] with or without 10 nM NAA. (E and F) NBD-auxin distribution at the root apex in the *DR5::tdTomato-NLS* line. The values presented in parentheses indicate the concentration of chemicals (μ M). The arrows indicate the QC region.

Fluorescent Auxin Distribution Mimics Native Auxin Accumulation in Vivo

Fluorescent NBD-auxin analogs are distributed to form an asymmetrical gradient in *Arabidopsis* roots. To examine whether the distribution of NBD-auxins mimics the endogenous auxin gradient in vivo, we analyzed fluorescence images of NBD-NAA in planta in different developmental stages and tissues and in response to environmental stimuli. At the very early seedling stage, seedlings treated with NBD-NAA showed similar fluorescence images as the *DR5::GFP* line (Appendix A Fig. S5.12). Polar transport of auxin is essential for lateral root formation, and auxin accumulates at high levels in the primordia of lateral roots (Fig. 5.5A) (Benková et al., 2003). NBD-auxins were selectively accumulated in the primordia of lateral roots and showed a similar pattern to *DR5::GFP* expression (Fig. 5.5A–C). The development of the embryo is regulated by the asymmetric auxin distribution via PIN efflux carriers (Friml et al., 2003). NBD-NAA distribution showed a similar pattern to *DR5::GFP* expression in embryos (Fig. 5D and E). Gravity signals regulate the auxin transport system to generate an asymmetric auxin distribution. Consistent with previous reports on the gravitropic response of the *DR5* reporter system (Friml et al.,

2002), NBD-NAA was distributed on the elongated side of the hypocotyl, across gravi-stimulated hypocotyls (Fig. 5.5F and H). In contrast, symmetric fluorescent signals were detected in vertically grown straight hypocotyl (Fig. 5.5G). To examine the transport of NBD-auxins in shoots, NBD-auxins were placed on the shoot apex and then incubated vertically. The distribution rate of NBD-auxin in the etiolated hypocotyl of the *pin3 pin7* mutant was slightly lower than the wild type (Fig. 5.5 I and J, Appendix A Fig. S5.13A). The fluorescent signal of NBD-auxins along the epidermal cells was clearly observed, and this transport of NBD-NAA was reduced by excess NAA and TIBA (Appendix A Fig. S5.13B,C). However, NBD-auxins were less accumulated in the deeper cell layers or in the central cylinder (Appendix A Fig. S5.13C,D), although the *DR5* reporter signal was shown in both the epidermal cells and the central cylinder (Christie et al., 2011). To confirm that the NBD-auxin distribution mimics the auxin gradient in other plant species, the distribution of NBD-NAA was observed in rice roots. In accordance with the distribution observed in *Arabidopsis* roots, NBD-NAA showed a similar pattern to the auxin-induced *DR5::GUS* response in rice roots (Fig. 5.5 K and L) (Inukai et al., 2005).

Subcellular Distribution of Fluorescent Auxins

DR5 and *DII-VENUS* auxin sensors allow for the clear visualization of intercellular auxin gradients in tissues. However, these SCF^{TIR1}-based systems are unable to visualize subcellular auxin gradients. In comparison, fluorescent auxin analogs display a high spatial resolution due to being small molecules. To investigate the subcellular auxin distribution, we initially visualized the distribution of subcellular NBD-auxins in tobacco BY-2 cultured cells. The auxin transport

inhibitors NPA and TIBA induced the accumulation of cellular NBD-NAA, thus enhancing the fluorescent signal within a cell (Fig. 5.6 A–C, Appendix A Fig. S5.14). However, NBD-benzoic acid and NBD-indole did not exhibit clear signals in cultured cells (Appendix A Fig. S5.2C). Additionally, NBD-auxins were not co-localized with the tonoplast marker VHA-a3-mRFP (Brux et al., 2008) (Appendix A Fig. S5.15), suggesting that the localization of NBD-auxins was not due to the nonspecific binding of the NBD fluorophores to organelles or membranes. Several auxin transporters, such as PIN5, PIN8, and PILS, are subcellularly localized to the endoplasmic reticulum (ER) (Barbez et al., 2012; Barbez et al., 2013; Barbez and Kleine-Vehn, 2013). NBD-auxin signals showed a similar localization pattern to the signals of PIN5-GFP and PIN8-GFP observed in BY-2 cells (Fig. 5.6, Appendix A Fig. S5.14) (Ganguly et al., 2010; Barbez et al., 2013), and NBD-auxin signals co-localized well with the fluorescent signals from ER-Tracker. In the wild-type root, NBD-NAA accumulated at the root hair and co-localized well with ER-Tracker (Fig. 5.6G–L). To further examine the subcellular distribution of NBD-auxins, the *Arabidopsis* root expressing the ER-retained CFP-HDEL protein (CFP-ER) was used. NBD-auxins were identically localized to CFP-HDEL (Fig. 5.6M–O, Appendix A Fig. S5.16), confirming that NBD-auxin is preferably localized to the ER. The treatment of roots with TIBA highly accumulated NBD-NAA to form a steep gradient of NBD-NAA in the roots (Appendix A Fig. S5.16C). On the contrary, CFP-ER was uniformly distributed even in TIBA-treated roots. These results implied that NBD-auxins highly accumulate in the cytosol when auxin efflux transport is blocked.

Discussion

We herein demonstrate that fluorescently labeled auxin molecules are able to selectively monitor auxin transport sites. Our NBD-auxins displayed a similar auxin distribution image generated by SCF^{TIR1}-based sensors. The pharmacological and genetic evidence convincingly shows that the asymmetric gradient of NBD-auxins is established by the auxin transport machinery. Sokołowska *et al.*, (2014) recently reported fluorescently labeled IAA analogs to be active auxins. In these analogs, the fluorescent dyes fluorescein isothiocyanate (FITC) or rhodamine isothiocyanate (RITC) were directly conjugated to IAA at the indole NH group. These FITC/RITC-conjugated IAAs were reported to retain auxin-like activity in oat coleoptiles and *Arabidopsis* root (Sokołowska *et al.*, 2014), suggesting that these conjugated IAAs might be active toward TIR1/AFB–Aux/IAA receptor complexes. Our fluorescent auxin analogs are designed to be active in the auxin transport system but inactive for auxin signaling (Appendix A Fig. S5.2B), indicating that the concept of our auxin analogs is quite different from that of FITC/RITC-conjugated IAAs (Sokołowska *et al.*, 2014). The ABP1 and SCF^{TIR1} signaling pathways both affect the polar auxin stream by modulating the localization and abundance of PIN proteins at the plasma membrane (Sauer and Kleine-Vehn, 2011; Baster *et al.*, 2012). Therefore, active analogs for auxin signaling can also impact auxin transport and hence disrupt the native auxin gradient. Previous studies have demonstrated that auxin biosensors, such as *DR5* reporters and the *DII-VENUS* system, display relative cellular IAA levels as the final output of IAA transport, biosynthesis, and metabolic pathways; however,

their sensitivity is primarily governed by the expression of TIR1/AFB receptor proteins and their posttranscriptional regulation (Parry et al., 2009).

This study also demonstrated that local auxin biosynthesis plays a crucial role in the formation of auxin maxima in the QC region (Fig. 5.4). Petersson et al. demonstrated that de novo synthesized IAA accumulated at the root apex, thereby indicating that a source of IAA exists in the most apical region of *Arabidopsis* primary roots (Petersson et al., 2009). Recent studies have shown that the expression of IAA biosynthesis genes is mainly localized near the QC region (Stepanova et al., 2008; Zhou et al., 2010; Chen et al., 2014). Our fluorescent NBD-auxins were not accumulated in the QC region in our experimental conditions. NBD-auxins were incorporated from the surface of whole tissue and then distributed by the auxin transport system. This distribution process does not represent the native condition because endogenous IAA was locally supplied from specific auxin biosynthetic cells. Similar to the NBD-auxins, the *DR5* and *DII-VENUS* response images to exogenous auxin supported that auxin transport would not largely contribute to the formation of auxin maxima at the QC (Figs. 6.1C, 6.4D), confirming that NBD-auxins can mimic auxin transport sites at the root apex.

Our findings demonstrate the power of fluorescently labeled hormones designed to be selective for transport systems with a high spatial resolution. However, in the present work, we cannot discuss the kinetics and affinity of these labeled analogs in relation to distinct auxin transporters, such as PINs, ABCBs, and AUX1/LAX, due to the nonspecific binding of the analogs in the yeast system used for the alkoxy-auxin analogs (Tsuda et al., 2011). In the shoot, it seems that NBD-

auxins were not efficiently transported by auxin transporters localized in the central cylinder (Appendix A Fig. S5.13). These results imply that NBD-auxins might aggregate locally at application sites; therefore, NBD-auxins are not versatile for the visualization of auxin transport streams in the shoot. Several ER-localized auxin transporters, such as PIN5, PIN8, and PILS, play a role in subcellular auxin homeostasis (Barbez et al., 2012; Barbez et al., 2013; Barbez and Kleine-Vehn, 2013). Because of the general nature of small-molecule compounds, a small fraction of NBD-auxins might be passively diffused and nonspecifically bound to organelle membranes. Nevertheless, NBD-auxin robustly accumulated in the ER of *Arabidopsis* and tobacco cells, and cytosolic NBD-auxin levels were highly enhanced by auxin transport inhibitors. This evidence indicates that NBD-auxins can facilitate the visualization of the subcellular auxin gradient in cells.

Our fluorescent auxin analogs will provide insights into auxin biology in combination with multiple tools such as SCF^{TIR1}-based sensors (Brunoud et al., 2012; Barbez et al., 2013), pharmacological auxin probes (He et al., 2011; Nishimura et al., 2014), and mathematical modeling (Band et al., 2014).

Materials and Methods

Synthesis and Properties of Fluorescent Auxin Analogs. Full synthetic procedures and characterization of compounds are described in Appendix A, Materials and Methods.

Plant Materials and Growth Conditions. *Arabidopsis thaliana* ecotype Columbia-0 was used as the wild-type control. Seeds were stratified for 2 d at 4 °C and cultured on germination medium (GM) (Oono et al., 1998) on soft gel plates (0.8 g/L gellan gum) or vertical agar plates (12 g/L agar) at 24 °C under continuous light for all assays. The mutant and transgenic *A. thaliana* lines used in this work are described in Appendix A, Materials and Methods. *Arabidopsis* MM1 and tobacco cultured BY-2 cells were maintained on modified Murashige and Skoog (MS) medium on a rotary shaker (100 rpm) at 24 °C in the dark.

Imaging and Image Analysis. Fluorescence images were recorded with a fluorescence microscope (Olympus; BX-50) and a laser scanning confocal microscope (Olympus; FV-1200). Typically, the seedlings were incubated with half-strength MS medium containing NBD-analogs for 15–20 min at 24 °C in the dark, and fluorescence images were then immediately recorded. Complete methods are described in Appendix A, Materials and Methods.

Acknowledgements

We thank Drs. Hironori Kaminaka and Yoshiaki Inukai for providing materials, and Prof. Hyung-Taeg Cho and Dr. Hiroyuki Kasahara for critical reading of the manuscript. This work was funded by grants from the Japan Society for the Promotion of Science; Grant-in-Aid for Scientific Research (KAKENHI) 23510285 and 25114518 (to K.H.); and US Department of Energy, Chemical Sciences,

Geosciences, and Biosciences Division, Basic Energy Sciences Grant DE-FG02-06ER15804 (to M.K.J. and A.S.M.).

Chapter 6. Computational modelling and heterologous expression

Summary

Computational modeling indicates plant ABCB transporters share a high degree of structural conservation with polyspecific multidrug ABCB transporters in mammals. Despite this similarity the best characterized ABCB transporters exhibit narrow specificities for the phytohormone auxin and similar auxin analogs. In this chapter, computational modelling was used to identify substrate binding sites associated with polyspecific substrate transport and primary sites for determining substrate specificity. To examine the contribution of specific amino acid residues to substrate binding and activity mutational analysis and expression in heterologous systems was investigated.

Introduction

The use of modelling and *in silico* substrate docking has been widely used in attempts to determine substrates of ABC transporters, particularly for mammalian ABCB1 (Chufan et al., 2013; Pan and Aller, 2015; Subhani et al., 2015). These efforts have been aided by the determination of several high resolution crystal structures and have identified substrate binding sites within the transmembrane helices (Aller et al., 2009; Li et al., 2014a; Szewczyk et al., 2015). The narrow substrate specificities of plant ABCB transporters compared to mammalian homologs suggests specific sequence differences within these sites contribute to substrate recognition. However, phylogenetic and amino acid comparison alone have not been

sufficient in determining substrate specificity and activity (Geisler and Murphy, 2006; Knöller et al., 2010; Kaneda et al., 2011).

Previous structural modelling and docking analyses have identified two plant specific putative auxin binding sites associated with the inner-leaflet of the plasma membrane that are hypothesized to confer substrate specificity (Yang and Murphy, 2009; Bailly et al., 2011). In this chapter, these analyzes were expanded to include several newly characterized plant ABCB transporters. To further analyze the contribution of specific amino acid residues to substrate recognition and activity, ABCB19 and site-directed ABCB19 mutants were analyzed in heterologous systems.

Results

Sequence analysis of Arabidopsis ABCB transporter NBDs

The majority of the *Arabidopsis* ABCB transporters have conserved sequences in the canonical nucleotide-binding domain (NBD) motifs. Of the 21 full length ABCBs only ABCB6 and ABCB20 have significant alterations in NBD sequences. Modelling of ABCB6 reveals these substitutions do not cause any major conformational shifts within the NBDs (Fig. 6.1 A and B). These residues, however, are all within the NBD regions where highly coordinated interactions occur between several residues, ATP, Mg²⁺, and water (Fig. 6.1 C). Mutations at key positions have been shown to have a significant impact on activity. For instance, introduction of a polar threonine residue in place of the non-polar glycine in the NBD1 signature sequence (LSGGQ→LSTGQ) reduced ATPase activity >80% in the bacterial

heterodimeric exporter EfrCD (Hürlimann et al., 2017). In human ABCB1, signature sequence mutants G534V and G534D independently reduce ATPase activity >95% (Bakos et al., 1997). ABCB6 and ABCB20 have several alterations in their respective ATP-binding cassette motifs that would likely cause both steric and charge alterations and reduced ATPase activity. A number of ABC transporters, including CFTR, have been reported to maintain activity despite having one “degenerate” nucleotide-binding site that is able to bind but not hydrolyze ATP. This does not appear to be the case with ABCB6 and ABCB20 as each have non-canonical sequences in both nucleotide-binding sites. The groups of ABCB15/16/17/18 and ABCB2/10 have L→M mutations in the signature sequence (LSGGQ) in the NBD1 and NBD2, respectively, but these changes are not predicted to have any impact on protein function. Development of a system to test for ATPase activity is needed to test the effects of these mutations.

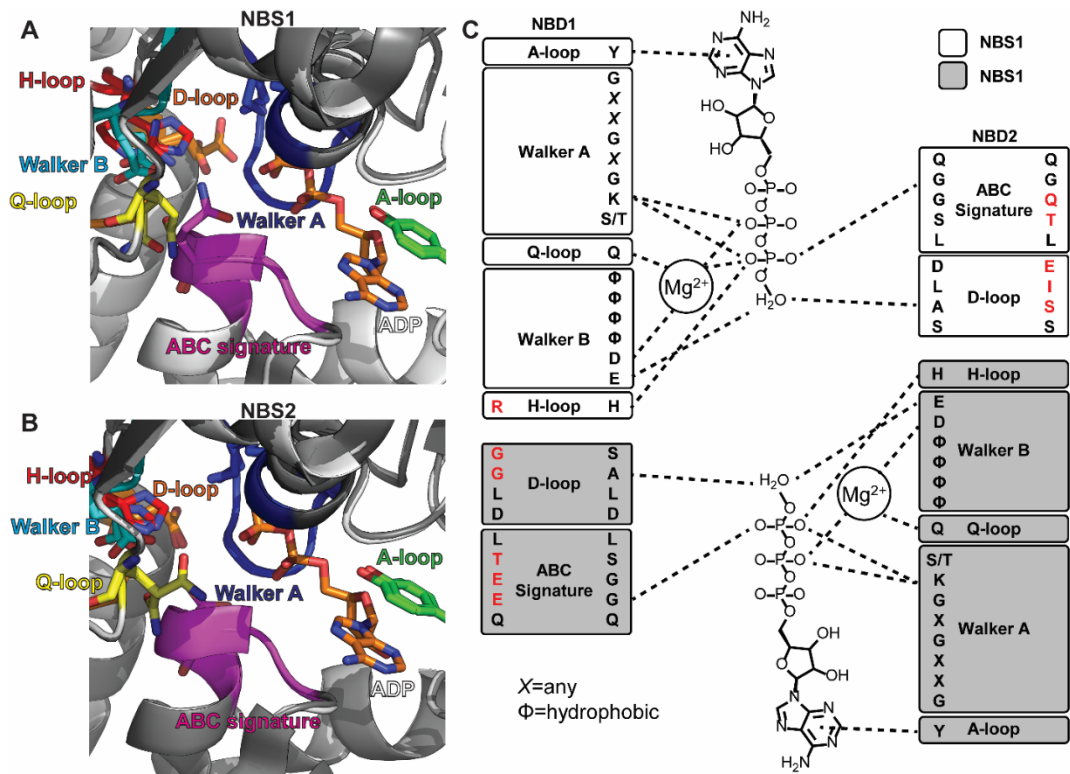


Figure 6.1. Comparison of ABCB6 and Sav1866 nucleotide binding domain (NBD) dimer organization. (A-B) ATP binding pockets of ABCB6. Homology model of ABCB6 was threaded on Sav1866 (PDB 2HYD). Sticks are shown for the A-loop tyrosine (green), Walker A lysine (blue), Walker B glutamate (cyan), D-loop aspartate (orange), H-loop histidine (red), Q-loop glutamine (yellow), and the second glycine in the ABC signature sequence (pink). (C) Schematic of the NBD dimer coordination with ATP. Letters in black are the canonical motif sequences. Red letters are residues in ABCB6 that are not conserved.

Computational modelling predicts auxin binding sites

To identify ABCB transporters capable of transporting auxin, docking of IAA to inner-leaflet associated binding sites was compared between homology models of

Arabidopsis ABCB19, 2, 10, 11, 21, and 14, and rice (*Oryza sativa*) OsABCB14 threaded on the murine ABCB1 (MmABCB1, PDB: 4M1M) (Fig. 6.2 A). ABCB19, which has been shown to have high specificity for IAA (Yang and Murphy, 2009), had docking affinities of -6.4 and -5.5 kcal/mol for each of the binding sites, respectively. ABCB21 and OsABCB14, which have also been characterized as auxin transporters (Chapter 3 and 4) (Kamimoto et al., 2012; Xu et al., 2014), show IAA docking energies comparable to that of ABCB19. ABCB14, which was originally characterized as a malate and citrate transporter (Lee et al., 2008) and later implicated in auxin transport (Kaneda et al., 2011), also exhibits comparable binding to ABCB19. In contrast, ABCB2, which does not transport IAA when heterologously expressed in *S. pombe* (Yang and Murphy, 2009), has lower affinities for IAA at both sites. ABCB10 binding is comparable to ABCB19 in site 1 and substantially higher in site 2. ABCB11 has a docking energy comparable to ABCB19 in site 1 and reduced affinity in site 2.

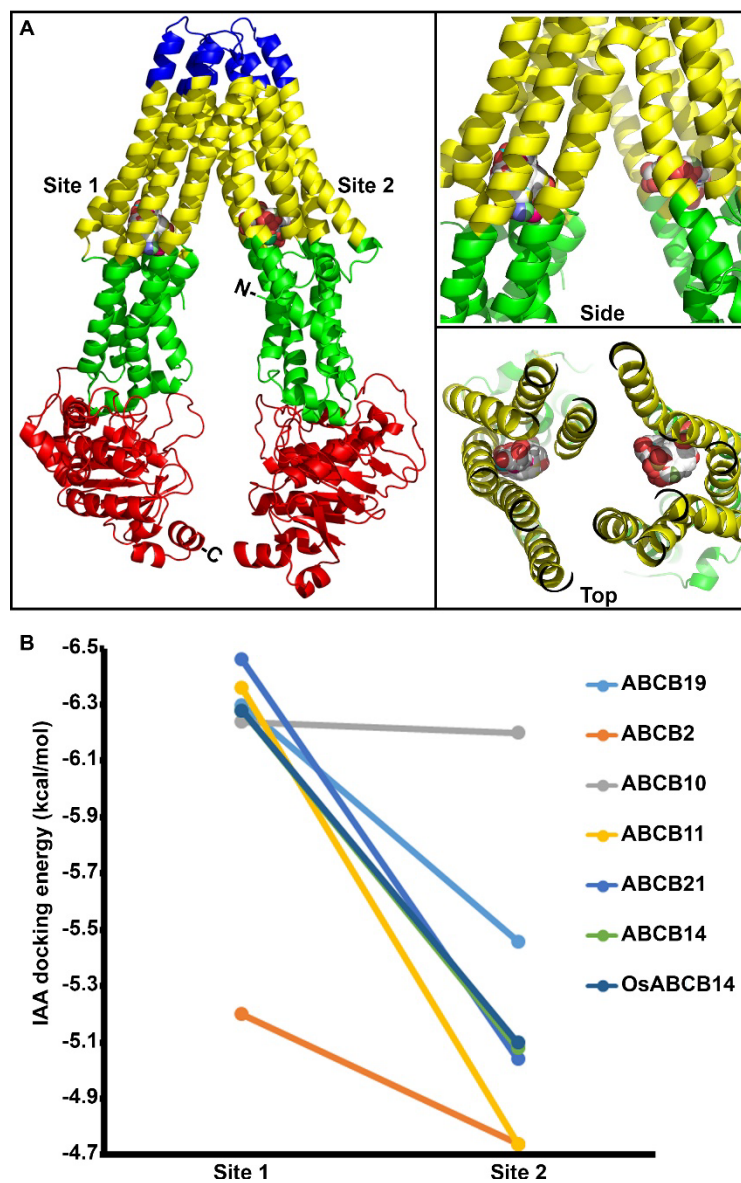
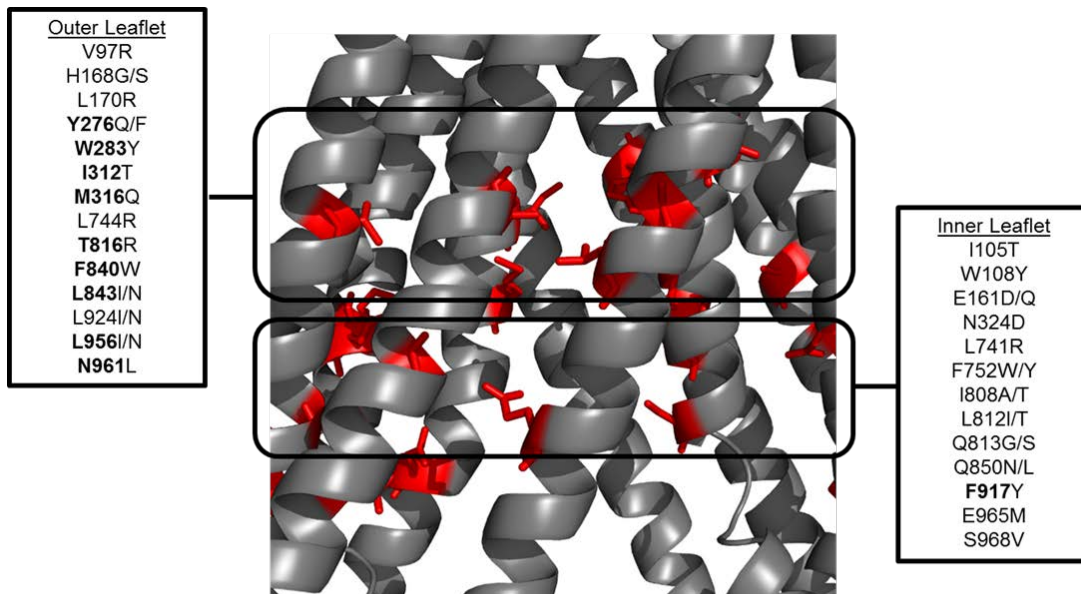


Figure 6.1 Docking of IAA to the inner leaflet associated binding sites. (A) Homology modelling and IAA docking simulation for ABCB19 in inward facing conformation. White and red spheres represent positions of IAA binding. **(B)** Mean docking energies for the top 5 IAA binding poses within each binding pocket.

These results support a role for the two inner-leaflet associated binding sites contributing differentially to substrate specificity, with site 1 functioning as the primary site for IAA recognition (Fig. 6.2 B) (Bailly et al., 2011). All transporters characterized as having some capacity for IAA transport (ABCB19, 14, 21, and OsABCB14) group together in site 1 binding. Site 1 binding affinities for ABCB11 also group with these transporters, which supports the activity observed when expressed in *S.pombe* (Chapter 4). Modelling also predicts ABCB10 may function as an auxin transporter, however, *abcb10* mutants do not show auxin related phenotypes and *ABCB10* expression is very low *in planta* (Chapter 3 and 4).

Mutational analysis of ABCB19 in Schizosaccharomyces pombe

To further investigate the contribution putative inner- and outer-leaflet associated auxin binding sites make to auxin transport, site-directed mutants of ABCB19 were generated and assayed for transport activity in *S.pombe*. Amino acid residues within 5 Å of the predicted IAA binding pockets were considered candidates for contribution to substrate recognition (Fig. 6.2).



BOLD = equivalent to residues identified in HsABCB1

Figure 6.2. Amino acid residues associated auxin binding in ABCB19. Amino acid residues that were within 5 Å of the inner and outer leaflet auxin binding pockets are colored red and listed in boxes. Residues in bold are associated with substrate recognition in human ABCB1. Also listed in boxes are site-directed mutants used for analyzing substrate specificity.

Several of these mutations lead to decreases in ABCB19 transport activity (Fig. 6.4). For example, mutation of valine 97 to arginine (V97R) or histidine 168 to glycine (H168G), which correspond to residues associated with the outer membrane leaflet, resulted in defects in IAA export activity. However, it quickly became apparent that without the ability to test transport activity and ATPase activity, changes in specificity or changes in activity could not be separated.

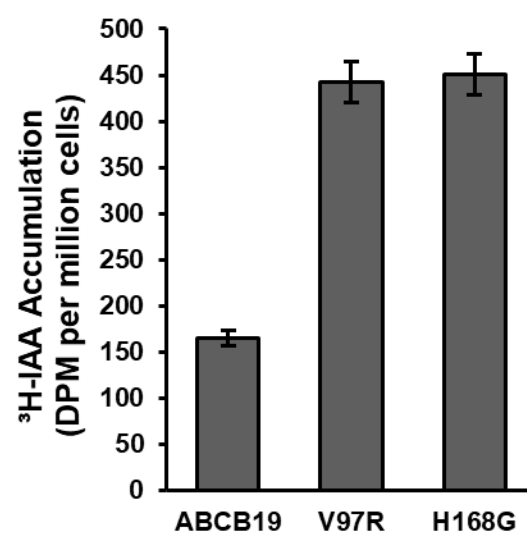


Figure 6.4 Mutations in ABCB19 binding pockets reduce transport activity.

Analysis of ABCB19 in Lactococcus lactis

A number of publications have used *Lactococcus lactis* for expression of membrane transporters, including human ABCG2/BCRP (Janvilisri et al., 2003) and the *Arabidopsis* HMA P-type ATPase transporters (Frelet-Barrand et al., 2010). *L.lactis* is a Gram-positive bacterium with a single outer membrane and low proteolytic activity (Kunji et al., 2003). Expression in *L.lactis* can be tightly controlled using the nisin-controlled gene expression (NICE) system (de Ruyter et al., 1996). The greatest benefit to using *L.lactis* system is the ability to make inverted membrane vesicles (Fig. 6.6). With an inverted vesicle system the dependence on substrate uptake prior to measuring efflux is eliminated, allowing for the use of multiple substrates simultaneously and a more robust characterization of specificity. Additionally, ATPase activity can be measured in the isolated membranes.

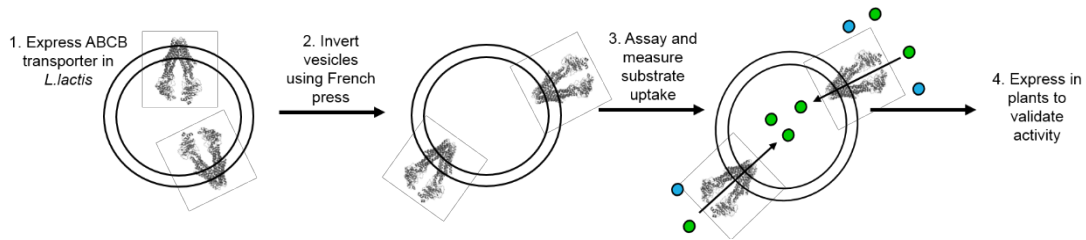


Figure 6.6. ABCB19 exhibits auxin efflux activity that is sensitive to transport inhibitors in *L.lactis* whole cells.

Expression of ABCB19 results in a decreased in net ^3H -IAA uptake of about 20% in whole *L.lactis* cells (Fig. 6.7 A). This activity was sensitive to competition with cold IAA (5:1 molar ratio) and the polar auxin transport inhibitor NPA (Fig. 6.7 B). Recently, ABCB19 was reported to exhibit channel activity that is sensitive to the chloride channel inhibitor NPPB when expressed in human embryonic kidney cells, however, auxin transport could not be detected in this system (Cho et al., 2014). When expressed in *L.lactis*, treatment with NPPB reduced ^3H -IAA accumulation (Fig 6.8), providing a link between ABCB19 NPPB-sensitivity and auxin transport activity. When membranes were isolated from cells expressing ABCB19, net uptake into the membrane vesicles could be detected after 5 and 10 minutes (Fig 6.7 C). This is the first time a plant ABCB transporter has been assayed in isolated membrane vesicles. Attempts were made to optimize the timing of maximum protein expression, however, HIS-tagged ABCB19 was not detected by western blot.

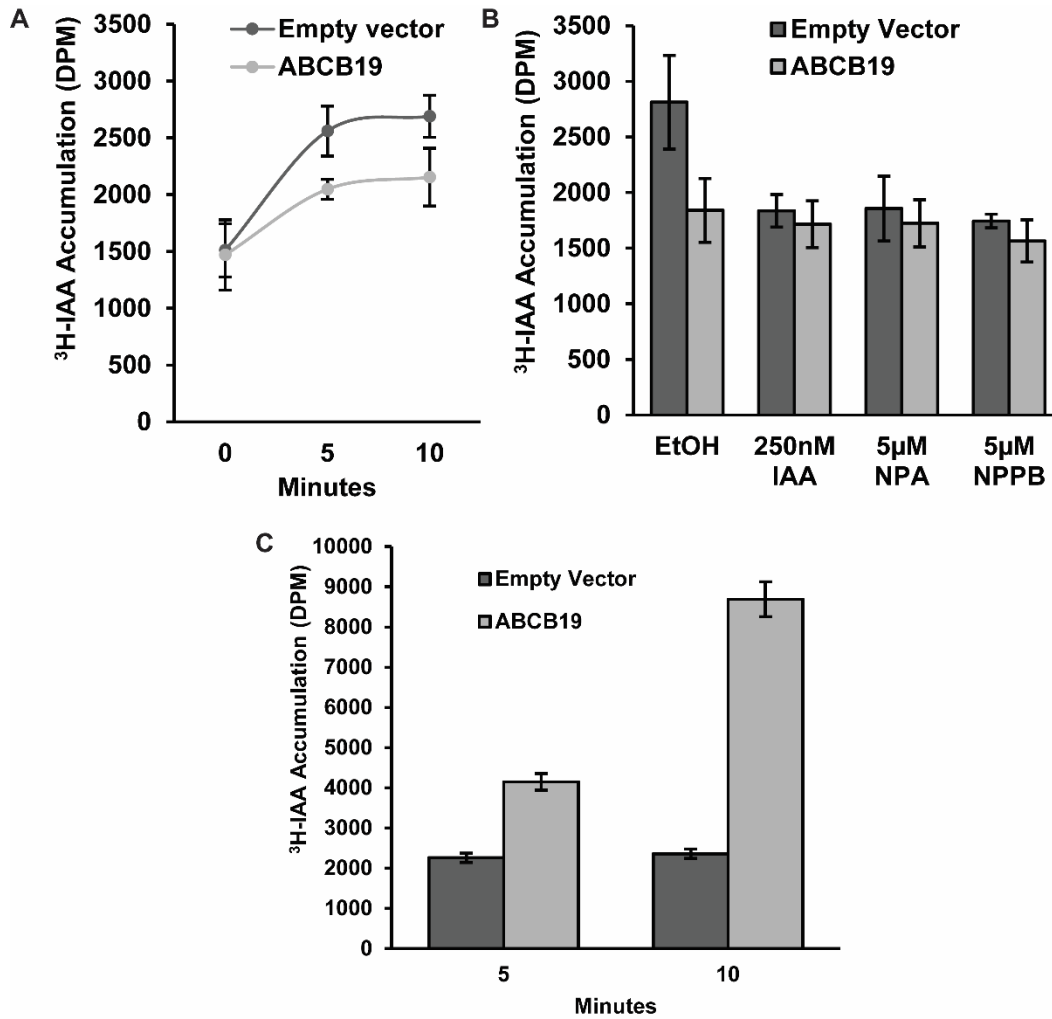


Figure 6.7. Auxin transport activity of ABCB19 in expressed in *Lactococcus lactis*. (A) ABCB19 exhibits auxin efflux in *L. Lactis* whole cells. (B) ABCB19 mediated auxin efflux is sensitive to competition with IAA and auxin transport inhibitors in *L. Lactis* whole cells. (C) ABCB19 exhibits auxin transport activity in *L. Lactis* inverted membrane vesicles.

Discussion

Homology modelling and docking can be a powerful tool for protein structure determination and prediction of activities for proteins that cannot be determined from sequence alignments alone (Knöllner et al., 2010). Previous analyses have identified two putative auxin binding sites associated with the inner-leaflet of the plasma membrane that are predicted to confer substrate specificity in ABCB auxin transporters (Yang and Murphy, 2009; Bailly et al., 2011). An additional binding pocket that resides between the membrane bilayers is associated with broad specificity substrate exclusion from the membrane.

In this chapter, previous modelling efforts were repeated to include several newly characterized plant ABCB transporters. From these results site 1 appears to function as the primary site for IAA recognition (Fig. 6.1), which is consistent with a previous report (Bailly et al., 2011). In line with modelling, biochemical, and mutational analyses, ABCB19 is predicted to exhibit a high level of substrate specificity. Equivalent IAA binding affinities in site 1 are consistent throughout the known *Arabidopsis* auxin transporters ABCB19, 11, and 21 and the rice auxin transporter OsABCB14. These results also predict much weaker affinities for the non-auxin transporter ABCB2.

To further analyze the contribution of specific amino acid residues to substrate specificity, site-directed mutants in ABCB19 were generated. While reductions in transport were observed in ABCB19 mutants, it was not possible to determine if these alterations were due to reduced transport activity or reduced ATPase/overall activity.

A widely used heterologous system for examining ABC transporter function is expression in *Lactococcus lactis*. Expression in *L. Lactis* has the benefit of being able to analyze transport activity in whole cells, and transport and ATPase activity in inverted membrane vesicles. When expressed in *L. Lactis* ABCB19 exhibited auxin efflux activity that was sensitive to established auxin transport inhibitors. Further, ABCB19 also exhibited net uptake activity into inverted membrane vesicles. However, since the protein could not be detected by western blotting, these activities cannot be directly attributed to ABCB19. Analysis of the genome reveals *L. Lactis* lacks proteins with any significant homology to the FKBP42 or its chaperone HSP90. It is hypothesized that co-expression with FKBP42 and HSP90 would significantly increase ABCB19 stability and activity but those experiments were not made here.

Analyzing transporter activity using heterologous systems remains a challenge. Systems that work for one protein may not work for another, even in cases of proteins with significant similarity. Differences between eukaryotic and prokaryotic transcriptional, translational, and post-translational processes could play into the difficulties in expressing *Arabidopsis* ABCB19 in *L. Lactis*. Other eukaryotic heterologous systems have been used to express *Arabidopsis* ABCB transporters and analyze specificity including HeLa, human embryonic kidney, and SF9 cells (Terasaka et al., 2005; Titapiwatanakun and Murphy, 2009; Cho et al., 2014). Previously, specificity was analyzed for ABCB4 using vanadate trapping in SF9 cells (Terasaka et al., 2005). Efforts to express ABCB19 in SF9 cells are underway.

Materials and Methods

Homology modelling and docking. The amino acid sequences of *Arabidopsis* ABCB transporters were retrieved from TAIR (AtABCB1: AT2G36910.1, AtABCB2: AT4G25960.1, AtABCB3: AT4G01820.1, AtABCB4: At2G47000.1, AtABCB5: AT4G01830.1, AtABCB10: At1G10680.1, AtABCB11: AT1G02520.1, AtABCB12: AT1G02530.1, AtABCB13: AT1G27940.1, AtABCB14: At1G28010.1, AtABCB15: AT3G28360.1, AtABCB16: AT3G28380.1, AtABCB17: AT3G28390.1, AtABCB18: AT3G28415.1, AtABCB19: AT3G28860.1, AtABCB21: AT3G62150.1) and rice ABCB transporters from the SALK Institute Genomics Analysis Laboratory (OsABCB10: Os05g04610, OsABCB14: Os04g38570). Initially three homology models were build using the iTASSER (Roy et al., 2010) and Phyre2 (Kelley and Sternberg, 2009) servers, and the Modeller v9.14 (Eswar et al., 2006) program with the multidrug exporters MmABCB1 (PDB: 4M1M, open conformation) and Sav1866 (PDB: 2HYD, closed conformation) as templates. These three models were then used as templates to build a final ABCB transporter model using Modeller v9.14. Regions not included within the MmABCB1 crystal structure, i.e. the N-terminus and linker domain were removed due to high variability in the structure prediction in these regions. All final models were subjected to energy minimization using the YASARA energy minimization server. The quality of the final models was assessed using the ERRAT2, RAMPAGE and QMEAN servers. For the docking 60 IAA poses generated using AutoDock Vina (Seeliger and de Groot, 2010).

Yeast transport assays. Yeast assays were conducted as described in Yang and Murphy, 2009.

Site-directed mutagenesis and cloning. ABCB19 sequence was amplified with BP Gateway primers using Herculase II Fusion DNA polymerase (Agilent Technologies) then cloned into the pDONR/zeo Gateway donor vector (Life Technologies) by BP recombination and confirmed by sequencing. ABCB19 was then transferred to pPTPi-G17 (Douillard et al., 2011), a nicin-inducible *L. lactis* expression vector with an N-terminal His₆ tag, by LR recombination (Life technologies). pPTPi-G17-ABCB19 was then transformed into *L. lactis* strain NZ9000 by electroporation. Positive transformants were verified by PCR and restriction digestion.

Growth and induction of *L. Lactis*. *L. lactis* expressing empty vector or ABCB19 were grown overnight (static, 30°C) in GM17 media containing 5µg/ml tetracycline. 1 ml culture was used to inoculate 50 ml fresh media and grown 90 RPM, 30°C. Protein production was induced by addition of 5ng/ml nisaplin (in 0.05 acetic acid) when cultures reached OD₆₀₀ 0.4-0.5.

Preparation of inverted membrane vesicles. Cell pellets were be resuspended in 100 mM K-HEPES (pH 7.0) with 1 mM PMSF, 20 mg/l leupeptin, 200 mg/l pepstatin, and 40 mg/l aprotinin. Lysozyme was be added to a final concentration of 2 mg/ml, and the suspensions incubated 30°C for 30 min to digest the cell wall. Cells were then lysed by three passages through a French press cell disruptor at 20,000 psi.

10 $\mu\text{g/ml}$ DNase, 2 $\mu\text{g/ml}$ RNase, 10 mM MgSO_4 , and 15 mM K-EDTA (pH 7.0) will be added and the suspension incubated for 30 min at 30°C. Unbroken cells and cell debris were removed by centrifugation at 4°C, 13,000 x g for 15 min. Inside-out membrane vesicles were collected by centrifugation at 4°C, 125,000 x g for 50 min and resuspended in 100 mM K-HEPES (pH 7.0) containing 10% glycerol.

Transport assays in *L.lactis*. For whole cell assays, 100 μl cell culture was aliquoted into pre-chilled Eppendorf tubes and incubated 25 min on ice. 1 μl ^3H -IAA (40nM final conc.) was added, samples were vortexed briefly then incubated 30°C. Cells were collected by centrifugation 30 sec, 8,000 x g, 4°C, washed once with cold GM17 (pH 4.5) then resuspended in 250 μl cold water. Cells were added to 5ml scintillation cocktail and analyzed for ^3H -IAA accumulation. For inhibitors and competition assays 250nM cold IAA, 5 μM NPA or 5 μM NPPB was added at room temperature just prior to addition of ^3H -IAA on ice. Cells were incubated 30°C for 8 min. For assays with isolated membranes,

Conclusions

In this dissertation, I identify a primary function of ABCB auxin transporters in excluding auxin from the plasma membrane at points of efflux. This exclusionary function is not dynamic but is necessary to maintain auxin transport streams during plant growth and development. This is demonstrated in the severe dwarfism and reductions in auxin transport in *abcb1abcb19* double mutants.

In seedlings, ABCB1 and ABCB19 function primarily in excluding auxin from the shoot apex and keeping auxin within the rootward auxin transport stream in the hypocotyl and root. By expression, I establish that ABCB19 is the primary ABCB auxin transporter and contributions to auxin transport from other ABCBs are supplementary. One of these supplementary transporters is *ABCB21*. From my analysis I determined ABCB21 functions with ABCB19 in maintaining the rootward auxin transport stream by excluding auxin from entering the surrounding tissues. A phenotypic analysis of several other ABCB transporter mutants did not point to any obvious additional candidates. Analysis of expression and mutant phenotypes indicate most ABCB transporters are not expressed in seedlings but are more likely to contribute to auxin transport in mature tissues.

In mature tissues, loss of ABCB1 and ABCB19 results in pooling of auxin in the inflorescence shoot apex, supporting a role in exclusion of auxin from the apical regions between seedlings and mature tissues. The lack of defects organ formation in *abcb1* and *abcb19* mutants but severely stunted growth in *abcb1abcb19*, again, points to a dull but necessary exclusionary function. Consistent with what is observed in seedlings, I determined ABCB19 is the primary ABCB auxin transporter. I further

determined that ABCB6 mediates rootward auxin transport in inflorescence stems, ABCB21 contributes to auxin distribution in leaves, and ABCB11 mediates auxin transport in young flowers. However, auxin related phenotypic differences are only observed in triple mutant backgrounds and single *abcb11* and *abcb21* mutants do not exhibit any obvious phenotypic differences from wild type plants. This further suggests their contributions to auxin transport are supplementary to that of ABCB19. The levels of ABCB6 supplementary activity to ABCB19, and ABCB1, remain to be determined.

In order to better understand on the molecular level how ABCB transporters mediate exclusion of auxin from the membrane I analyzed transport of fluorescently-tagged auxins synthesized by Dr. Ken-Ichiro Hayashi. The original hypothesis was that ABCB transporters were less specific than AUX1/LAX or PIN proteins, and would be able to actively transport the fluorescent auxins by excluding them from the membrane. My analysis of these tagged auxins determined they mirror the distribution of native auxin *in vivo*. Further, analysis indicated the fluorescent-auxin auxins partition into membranes at sites of auxin transport but it remains unclear whether these auxins primarily are labelling membranes or proteins. Most significantly, I determined that the fluorescent auxin were not actual substrates of the AUX1/LAX, PINs or ABCBs and were not useful for study of the primary auxin transporters.

Despite the development of several tools to study auxin transport *in planta*, it appears the best way to determine how ABCB transporters confer substrate specificity is with the use of heterologous expression systems. Here, I used homology

modelling and expression in heterologous expression systems in an attempt to identify the molecular mechanisms of ABCB transporter specificity and activity. From my analysis, I identify putative substrate binding sites that support a primary function of ABCB transporters in exclusion of auxin from the membrane. Analysis of mutations within these binding sites reduced auxin transport in ABCB19 when expressed in *S.pombe*. It was not possible to determine if these reductions were due to changes in specificity or activity. Attempts to analyze the contribution of these binding sites to specificity and activity in other heterologous systems are ongoing.

Since beginning this dissertation research, the field of auxin transport has advanced tremendously. However, the question of how ABCB transporters work remains largely unknown. In this dissertation I identified a primary role for ABCB transporters in excluding auxin from the membrane. What we still don't know is how, on the molecular level, the interactions between ABCB transporters, the membrane environment, and their substrates determines specificity.

Appendices

Appendix A. Supplementary information for Chapter 5

Auxin transport sites are visualized in planta using fluorescent auxin analogs

Ken-ichiro Hayashi, Shouichi Nakamura, Shiho Fukunaga, Takeshi Nishimura, Mark Jenness, Angus Murphy, Hiroyasu Motose, Hiroshi Nozaki, Masahiko Furutani, Takashi Aoyama

In the interest of space, only supplemental figures have been included here. The full supporting information for this publication, including fluorescent auxin synthesis, can be found at:

<http://www.pnas.org/content/pnas/suppl/2014/07/19/1408960111.DCSupplemental/pnas.1408960111.sapp.pdf>

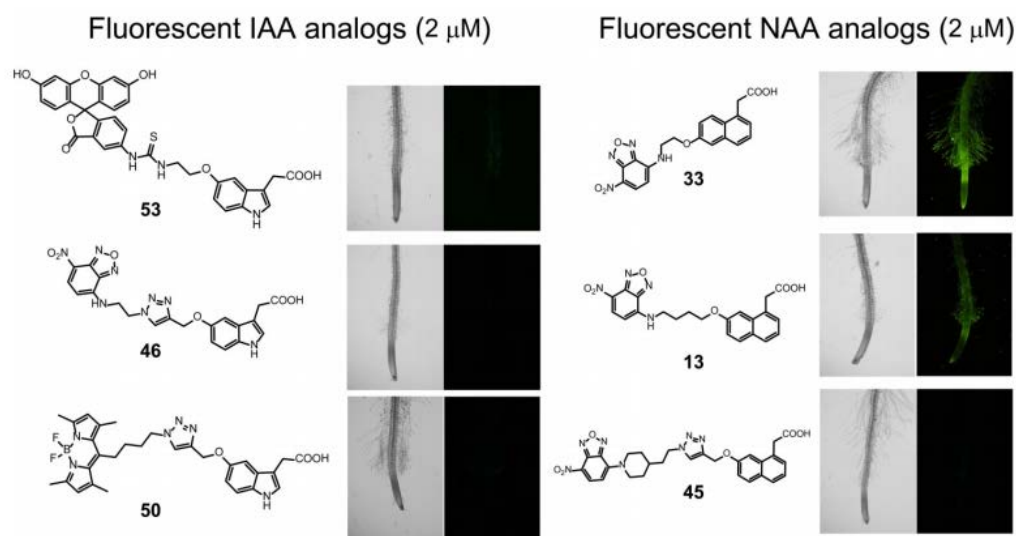


Fig. S5.1. Structures of fluorescently labeled auxins and fluorescence images of *Arabidopsis* roots. 6-d-old seedlings were treated with medium containing 2 μ M fluorescent probes for 15 min. Fluorescent microscopy images were generated using FITC filter sets. Compounds 13: 2-(7-(2-((7-nitrobenzo[c][1,2,5]oxadiazol-4-yl)amino)ethoxy)naphthalen-1-yl)acetic acid, 33: 6-[2-(7-nitrobenzo[1,2,5]oxadiazol-4-ylamino)ethoxy]naphthalen-1-yl acetic acid, 45: [7-(1-{2-[1-(7-Nitro-benzo[1,2,5]oxadiazol-4-yl)-piperidin-4-yl]-ethyl}-1H-[1,2,3]triazol-4-ylmethoxy)naphthalen-1-yl]acetic acid, 46: [5-(1-{2-[1-(7-Nitro-benzo[1,2,5]oxadiazol-4-yl)-piperidin-4-yl]-ethyl}-1H-[1,2,3]triazol-4-ylmethoxy)-1H-indol-3-yl]acetic acid, 50: BODIPY-labeled IAA, 10-(4-(4-(((3-(carboxymethyl)-1H-indol-5-yl)oxy)methyl)-1H-1,2,3-triazol-1-yl)butyl)-5,5-difluoro-1,3,7,9-tetramethyl-5H-dipyrrolo[1,2-c:2',1'-f][1,3,2]diazaborinin-4-ium-5-uide, 53: FITC-labeled IAA, 2-(5-(2-(3-(3',6'-dihydroxy-3-oxo-3H-spiro[isobenzofuran-1,9'-xanthen]-5-yl)thioureido)ethoxy)-1H-indol-3-yl)acetic acid.

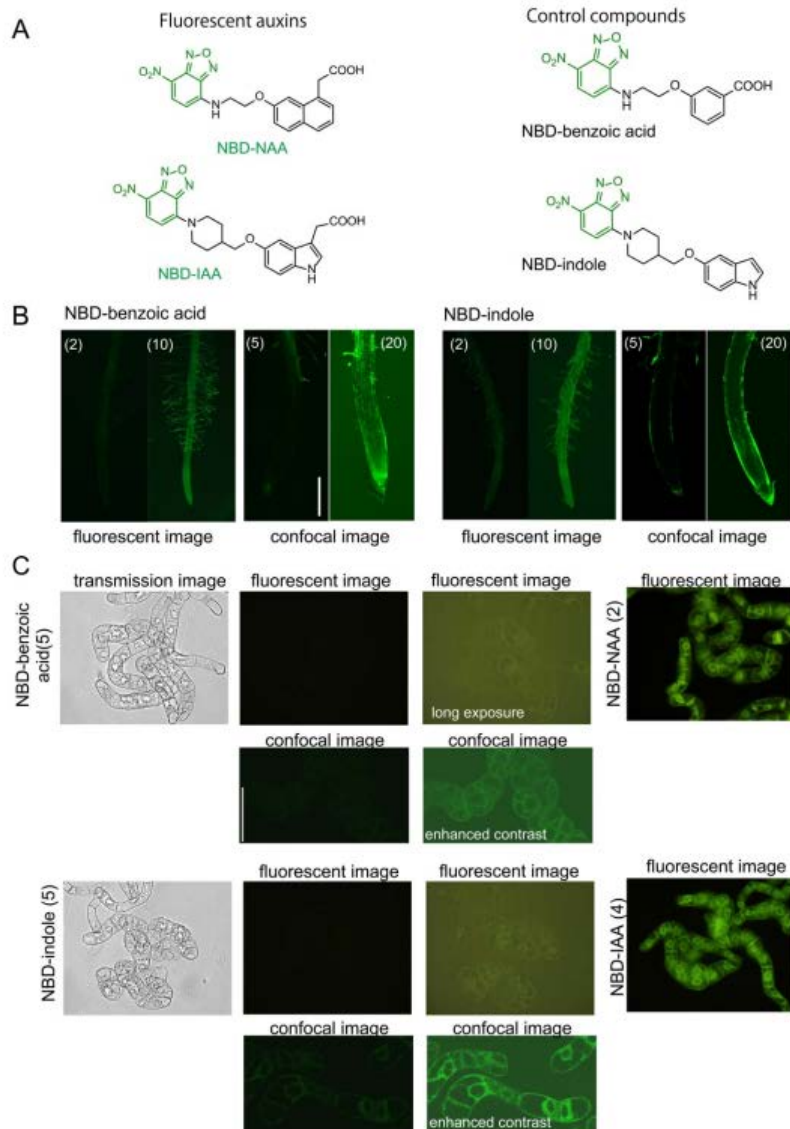


Fig. S5.2. Distribution of NBD-benzoic acid and NBD-indole in *Arabidopsis* root and tobacco BY-2 cells. (A) Structures of NBD-benzoic acid and NBD-indole used for control. (B) Distribution of NBD-benzoic acid and NBD-indole in *Arabidopsis* roots. 6-d-old wild-type seedlings were treated with medium containing NBD-labeled chemicals for 15 min. The values presented in parentheses indicate the concentration of chemicals (μM). Scale bar represents 100 μm . (C) The tobacco BY-2 cells were treated with 5 μM NBD-benzoic acid and 5 μM NBD-indole for 15 min. The control

compounds NBD-benzoic acid and NBD-indole did not show a clear fluorescent signals. Fluorescence images of roots and cells were recorded under identical conditions by fluorescent microscopy (fluorescent image) and confocal laser scanning microscopy (confocal image). The values in parentheses indicate the concentrations of chemicals (μM).

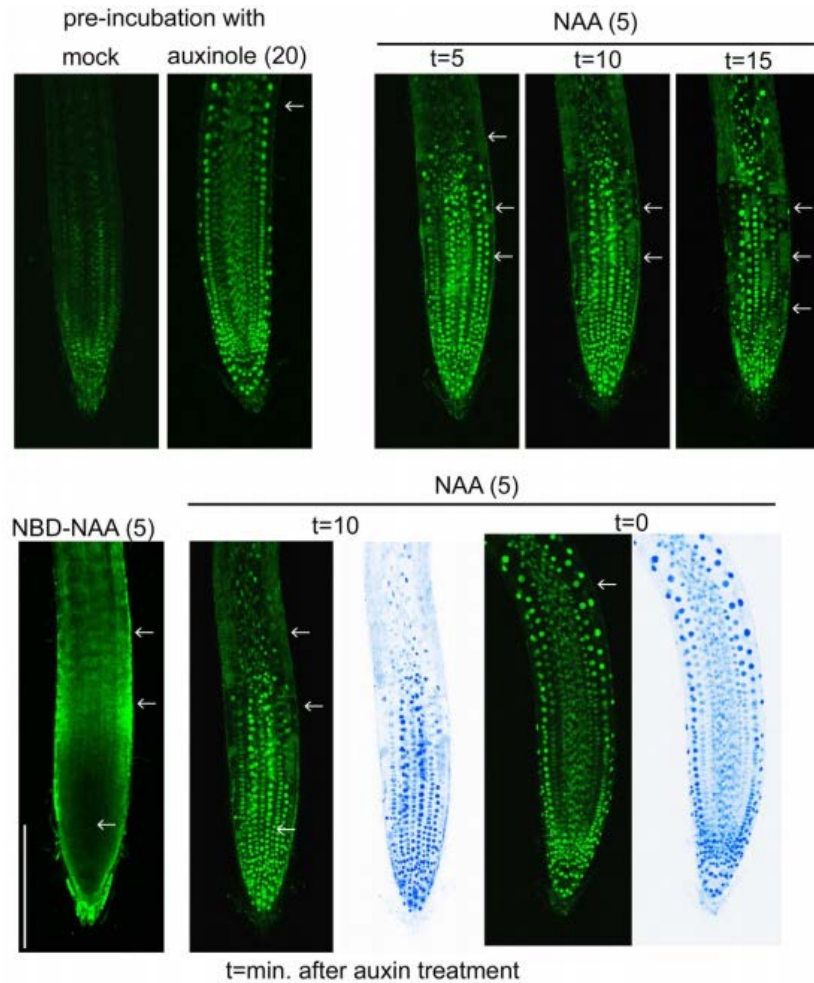


Fig. S5.3. Visualization of exogenous NAA distribution by using *DII-VENUS* system. 6-d-old *DII-VENUS* seedlings were incubated for 6 h with/without 10 μ M auxinole, specific antagonist for TIR1/AFB auxin receptor to block the degradation of *DII-VENUS* reporter protein regulated by endogenous auxin. The *DII-VENUS* roots were washed out with fresh medium and treated with exogenous NAA. Fluorescent confocal images of roots were recorded under the identical conditions at regular intervals. The values presented in parentheses indicate the concentration of chemicals (μ M). Scale bar represents 200 μ m. Auxinole uniformly accumulated the *DII-VENUS*

reporter protein by repressing the endogenous IAA activity. The distribution profile of NAA was estimated from the NAA-induced degradation pattern of DII-VENUS protein in root.

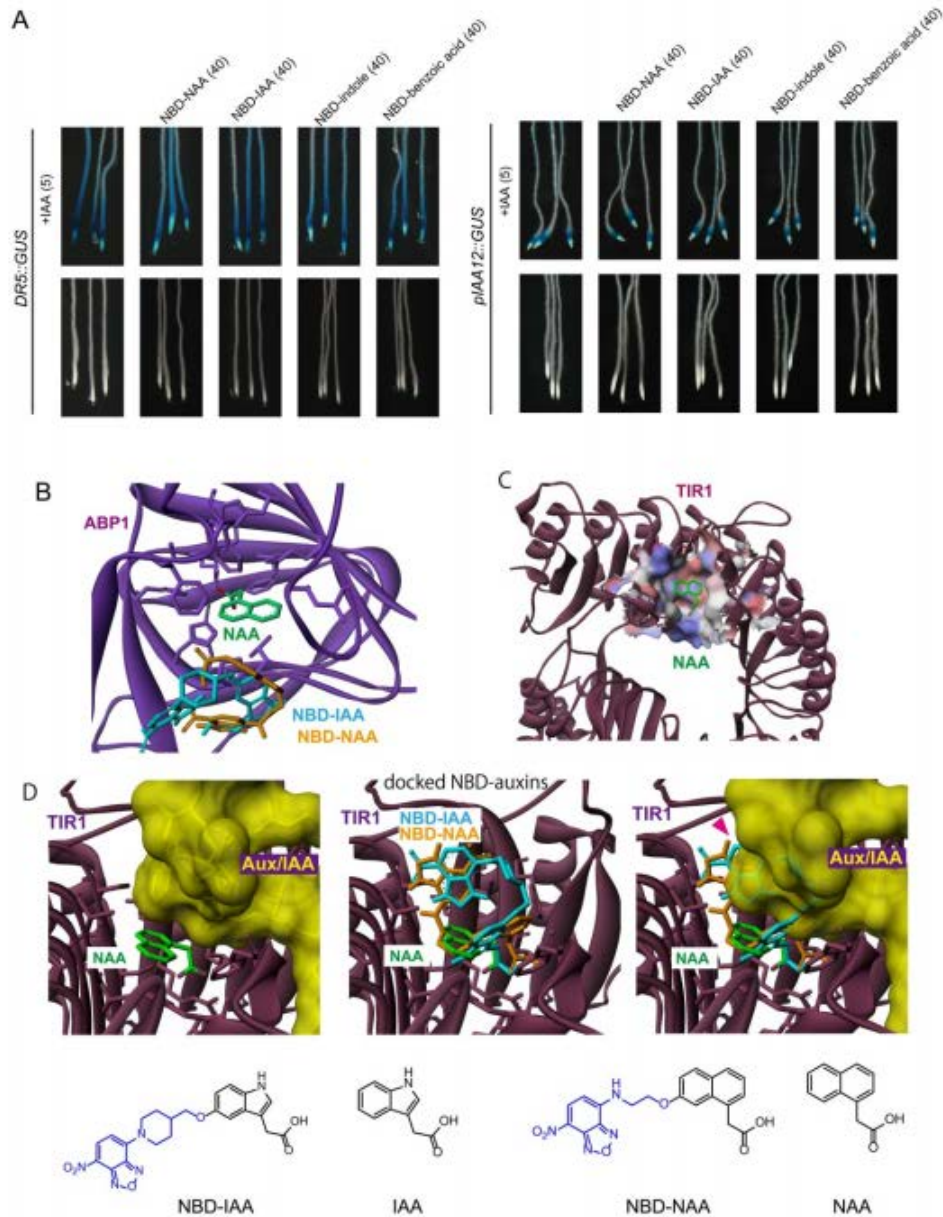


Fig. S5.4. Effects of NBD-analogs on auxin-responsive gene expression and molecular docking analysis of the auxin receptors TIR1 and ABP1. (A) 6-d-old *DR5::GUS* (left) and *pIAA12::GUS* (right) lines were incubated with/without 5 μM IAA, together with NBD-auxins, for 5 h or 16 h, respectively. NBD-IAA, -NAA, -indole and -benzoic acid were inactive regarding IAA-induced gene expression. The values in parentheses indicate the concentrations of chemicals (μM). (B–D)

Molecular docking calculations for NBD-IAA and NBD-NAA at the auxin-binding pockets of *Arabidopsis* Auxin-Binding Protein 1 (ABP1) and TIR1. The NAA molecule within the crystal structures of ABP1 and TIR1 is shown in green. The crystal structure of the ABP1-NAA complex was obtained from a protein data bank [PDB ID, 1LRH]. (B) Blue- and orange-colored molecules represent the predicted binding conformation of NBD-IAA and NBD-NAA to ABP1. The NBD-auxins cannot fit into narrow cavity of the auxin-binding site of ABP1. (C) Structure of the TIR1-NAA complex [PDB ID, 2P1O]. (D) Left panel: The green NAA molecule was placed in a small cavity formed with TIR1 and Aux/IAA (auxin-binding pocket). Middle panel: the blue and orange molecules represent the predicted binding conformations of NBD-IAA and NBD-NAA at the TIR1 auxin-binding site. The NBD-auxins crush the Aux/IAA protein at the TIR1-binding site (red arrow); therefore, the NBD-auxins cannot function as active auxins in the TIR1-Aux/IAA receptor complex.

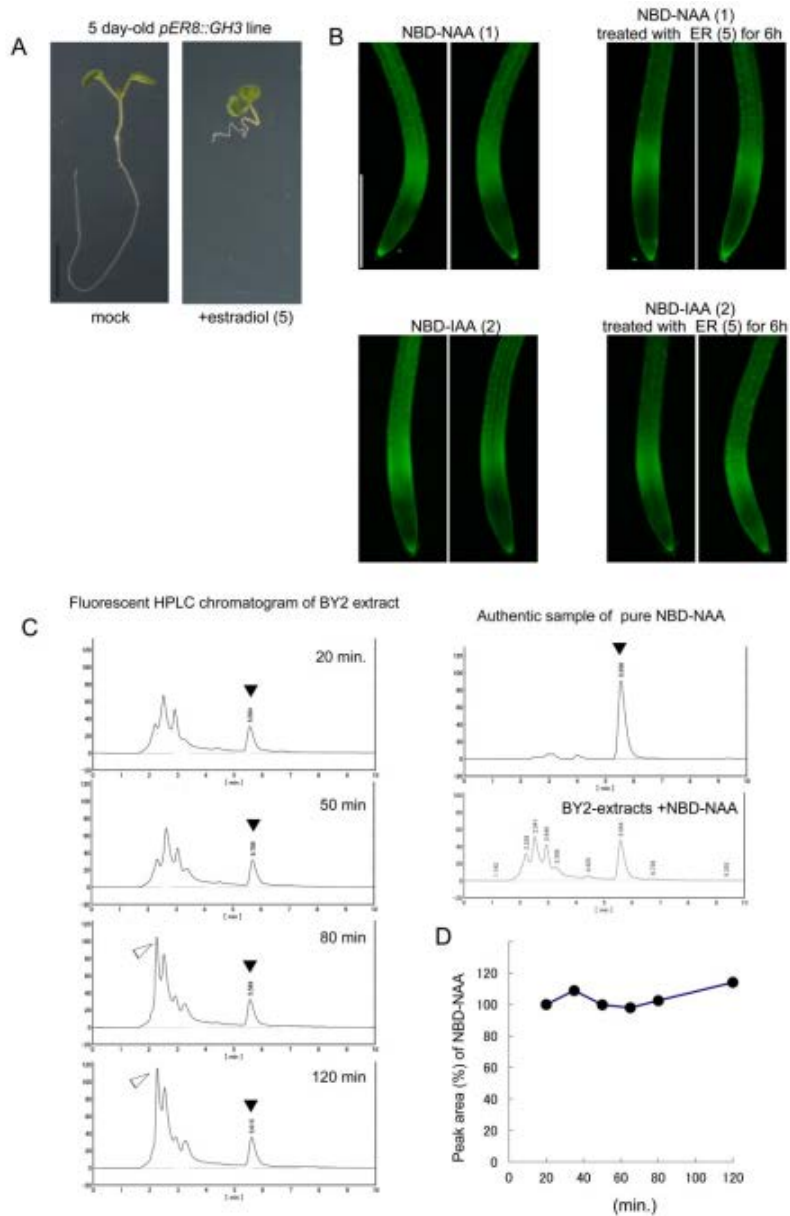


Fig. S5.5. Distribution of NBD-auxins in GH3-overexpressing roots and stability of NBD-NAA in suspension-cultured tobacco BY2 cells. (A) *Arabidopsis* estradiol-inducible *pER8::GH3.6* overexpression line (GH3ox) showed auxin-deficient root phenotype grown with 5 μ M estradiol. Scale bar represents 5 mm. (B) 5-d-old GH3ox seedling was incubated with liquid GM medium containing 5 μ M estradiol for 6 h to induce GH3 protein. After induction of the GH3 enzyme, the seedlings were treated

with medium containing NBD-auxins for 20 min (left panel) or 40 min (right panel), and fluorescence images of roots were subsequently recorded. The values in parentheses indicate the concentrations of chemicals (μM). The fluorescence images showed no effects of GH3 overexpression until 40 min, suggesting that NBD-auxins are a poor substrate for the GH3 enzyme. Scale bar represents 500 μm . (C)

Fluorescent HPLC chromatogram of extracts from tobacco BY2 cells treated with NBD-NAA. BY-2 cells were incubated with 2 μM NBD-NAA at 24°C, and 0.5 ml aliquots of the cultures were collected at regular intervals. A methanol extract from the harvested cells was analyzed via fluorescent HPLC. As a control, NBD-NAA was added to methanol extracts from non-treated cells. The fluorescent HPLC chromatogram was not altered until 50 min of the incubation period had elapsed. (D)

The peak levels of NBD-NAA (HPLC chromatogram) extracted from the cells were maintained during incubation.

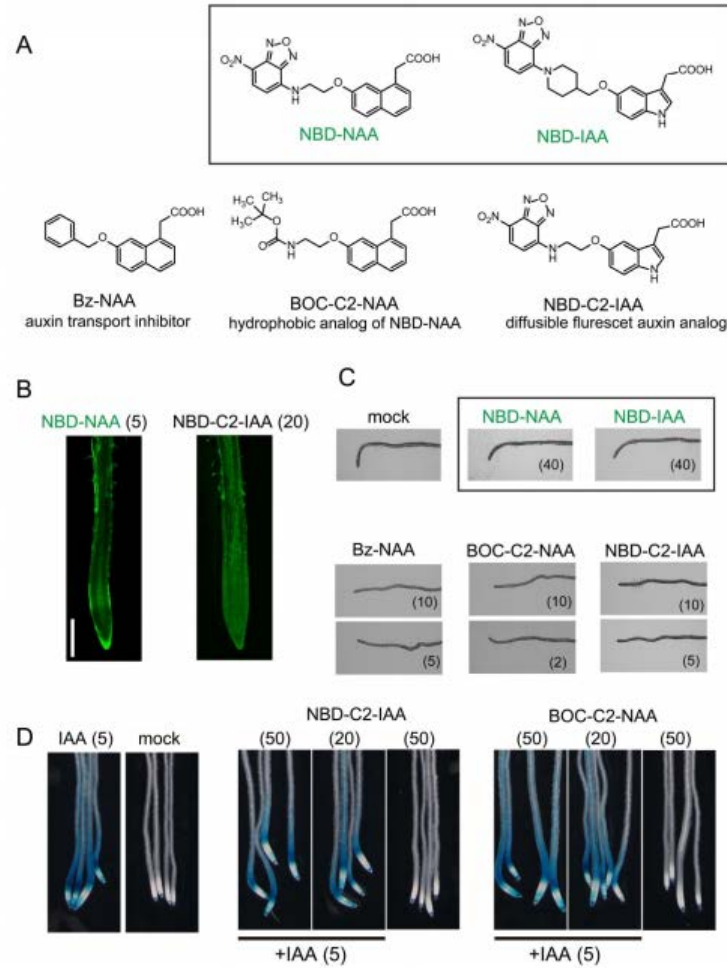


Fig. S5.6. Effects of NBD-auxins and auxin analogs on *Arabidopsis* root gravitropism. (A) Structures of the diffusible fluorescent NBD-auxin NBD-C2-IAA, lipophilic analogs of NBD-NAA BOC-C2-NAA, and auxin transport inhibitors Bz-NAA. (B) Distribution of the diffusible fluorescent NBD-auxin NBD-C2-IAA. 6-d-old seedlings were treated with 10 μ M NBD-C2-IAA for 20 min. In contrast to the asymmetric fluorescent signal of NBD-NAA, a uniform fluorescent signal of NBD-C2-IAA was observed in the root tips. Scale bar represents 200 μ m. (C) Roots (6-d-old) were placed on GM agar plates containing chemicals. The seedlings were grown in the dark for 5 h after rotating the plates at 90° angle against vertical direction. The

values in parentheses indicate the concentrations of chemicals (μM). Bz-NAA, alkoxy-NAA showed potent inhibition of root gravitropism. BOC-C2-NAA, hydrophobic analogs of NBD-NAA, and diffusible NBD-C2-IAA exhibited potent inhibition. These alkoxy auxin analogs are expected to be recognized by auxin transporters and then perturb endogenous auxin movements via competitive inhibition of auxin transport. These data suggest that the membrane permeability of analogs strongly influences inhibitory activity against root gravitropism. (D) Effects of NBD-C2-NAA and BOC-C2-NAA on *DR5::GUS* expression. NBD-C2-NAA and BOC-C2-NAA did not affect *DR5::GUS* expression, indicating that both analogs did not act as auxin nor anti-auxin in SCF^{TIR1}/AFB pathway.

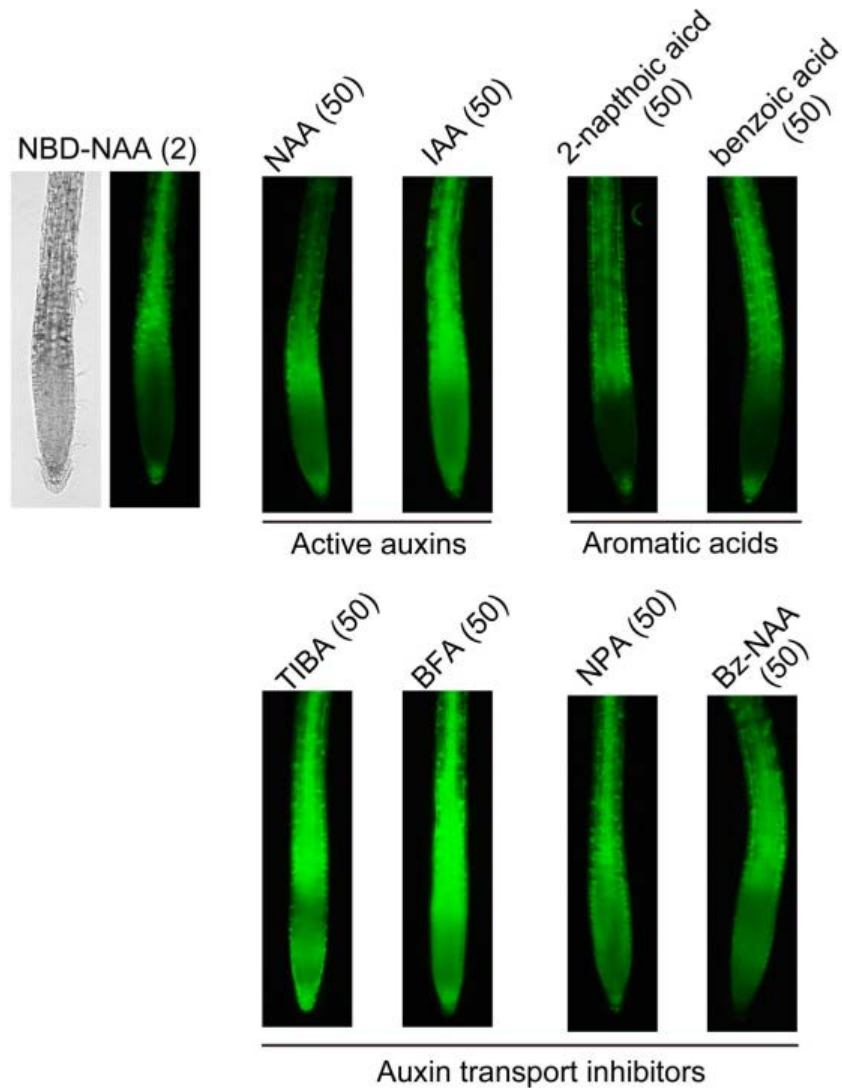


Fig. S5.7. Effects of auxin and transport inhibitors on the NBD-NAA distribution in *Arabidopsis* roots. 6-d-old *Arabidopsis* seedlings were incubated with liquid GM medium containing auxin or aromatic acids for 30 min or with auxin transport inhibitors for 60 min. NBD-NAA was then added to the medium, followed by incubation for another 20 min. Fluorescence images of roots were recorded under identical conditions. The values in parentheses indicate the concentrations of chemicals (μM). IAA and NAA enhanced NBD-NAA accumulation in the meristematic zone, whereas aromatic acids did not. The auxin transport inhibitors

2,4,5-triiodobenzoic acid (TIBA), brefeldin A (BFA), 1-N-naphthylphthalamic acid (NPA), and 7-benzyloxy-NAA (Bz-NAA) increased NBD-NAA accumulation to the same extent as active auxins.

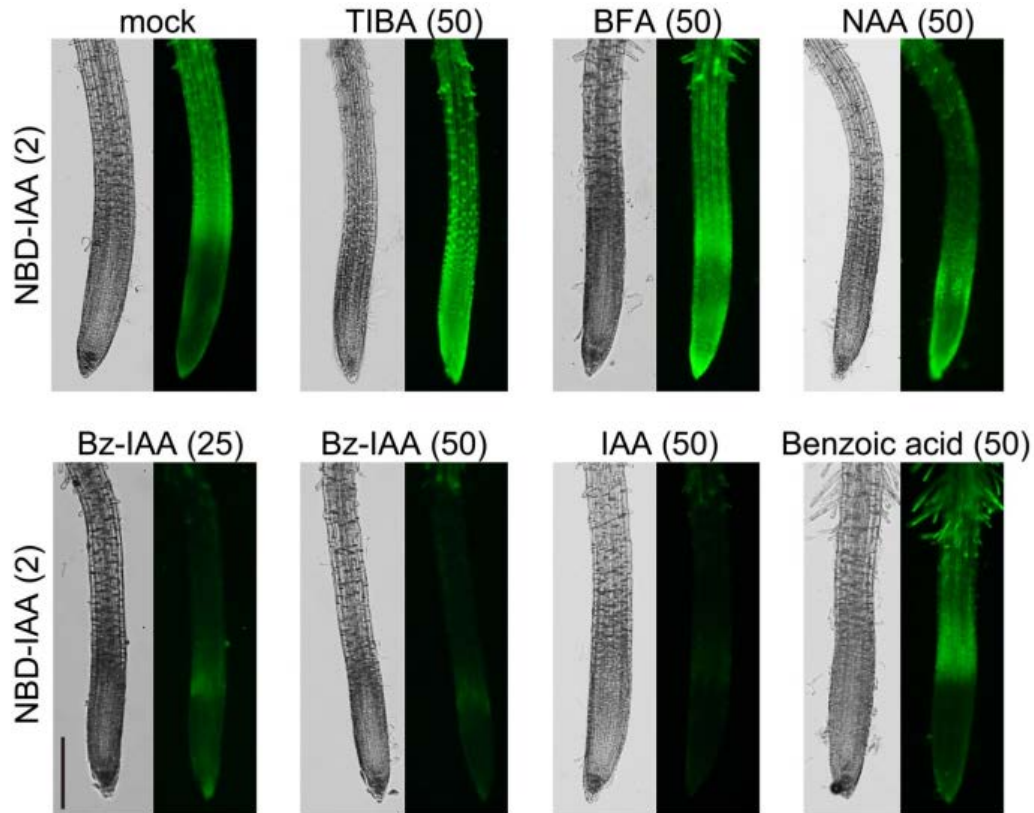


Fig. S5.8. Effects of auxin and transport inhibitors on NBD-IAA distribution in *Arabidopsis* roots. 6-d-old *Arabidopsis* seedlings were incubated with liquid GM medium containing auxin or auxin transport inhibitors for 60 min. NBD-IAA was then added to the medium, followed by incubation for another 20 min. Fluorescence images of roots were recorded under identical conditions. The values in parentheses indicate the concentrations of chemicals (μM). NAA and the auxin transport inhibitors TIBA and BFA enhanced NBD-IAA accumulation in the meristematic zone, whereas benzoic acids did not. IAA and 5-Benzyloxy-IAA (Bz-IAA) reduced the fluorescent signals via competitive inhibition of AUX1/LAX-mediated NBD-IAA import. Scale bar represents 200 μm .

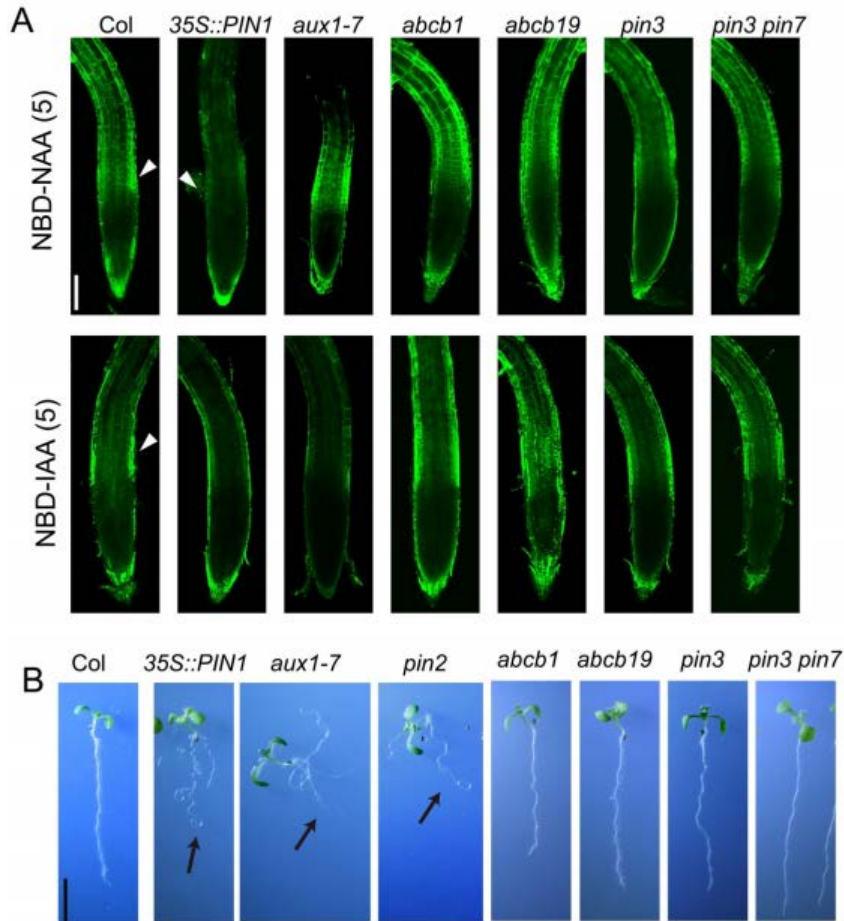


Fig. S5.9. Distribution of NBD-auxins in *Arabidopsis* transport mutants

35S::PIN1, *aux 1-7*, *abcb1*, *abcb19*, *pin3* and *pin3pin7*. (A) 6-d-old *Arabidopsis* seedlings incubated with liquid GM medium containing 5 μ M NBD-IAA and 5 μ M NBD-NAA for 20 min. Fluorescent confocal images of roots were recorded under identical conditions. The accumulation of NBD-auxins in the elongation zone was disappeared in PIN1 overexpression (*35S::PIN1*) mutant. The fluorescent signal of NBD-IAA was reduced in *aux1-7* roots due to a loss-of-function mutation in *aux1* importer. On the contrary, NBD-NAA is expected to bypass the AUX1 importer in the same manner as original NAA molecule. The *abcb1*, *abcb19*, *pin3* and *pin3 pin7* mutants showed similar distribution profile of NBD-auxins to that in wild-type (Col).

Scale bar represents 100 μm . The values in parentheses indicate the concentrations of chemicals (μM). (B) Root phenotypes in *35S::PIN1*, *aux1-7*, *pin2/eir1-1*, *abcb1*, *abcb19*, *pin3* and *pin3pin7*. The *35S::PIN1*, *aux1-7* and *pin2/eir1-1* mutants displayed highly agravitropic root phenotype. These agravitropic root phenotype would be correlated with abnormal distribution pattern of NBD-auxins. Scale bar represents 5 mm.

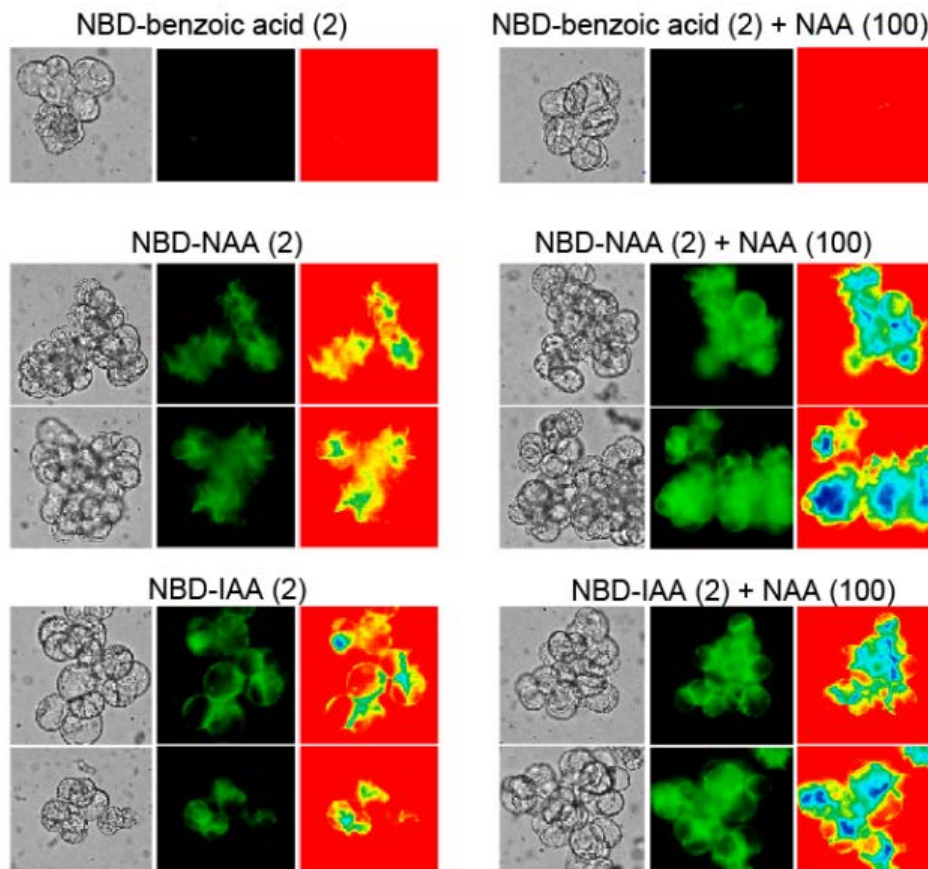


Fig. S5.10. The excess NAA accumulated NBD-auxins in *Arabidopsis* cultured cell. *Arabidopsis* MM1 cultured cell were incubated with 100 μ M NAA for 10 min and then treated with 2 μ M NBD-analogs with/without 100 μ M NAA for 30 min. The values in parentheses indicate the concentrations of chemicals (μ M).

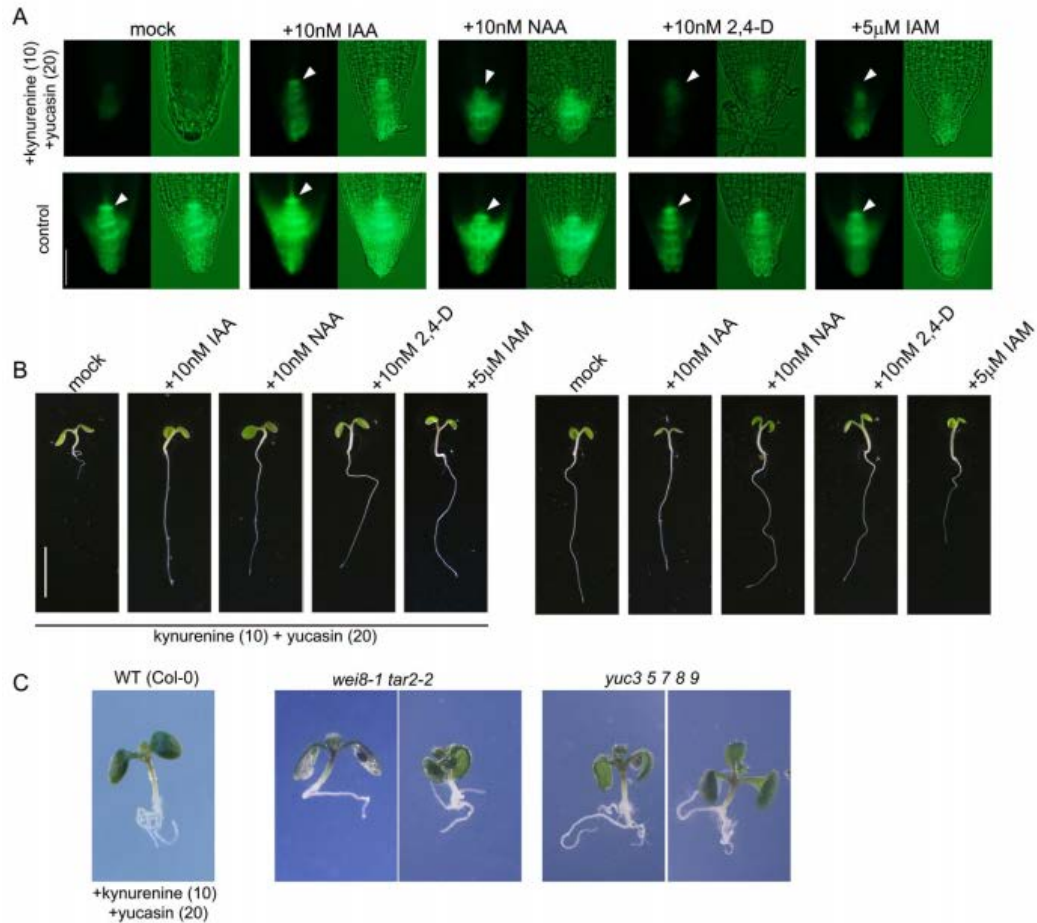


Fig. S5.11. Effects of exogenous auxins on the *DR5::GFP* expression profile in endogenous auxin-depleted roots. *DR5::GFP* line were grown for 5 days on medium containing auxin biosynthesis inhibitors (10 μ M kynurenine, a TAA1 inhibitor, and 20 μ M yucasin, a YUC inhibitor) with/without auxins. (A) *DR5::GFP* maxima in endogenous auxin-deficient (upper) and control (lower) roots. The *DR5::GFP* expression profile in the root apex was not fully restored by the application of exogenous auxins. (B) Phenotype of endogenous auxin-deficient and control seedlings in the presence of exogenous auxins. The application of exogenous auxins restored the growth defects observed in auxin-deficient seedlings. The values in parentheses indicate the concentrations of chemicals (μ M). (C) The phenotype of

auxin biosynthesis mutants *wei8-1 tar2-2*, *yuc 3 5 7 8 9* and wild-type plant (*Col-0*)
treated with kynurenine and yucain. The values in parentheses indicate the
concentrations of chemicals (μM).

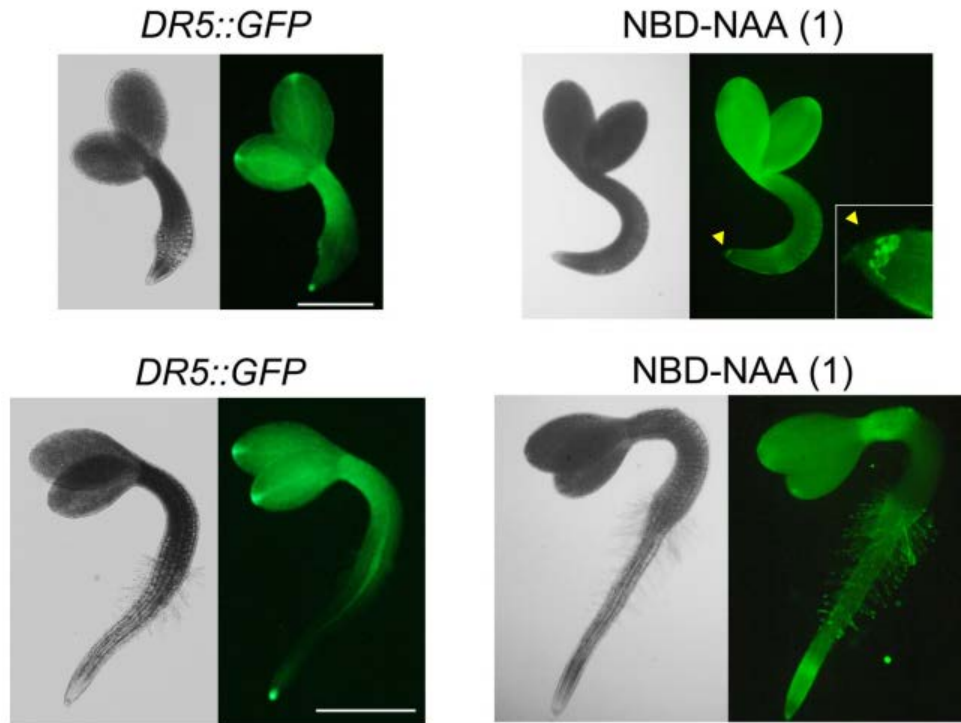


Fig. S5.12. Distribution of NBD-NAA in *Arabidopsis* seedlings. The wild-type seedlings (just germinated and 2-days old) were incubated with liquid GM medium containing 1 μM NBD-NAA for 20 min. The fluorescent image of *DR5::GFP* seedlings was obtained at same growth period. Scale bar represents 500 μm . The values in parentheses indicate the concentrations of chemicals (μM).

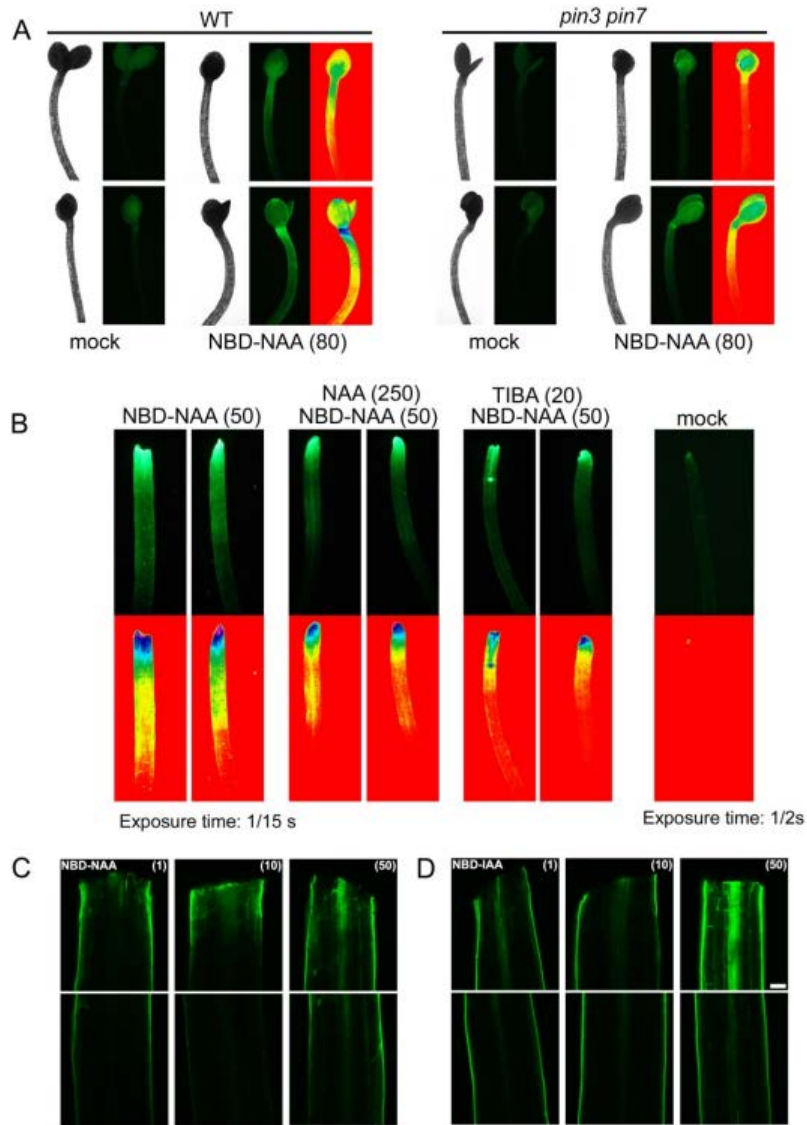


Fig. S5.13. Transport of NBD-auxin in *Arabidopsis* hypocotyl. (A) Distribution of NBD-NAA in 4-d-old etiolated *Arabidopsis* hypocotyls of wild-type (Col-0) and *pin3 pin7* mutant. 0.2 μ l droplet of 0.1 % agarose containing 80 μ M NBD-NAA was placed on apical cotyledon, and then incubated for 4 h in the dark. (B) Effects of NAA and auxin transport inhibitor on NBD-NAA transport in decapitated etiolated hypocotyls. The decapitated hypocotyls were inverted in 5 μ l of medium containing NAA or TIBA in 0.5 ml microcentrifuge tubes and incubated for 1 h in the dark.

0.1% agar solution (5 μ l) of NBD-NAA was added into the tube at 50 μ M final concentration, and then incubated for additional 3h. (C, D) Distribution of NBD-auxins in decapitated etiolated hypocotyls. The decapitated hypocotyls were inverted in 15 μ l of medium containing NBD-auxin in 1.5 ml microcentrifuge tubes and incubated for 2-3 h in the dark. Scale bar represents 50 μ m. Upper panels show decapitation site, lower panels areas 1-2mm below decapitation site.

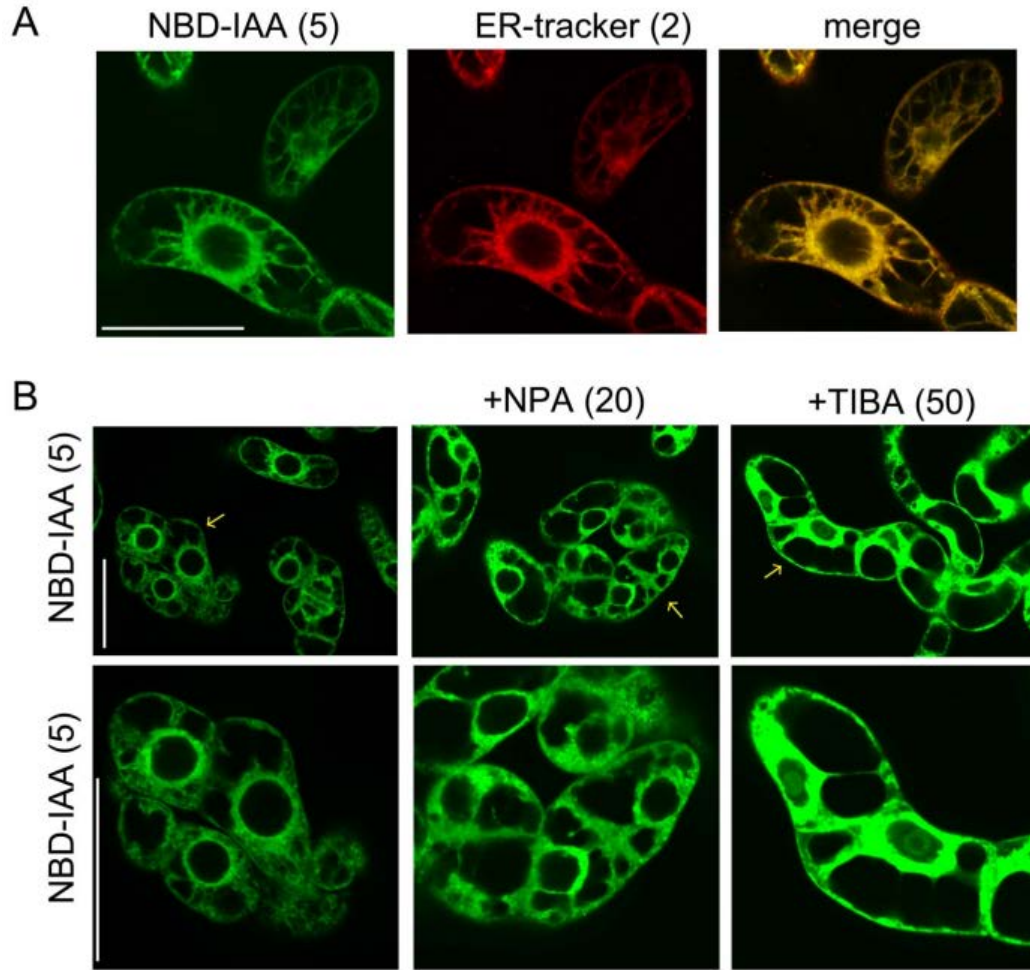


Fig. S5.14. Subcellular distribution of NBD-IAA in tobacco suspension BY-2 cells. (A) Subcellular distribution of NBD-IAA in tobacco BY2 cells. The cells were incubated with NBD-IAA and ER-tracker for 20 min. (B) Auxin transport inhibitors, NPA and TIBA accumulated subcellular NBD-IAA in tobacco BY2 cells. The cells were pre-incubated with auxin transport inhibitors, NPA or TIBA for 4 h and then NBD-IAA was added. The confocal images were recorded after 20 min incubation. The values in parentheses indicate the concentrations of chemicals (μM). Scale bar represents 50 μm .

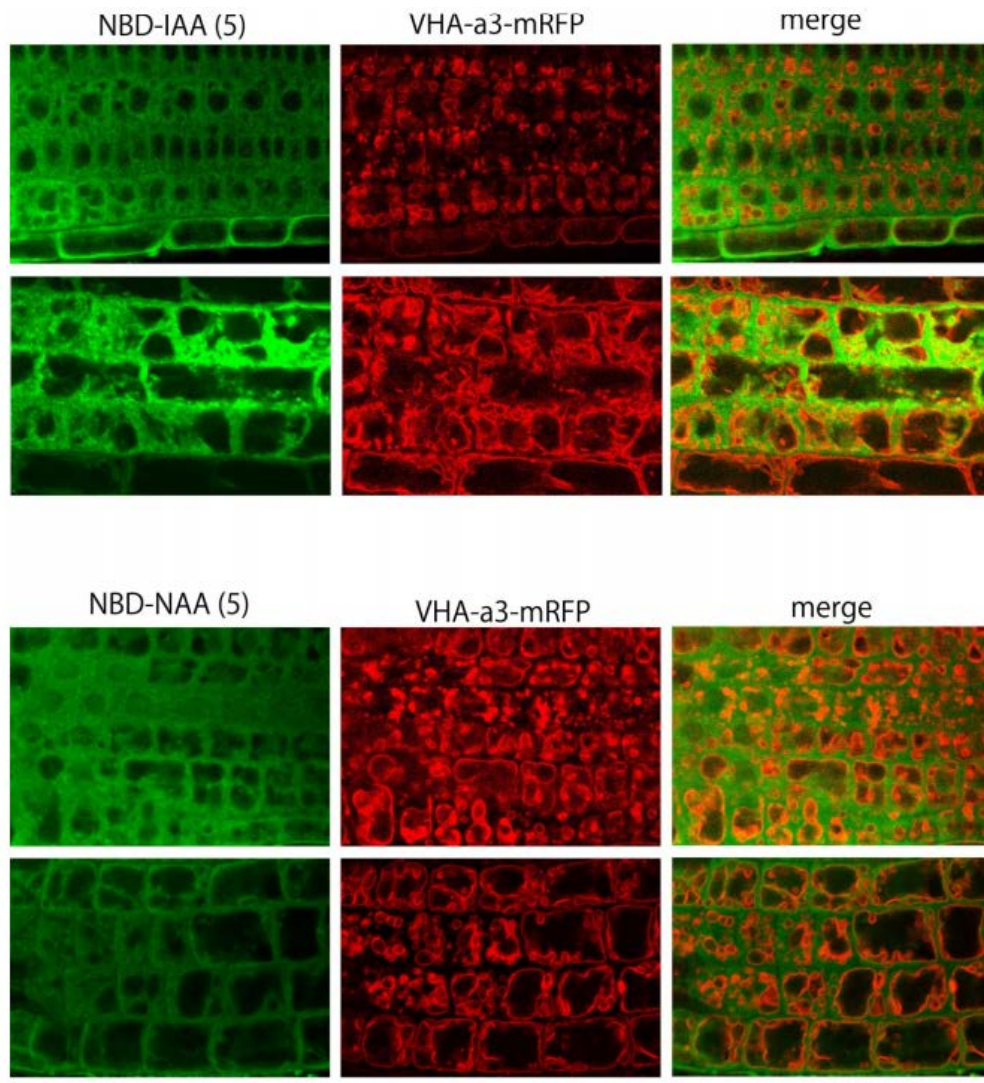


Fig. S5.15. Subcellular distribution of NBD-IAA in root expressing tonoplast marker, VHA-a3-mRFP. Subcellular distribution of NBD-auxin in root expressing tonoplast marker, VHA-a3-mRFP. The root was treated with 5 μ M NBD-auxin for 30 min. The values in parentheses indicate the concentrations of chemicals (μ M). Scale bar represents 50 μ m.

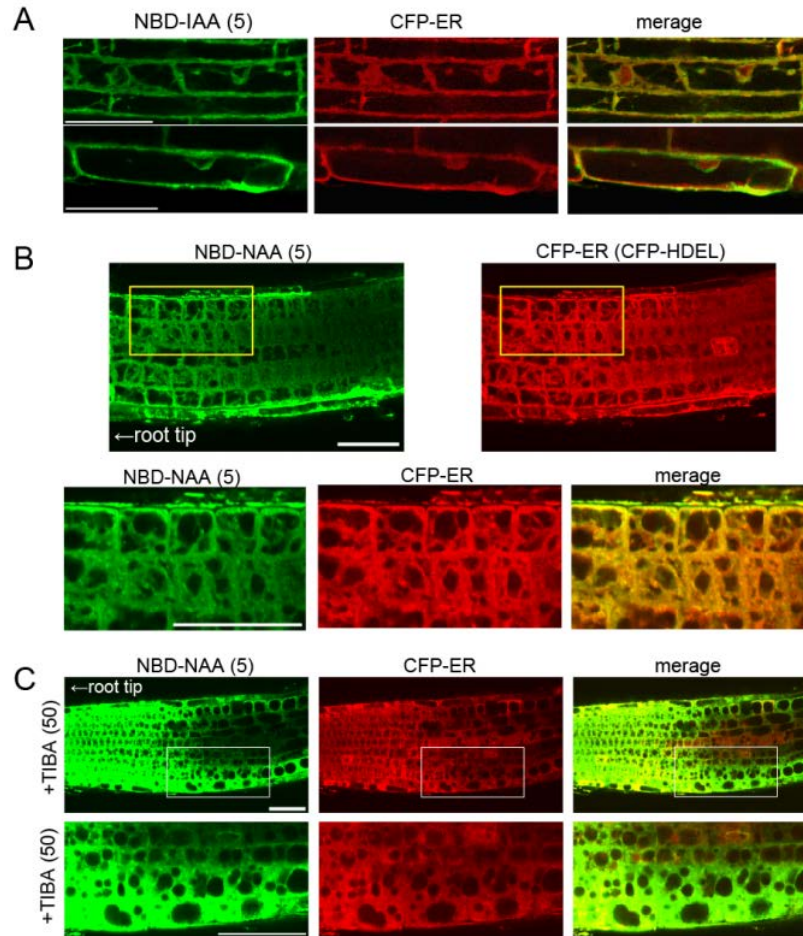


Fig. S5.16. Subcellular distribution of NBD-IAA in root expressing ER marker, CFP-HDEL. (A) Subcellular distribution of NBD-IAA in root expressing ER marker, CFP-HDEL (CFP-ER: ABRC CS16250 line). The root was treated with 5 μM NBD-IAA for 20 min. (B) Subcellular distribution of NBD-NAA in root cell expressing ER marker, CFP-ER. The CFP-ER root was treated with 5 μM NBD-NAA for 20 min. (C) The CFP-ER seedling was incubated with 50 μM TIBA for 4h and the NBD-NAA was added to final concentration of 5 μM. The root was incubated for additional 20 min. The values in parentheses indicate the concentrations of chemicals (μM).

Scale bar represents 20 μm.

Appendix B. Lines used in this dissertation.

Gene Locus	Protein	Mutant	T-DNA Insertion	Reference
AT2G36910	ABCB1	<i>abcb1-1 (pgp1-1)</i>		Noh et al., 2001*
		<i>abcb1-100</i>		Lin and Wang, 2005
AT4G25960	ABCB2	<i>abcb2-1</i>	Salk_025155	
		<i>abcb2-2</i>	WiscDsLox340 G08	
AT2G47000	ABCB4	<i>abcb4-1</i>	Salk_063720	Terasaka et al., 2005
AT2G39480	ABCB6	<i>abcb6-1</i>	Sail_7_C04.v1	
AT1G02520	ABCB11	<i>abcb11-1</i>	Salk_057628	
AT1G02530	ABCB12	<i>abcb12-1</i>	Salk_094249	Kaneda et al., 2011
AT1G28010	ABCB14	<i>abcb14-1</i>	Salk_016005	Kaneda et al., 2011
AT3G28345	ABCB15	<i>abcb15-3</i>	Salk_034562	
AT3G28860	ABCB19	<i>abcb19-1 (pgp19-1)</i>		Noh et al., 2001*
		<i>mdr1-101</i>		Lin and Wang, 2005
		GFP-ABCB19		Mravec et al., 2008
AT3G62150	ABCB21	<i>abcb21-1</i>	WiscDsLox1C2	Kamimoto et al., 2012
		<i>abcb21-2</i>	Gabi_954H06	
DII- VENUS				Brunoud et al., 2012

* Original Ws alleles from Noh et al. (2001) were backcrossed into Col-0 five times and were verified phyD+ by PCR.

Appendix C. Primers used in this dissertation.

RNAi Constructs		
Construct	5'-Sequence-3'	Sense
<i>B2/10-RNAi</i>	CACCCAGAGTCGCCAAGTACTCGT GTACGGTCCTCACATTCCCGA	For. Rev.
<i>B3/5/11/12-RNAi</i>	CACCCGCGAGGATAAGAAGTACATATC GATGTTATGAACTTCTTGTAAGCTGTTAATG	For. Rev.
<i>B13/14-RNAi</i>	CACCCTCGCGTTTCACAGAATGCT CATGACTATAGCATACCCTCCTC	For. Rev.

<i>B15/16/17/18-RNAi</i>	CACCCACTTCCTCTTCCAATAATAAA CTCCACATCAAGATGAAACTC	For. Rev.
Quantitative real-time PCR		
Gene	5'-Sequence-3'	Sense
<i>ABCB1</i>	TCTCTTGCTTTGGTACGGTG CTCGGTGCTGATTGTCCC	For. Rev.
<i>ABCB2</i>	TTCGTCGCCATCGGACTTATTGCT TTGTACGGTCCTCACATTCCCGAT	For. Rev.
<i>ABCB3</i>	GCCTATCGAGCGAGTGTTAAGCAA AGACATCGAACTTGCACCACAGT	For. Rev.
<i>ABCB4</i>	GAGACGCGAGTGAATCCGAA ATCATAACCCTGTTGCAGACCA	For. Rev.
<i>ABCB5</i>	GCTTTGGGTACATGGTTTGGTGGT ACAAGGTGATGCTTGCCCTAAAGC	For. Rev.
<i>ABCB6</i>	ACAACCGTTAACTCCTGTTTC CATTCCTCCTCATCATCCG	For. Rev.
<i>ABCB7</i>	CCGTTGGTGAACGTGGAGTA CCTGATCAAGCGCATCTTGC	For. Rev.
<i>ABCB9</i>	CGTAGTTTTGATGACCGTCG TTACAGCAACCTTCCACACT	For. Rev.
<i>ABCB10</i>	ATCGCAGAAGAGGTGATCGGGAAT AATGCAACGAACCAAGCCCTAGTC	For. Rev.
<i>ABCB11</i>	CGCAGCTCATTTCGATTACAAG ACGAAGTTCCCTCCATTGAC	For. Rev.
<i>ABCB12</i>	TGCTTCCCTTGTTTCAGCTTCA GCTACATAAACTTGCATACAACAACATAA	For. Rev.
<i>ABCB13</i>	TCTCATTGCGGCTTCACTTACCGA GACAAAGGCATTCTTGGTGGGCTT	For. Rev.
<i>ABCB14</i>	CTGCTAAAGCAGCCAACGCAGATT TGCCCTCCTGAAAGTTGAGTTCCT	For. Rev.
<i>ABCB15</i>	TCGTTAGTGGGTGATCGAATGGCA ACCCGACGAGGTGATGAGCAAACA	For. Rev.
<i>ABCB16</i>	TTGGACAGCCAATCAGAGCGTGTA TCGTGCTAAGCCTATGTGCGATCA	For. Rev.
<i>ABCB17</i>	AAGCGGATCGGGTAAATCGACAGT TGCGACCTCAACCAATTCATTGC	For. Rev.
<i>ABCB18</i>	AAGCTTGGGTTGAGACAAGGGCTA ACCGAAGGTGACGCAAACAATGAC	For. Rev.
<i>ABCB19</i>	AGGATTGACCCGGATGATGCTGAT TCGGGTCTTGAAGGGTAAGCGAAA	For. Rev.
<i>ABCB20</i>	TCAGCAGAGATCTGAACACC GCAAGACACCTCAATCCAAC	For. Rev.
<i>ABCB21</i>	TCGCTCATACTGCTACAAGAAGATACTAAACA G CGAAAGAGACTTTCTTTTCTTTGATCGG	For. Rev.

<i>ABCB22</i>	TTCGTTGGGGAGAGACAAGC GACGTCTTGGATCACGAGGG	For. Rev.
<i>PP2A</i>	TCGTGGTGCAGGCTACACTTTC TCAGAGAGAGTCCATTGGTGTGG	For. Rev.
<i>ACT2</i>	ACACTGTGCCAATCTACGAGGGTT ACAATTTCCCGCTCTGCTGTTGTG	For. Rev.
Promoter:GUS Constructs		
Construct	5'-Sequence-3'	Sense
<i>ABCB11</i>	CACCTGGACCCTCATGTTTTTCCTT ATTTCCGGCGCTGACAAAAATCAG	For. Rev.
<i>ABCB21</i>	CACCAATTGTAAAGAAAAAGTTATGAGTC TGTTCTTTGATCCTATCAAGA	For. Rev.
Expression in <i>S.pombe</i>		
<i>ABCB11</i>	ATCATATGATGAACGGTGACGGCGCCAGAGAA G ATCCCGGGTCAATTAGAAGCAGTCATGTGAAG CTG	For. Rev.
<i>ABCB21</i>	GGGGACAAGTTTGTACAAAAAAGCAGGCTTCA TGGATAGTGTAATAGAATCAGAG GGGGACCACTTTGTACAAGAAAGCTGGGTCCT ATTATGTAGAAGCACTCAGATGAAGTTG	For. Rev.
Genotyping		
<i>b11-1</i> SALK_057628	TGGCATCTTGAATAAGAACCG ATTTTACGGGCAAGCAAAAAG	For. Rev.
WiscDsLox1C2	AATCGACAGTGATTGCGTTG TTAACCATAACCCGGTCCAA	For. Rev.
Gabi_954H06	TTCTCCACGATGACTCCATTC TCATTGTCTCCTGATTCCAGC	For. Rev.
LBb1.3	ATTTTGCCGATTTCCGGAAC	
p745	AACGTCCGCAATGTGTTATTAAGTTGTC	
o8409	ATATTGACCATCATACTCATTGC	

Bibliography

- Adamowski M, Friml J** (2015) PIN-dependent auxin transport: action, regulation, and evolution. *Plant Cell* **27**: 20–32
- Aller SG, Yu J, Ward A, Weng Y, Chittaboina S, Zhuo R, Harrell PM, Trinh YT, Zhang Q, Urbatsch IL, et al** (2009) Structure of P-glycoprotein reveals a molecular basis for poly-specific drug binding. *Science* (80-) **323**: 1718–22
- Ambudkar S V, Kim I-W, Sauna ZE** (2006) The power of the pump: mechanisms of action of P-glycoprotein (ABCB1). *Eur J Pharm Sci* **27**: 392–400
- Arase F, Nishitani H, Egusa M, Nishimoto N, Sakurai S, Sakamoto N, Kaminaka H** (2012) IAA8 Involved in Lateral Root Formation Interacts with the TIR1 Auxin Receptor and ARF Transcription Factors in Arabidopsis. *PLoS One* **7**: e43414
- Arsuffi G, Braybrook SA** (2018) Acid growth: an ongoing trip. *J Exp Bot* **69**: 137–146
- Bailly A, Wang B, Zwiewka M, Pollmann S, Schenck D, Lüthen H, Schulz A, Friml J, Geisler M** (2013) Expression of TWISTED DWARF1 lacking its in-plane membrane anchor leads to increased cell elongation and hypermorphic growth. *Plant J* n/a-n/a
- Bailly A, Yang H, Martinoia E, Geisler M, Murphy AS** (2011) Plant Lessons: Exploring ABCB Functionality Through Structural Modeling. *Front Plant Sci* **2**: 108
- Bainbridge K, Guyomarc'h S, Bayer E, Swarup R, Bennett M, Mandel T, Kuhlemeier C** (2008) Auxin influx carriers stabilize phyllotactic patterning.

Genes Dev **22**: 810–23

- Bakos E, Klein I, Welker E, Szabo K** (1997) Characterization of the human multidrug resistance protein containing mutations in the ATP-binding cassette signature region. *Biochem J* **323**: 777–783
- Band LR, Wells DM, Fozard JA, Ghetiu T, French AP, Pound MP, Wilson MH, Yu L, Li W, Hijazi HI, et al** (2014) Systems Analysis of Auxin Transport in the *Arabidopsis* Root Apex. *Plant Cell* **26**: 862–875
- Bandyopadhyay A, Blakeslee JJ, Lee OR, Mravec J, Sauer M, Titapiwatanakun B, Makam SN, Bouchard R, Geisler M, Martinoia E, et al** (2007) Interactions of PIN and PGP auxin transport mechanisms. *Biochem Soc Trans* **35**: 137–141
- Barbez E, Kleine-Vehn J** (2013) Divide Et Impera—cellular auxin compartmentalization. *Curr Opin Plant Biol* **16**: 78–84
- Barbez E, Kubeš M, Rolčík J, Béziat C, Pěňčík A, Wang B, Rosquete MR, Zhu J, Dobrev PI, Lee Y, et al** (2012) A novel putative auxin carrier family regulates intracellular auxin homeostasis in plants. *Nature* **485**: 119–22
- Barbez E, Laňková M, Pařezová M, Maizel A, Zažímalová E, Petrášek J, Friml J, Kleine-Vehn J** (2013) Single-cell-based system to monitor carrier driven cellular auxin homeostasis. *BMC Plant Biol* **13**: 20
- Baster P, Robert S, Kleine-Vehn J, Vanneste S, Kania U, Grunewald W, De Rybel B, Beeckman T, Friml J** (2012) SCFTIR1/AFB-auxin signalling regulates PIN vacuolar trafficking and auxin fluxes during root gravitropism. *EMBO J* **32**: 260–274
- Benková E, Michniewicz M, Sauer M, Teichmann T, Seifertová D, Jürgens G,**

- Friml JJ** (2003) Local, Efflux-Dependent Auxin Gradients as a Common Module for Plant Organ Formation. *Cell* **115**: 591–602
- Beveridge CA** (2000) Long-distance signalling and a mutational analysis of branching in pea. *Plant Growth Regul* **32**: 193–203
- Bhalerao RP, Eklöf J, Ljung K, Marchant A, Bennett M, Sandberg G** (2002) Shoot-derived auxin is essential for early lateral root emergence in *Arabidopsis* seedlings. *Plant J* **29**: 325–332
- Bhattacharya C, Bonfante P, Deagostino A, Kapulnik Y, Larini P, Occhiato EG, Prandi C, Venturello P** (2009) A new class of conjugated strigolactone analogues with fluorescent properties: synthesis and biological activity. *Org Biomol Chem* **7**: 3413
- Blakeslee JJ, Bandyopadhyay A, Lee OR, Mravec J, Titapiwatanakun B, Sauer M, Makam SN, Cheng Y, Bouchard R, Adamec J, et al** (2007) Interactions among PIN-FORMED and P-glycoprotein auxin transporters in *Arabidopsis*. *Plant Cell* **19**: 131–47
- Bouchard R, Bailly A, Blakeslee JJ, Oehring SC, Vincenzetti V, Lee OR, Paponov I, Palme K, Mancuso S, Murphy AS, et al** (2006) Immunophilin-like TWISTED DWARF1 modulates auxin efflux activities of *Arabidopsis* P-glycoproteins. *J Biol Chem* **281**: 30603–12
- Brown B, Phillips J** (1982) The Transport Behaviour of the Synthetic Auxin 2,4-Dichlorophenoxyacetic Acid in Decapitated Seedlings of Sunflower (*Helianthus annuus* L.). *Aust J Plant Physiol* **9**: 5
- Brunoud G, Wells DM, Oliva M, Larrieu A, Mirabet V, Burrow AH, Beeckman**

- T, Kepinski S, Traas J, Bennett MJ, et al** (2012) A novel sensor to map auxin response and distribution at high spatio-temporal resolution. *Nature* **482**: 103–6
- BruX A, Liu T-Y, Krebs M, Stierhof Y-D, Lohmann JU, Miersch O, Wasternack C, Schumacher K** (2008) Reduced V-ATPase Activity in the trans-Golgi Network Causes Oxylin-Dependent Hypocotyl Growth Inhibition in Arabidopsis. *PLANT CELL ONLINE* **20**: 1088–1100
- Busse JS, Evert RF** (1999) Vascular Differentiation and Transition in the Seedling of Arabidopsis thaliana (Brassicaceae). *Int J Plant Sci* **160**: 241–251
- Calderón Villalobos LIA, Lee S, De Oliveira C, Ivetac A, Brandt W, Armitage L, Sheard LB, Tan X, Parry G, Mao H, et al** (2012) A combinatorial TIR1/AFB–Aux/IAA co-receptor system for differential sensing of auxin. *Nat Chem Biol* **8**: 477–485
- Campanella JJ, Larko D, Smalley J** (2003) A molecular phylogenomic analysis of the ILR1-like family of IAA amidohydrolase genes. *Comp Funct Genomics* **4**: 584–600
- Cecchetti V, Brunetti P, Napoli N, Fattorini L, Altamura MM, Costantino P, Cardarelli M** (2015) ABCB1 and ABCB19 auxin transporters have synergistic effects on early and late Arabidopsis anther development. *J Integr Plant Biol* **57**: 1089–98
- Chaiwanon J, Garcia VJ, Cartwright H, Sun Y, Wang ZY** (2016) Immunophilin-like FKBP42/TWISTED DWARF1 Interacts with the Receptor Kinase BRI1 to Regulate Brassinosteroid Signaling in Arabidopsis. *Mol Plant* **9**: 593–600
- Chandler JW, Werr W** (2015) Cytokinin–auxin crosstalk in cell type specification.

Trends Plant Sci **20**: 291–300

Chen Q, Dai X, De-Paoli H, Cheng Y, Takebayashi Y, Kasahara H, Kamiya Y,

Zhao Y (2014) Auxin Overproduction in Shoots Cannot Rescue Auxin

Deficiencies in Arabidopsis Roots. *Plant Cell Physiol* **55**: 1072–1079

Chen R, Hilson P, Sedbrook J, Rosen E, Caspar T, Masson PH (1998) The

Arabidopsis thaliana AGRVITROPIC 1 gene encodes a component of the

polar-auxin-transport efflux carrier. *Proc Natl Acad Sci U S A* **95**: 15112–15117

Cho M, Henry EM, Lewis DR, Wu G, Muday GK, Spalding EP (2014) Block of

ATP-binding cassette B19 ion channel activity by 5-nitro-2-(3-

phenylpropylamino)-benzoic acid impairs polar auxin transport and root

gravitropism. *Plant Physiol* **166**: 2091–9

Cho M, Lee SH, Cho H-T (2007) P-glycoprotein4 displays auxin efflux transporter-

like action in Arabidopsis root hair cells and tobacco cells. *Plant Cell* **19**: 3930–

43

Christie JM, Yang H, Richter GL, Sullivan S, Thomson CE, Lin J,

Titapiwatanakun B, Ennis M, Kaiserli E, Lee OR, et al (2011) phot1

inhibition of ABCB19 primes lateral auxin fluxes in the shoot apex required for

phototropism. *PLoS Biol* **9**: e1001076

Chufan EE, Kapoor K, Sim H-M, Singh S, Talele TT, Durell SR, Ambudkar S V

(2013) Multiple transport-active binding sites are available for a single substrate

on human P-glycoprotein (ABCB1). *PLoS One* **8**: e82463

Conte SS, Lloyd AM (2011) Exploring multiple drug and herbicide resistance in

plants-Spotlight on transporter proteins. *Plant Sci* **180**: 196–203

- Cooper WC** (1935) Hormones in Relation To Root Formation on Stem Cuttings.
Plant Physiol **10**: 789–94
- Darwin C** (1880) The Power of Movement in Plants. John Murray, London
- Dawson RJP, Locher KP** (2006) Structure of a bacterial multidrug ABC transporter.
Nature **443**: 180–5
- Demir F, Hortrich C, Blachutzik JO, Scherzer S, Reinders Y, Kierszniowska S, Schulze WX, Harms GS, Hedrich R, Geiger D, et al** (2013) Arabidopsis nanodomain-delimited ABA signaling pathway regulates the anion channel SLAH3. Proc Natl Acad Sci **110**: 8296–8301
- Ding Z, Wang B, Moreno I, Dupláková N, Simon S, Carraro N, Reemmer J, Pěňčík A, Chen X, Tejos R, et al** (2012) ER-localized auxin transporter PIN8 regulates auxin homeostasis and male gametophyte development in Arabidopsis.
Nat Commun **3**: 941
- Douillard FP, Mahony J, Campanacci V, Cambillau C, van Sinderen D** (2011) Construction of two Lactococcus lactis expression vectors combining the Gateway and the NIsin Controlled Expression systems. Plasmid **66**: 129–135
- Dudler R, Hertig C** (1992) Structure of an mdr-like gene from Arabidopsis thaliana. Evolutionary implications. J Biol Chem **267**: 5882–5888
- Duhamel du Monceau H-L** (1758) La Physique des arbres, 1st ed.
- Eswar N, Webb B, Marti-Renom MA, Madhusudhan MS, Eramian D, Shen M-Y, Pieper U, Sali A** (2006) Comparative protein structure modeling using Modeller. Curr Protoc Bioinforma. doi:
10.1002/0471250953.bi0506s15.Comparative

Frelet-Barrand A, Boutigny S, Moyet L, Deniaud A, Seigneurin-Berny D, Salvi D, Bernaudat F, Richaud P, Pebay-Peyroula E, Joyard J, et al (2010)

Lactococcus lactis, an alternative system for functional expression of peripheral and intrinsic Arabidopsis membrane proteins. *PLoS One* **5**: e8746

Frelet-Barrand A, Kolukisaoglu HU, Plaza S, Rüffer M, Azevedo L, Hörtensteiner S, Marinova K, Weder B, Schulz B, Klein M (2008)

Comparative mutant analysis of Arabidopsis ABCC-type ABC transporters: AtMRP2 contributes to detoxification, vacuolar organic anion transport and chlorophyll degradation. *Plant Cell Physiol* **49**: 557–69

Friml J, Vieten A, Sauer M, Weijers D, Schwarz H, Hamann T, Offringa R, Jürgens G (2003) Efflux-dependent auxin gradients establish the apical-basal

axis of Arabidopsis. *Nature* **426**: 147–53

Friml J, Wiśniewska J, Benková E, Mendgen K, Palme K (2002) Lateral

relocation of auxin efflux regulator PIN3 mediates tropism in Arabidopsis.

Nature **415**: 806–9

Ganguly A, Lee SH, Cho M, Lee OR, Yoo H, Cho H-T (2010) Differential Auxin-

Transporting Activities of PIN-FORMED Proteins in Arabidopsis Root Hair

Cells. *PLANT Physiol* **153**: 1046–1061

Geisler M, Aryal B, di Donato M, Hao P (2017) A Critical View on ABC

Transporters and Their Interacting Partners in Auxin Transport. *Plant Cell*

Physiol **58**: 1601–1614

Geisler M, Blakeslee JJ, Bouchard R, Lee OR, Vincenzetti V, Bandyopadhyay A,

Titapiwatanakun B, Peer WA, Bailly A, Richards EL, et al (2005) Cellular

efflux of auxin catalyzed by the Arabidopsis MDR/PGP transporter AtPGP1.

Plant J **44**: 179–194

Geisler M, Girin M, Brandt S, Vincenzetti V, Plaza S, Paris N, Kobae Y,

Maeshima M, Billion K, Kolukisaoglu UH, et al (2004) Arabidopsis

immunophilin-like TWD1 functionally interacts with vacuolar ABC transporters.

Mol Biol Cell **15**: 3393–405

Geisler M, Kolukisaoglu HU, Bouchard R, Billion K, Berger J, Saal B, Frangne

N, Koncz-Kalman Z, Koncz C, Dudler R, et al (2003) TWISTED DWARF1, a

unique plasma membrane-anchored immunophilin-like protein, interacts with

Arabidopsis multidrug resistance-like transporters AtPGP1 and AtPGP19. Mol

Biol Cell **14**: 4238–49

Geisler M, Murphy AS (2006) The ABC of auxin transport: the role of p-

glycoproteins in plant development. FEBS Lett **580**: 1094–102

George A, Jones P (2014) Bacterial ABC Transporters: Structure and Function. Bact.

Membr. Struct. Mol. Biol.

Goldsmith MHM (1977) The Polar Transport of Auxin. Annu Rev Plant Physiol **28**:

439–478

Gottesman MM, Pastan I (1993) Biochemistry of multidrug resistance mediated by

the multidrug transporter. Annu Rev Biochem **62**: 385–427

Gray WM, Östin A, Sandberg G, Romano CP, Estelle M (1998) High temperature

promotes auxin-mediated hypocotyl elongation in Arabidopsis. Proc Natl Acad

Sci U S A **95**: 7197–7202

Han M, Park Y, Kim I, Kim E-H, Yu T-K, Rhee S, Suh J-Y (2014) Structural

- basis for the auxin-induced transcriptional regulation by Aux/IAA17. *Proc Natl Acad Sci U S A* **111**: 18613–8
- Hartwig T, Chuck GS, Fujioka S, Klempien A, Weizbauer R, Potluri DP V., Choe S, Johal GS, Schulz B** (2011) Brassinosteroid control of sex determination in maize. *Proc Natl Acad Sci* **108**: 19814–19819
- Hawkins C, Liu Z** (2014) A model for an early role of auxin in Arabidopsis gynoecium morphogenesis. *Front Plant Sci* **5**: 327
- Hayashi K -i.** (2012) The Interaction and Integration of Auxin Signaling Components. *Plant Cell Physiol* **53**: 965–975
- Hayashi K, Nakamura S, Fukunaga S, Nishimura T, Jenness MK, Murphy AS, Motose H, Nozaki H, Furutani M, Aoyama T** (2014) Auxin transport sites are visualized in planta using fluorescent auxin analogs. *Proc Natl Acad Sci U S A* **111**: 11557–62
- He W, Brumos J, Li H, Ji Y, Ke M, Gong X, Zeng Q, Li W, Zhang X, An F, et al** (2011) A Small-Molecule Screen Identifies l-Kynurenine as a Competitive Inhibitor of TAA1/TAR Activity in Ethylene-Directed Auxin Biosynthesis and Root Growth in *Arabidopsis*. *Plant Cell* **23**: 3944–3960
- Henrichs S, Wang B, Fukao Y, Zhu J, Charrier L, Bailly A, Oehring SC, Linnert M, Weiwad M, Endler A, et al** (2012) Regulation of ABCB1/PGP1-catalysed auxin transport by linker phosphorylation. *EMBO J* **31**: 2965–80
- Higgins CF** (1992) ABC transporters: from microorganisms to man. *Annu Rev Cell Biol* **8**: 67–113
- Higgins CF, Gottesman MM** (1992) Is the multidrug transporter a flippase? *Trends*

Biochem Sci **17**: 18–21

Ho C-H, Lin S-H, Hu H-C, Tsay Y-F (2009) CHL1 Functions as a Nitrate Sensor in Plants. Cell **138**: 1184–1194

Hürlimann LM, Hohl M, Seeger MA (2017) Split tasks of asymmetric nucleotide-binding sites in the heterodimeric ABC exporter EfrCD. FEBS J **284**: 1672–1687

Inukai Y, Sakamoto T, Ueguchi-Tanaka M, Shibata Y, Gomi K, Umemura I, Hasegawa Y, Ashikari M, Kitano H, Matsuoka M (2005) Crown rootless1, Which Is Essential for Crown Root Formation in Rice, Is a Target of an AUXIN RESPONSE FACTOR in Auxin Signaling. PLANT CELL ONLINE **17**: 1387–1396

Irani NG, Di Rubbo S, Mylle E, Van den Begin J, Schneider-Pizoń J, Hniliková J, Šíša M, Buyst D, Vilarrasa-Blasi J, Szatmári A-M, et al (2012) Fluorescent castasterone reveals BRI1 signaling from the plasma membrane. Nat Chem Biol **8**: 583–589

Ito H (2006) A Gain-of-Function Mutation in the Arabidopsis Pleiotropic Drug Resistance Transporter PDR9 Confers Resistance to Auxinic Herbicides. PLANT Physiol **142**: 63–74

Jacobs WP, Mccready CC, Osborne DJ (1966) Transport of the Auxin 2, 4-Dichlorophenoxyacetic Acid. Plant Physiol **41**: 725–730

Janvilisri T, Venter H, Shahi S, Reuter G, Balakrishnan L, van Veen HW (2003) Sterol transport by the human breast cancer resistance protein (ABCG2) expressed in Lactococcus lactis. J Biol Chem **278**: 20645–51

Jodoin J, Demeule M, Fenart L, Cecchelli R, Farmer S, Linton KJ, Higgins CF,

- Béliveau R** (2003) P-glycoprotein in blood-brain barrier endothelial cells: interaction and oligomerization with caveolins. *J Neurochem* **87**: 1010–23
- Kamimoto Y, Terasaka K, Hamamoto M, Takanashi K, Fukuda S, Shitan N, Sugiyama A, Suzuki H, Shibata D, Wang B, et al** (2012) Arabidopsis ABCB21 is a facultative auxin importer/exporter regulated by cytoplasmic auxin concentration. *Plant Cell Physiol* **53**: 2090–100
- Kamphausen T, Fanghänel J, Neumann D, Schulz B, Rahfeld JU** (2002) Characterization of Arabidopsis thaliana AtFKBP42 that is membrane-bound and interacts with Hsp90. *Plant J* **32**: 263–276
- Kaneda M, Schuetz M, Lin BSP, Chanis C, Hamberger B, Western TL, Ehltng J, Samuels AL** (2011) ABC transporters coordinately expressed during lignification of Arabidopsis stems include a set of ABCBs associated with auxin transport. *J Exp Bot* **62**: 2063–77
- Kang J, Park J, Choi H, Burla B, Kretschmar T, Lee Y, Martinoia E** (2011) Plant ABC Transporters. *Arab B.* doi: 10.1199/tab.0153
- Kelley LA, Sternberg MJE** (2009) Protein structure prediction on the Web: a case study using the Phyre server. *Nat Protoc* **4**: 363–371
- Knöllner AS, Blakeslee JJ, Richards EL, Peer WA, Murphy AS** (2010) Brachytic2/ZmABCB1 functions in IAA export from intercalary meristems. *J Exp Bot* **61**: 3689–96
- Koepfli JB, Thimann K V, Went FW** (1938) Phytohormones : Structure and Physiological Activity. *I. J. Biol. Chem.*
- Kögl F, Haagen-Smit AJ** (1931) Über die Chemie des Wuchsstoffs. Amsterdam

Proceedings Sect Sci **34**: 1411–1416

- Korasick DA, Westfall CS, Goo Lee S, Nanao MH, Dumas R, Hagen G, Guilfoyle TJ, Jez JM, Strader LC, Mark Estelle** by Molecular basis for AUXIN RESPONSE FACTOR protein interaction and the control of auxin response repression. doi: 10.1073/pnas.1400074111
- Křeček P, Skůpa P, Libus J, Naramoto S, Tejos R, Friml J, Zažímalová E** (2009) The PIN-FORMED (PIN) protein family of auxin transporters. *Genome Biol* **10**: 249
- Krouk G, Lacombe B, Bielach A, Perrine-Walker F, Malinska K, Mounier E, Hoyerova K, Tillard P, Leon S, Ljung K, et al** (2010) Nitrate-Regulated Auxin Transport by NRT1.1 Defines a Mechanism for Nutrient Sensing in Plants. *Dev Cell* **18**: 927–937
- Kubeš M, Yang H, Richter GL, Cheng Y, Mlodzińska E, Wang X, Blakeslee JJ, Carraro N, Petrášek J, Zažímalová E, et al** (2012) The Arabidopsis concentration-dependent influx/efflux transporter ABCB4 regulates cellular auxin levels in the root epidermis. *Plant J* **69**: 640–54
- Kunji ERS, Slotboom DJ, Poolman B** (2003) *Lactococcus lactis* as host for overproduction of functional membrane proteins. *Biochim Biophys Acta - Biomembr* **1610**: 97–108
- Kuromori T, Miyaji T, Yabuuchi H, Shimizu H, Sugimoto E, Kamiya A, Moriyama Y, Shinozaki K** (2010) ABC transporter AtABCG25 is involved in abscisic acid transport and responses. *Proc Natl Acad Sci* **107**: 2361–2366
- Lee M, Choi Y, Burla B, Kim Y-Y, Jeon B, Maeshima M, Yoo J-Y, Martinoia E,**

- Lee Y** (2008) The ABC transporter AtABCB14 is a malate importer and modulates stomatal response to CO₂. *Nat Cell Biol* **10**: 1217–23
- Lee M, Lee K, Lee J, Noh EW, Lee Y** (2005) AtPDR12 Contributes to Lead Resistance in Arabidopsis. *PLANT Physiol* **138**: 827–836
- Lewis DR, Miller ND, Splitt BL, Wu G, Spalding EP** (2007) Separating the roles of acropetal and basipetal auxin transport on gravitropism with mutations in two Arabidopsis multidrug resistance-like ABC transporter genes. *Plant Cell* **19**: 1838–50
- Lewis DR, Wu G, Ljung K, Spalding EP** (2009) Auxin transport into cotyledons and cotyledon growth depend similarly on the ABCB19 Multidrug Resistance-like transporter. *Plant J* **60**: 91–101
- Li J, Jaimes KF, Aller SG** (2014a) Refined structures of mouse P-glycoprotein. *Protein Sci* **23**: 34–46
- Li R, Li J, Li S, Qin G, Novák O, Pěňčík A, Ljung K, Aoyama T, Liu J, Murphy A, et al** (2014b) ADP1 affects plant architecture by regulating local auxin biosynthesis. *PLoS Genet* **10**: e1003954
- Linton KJ, Higgins CF** (2007) Structure and function of ABC transporters: The ATP switch provides flexible control. *Pflugers Arch Eur J Physiol* **453**: 555–567
- Locher KP** (2016) Mechanistic diversity in ATP-binding cassette (ABC) transporters. *Nat Struct Mol Biol* **23**: 487–493
- Löfke C, Luschnig C, Kleine-Vehn J** (2013) Posttranslational modification and trafficking of PIN auxin efflux carriers. *Mech Dev* **130**: 82–94
- Ludwig-Müller J** (2011) Auxin conjugates: their role for plant development and in

- the evolution of land plants. *J Exp Bot* **62**: 1757–1773
- Luo B, Xue X-Y, Hu W-L, Wang L-J, Chen X-Y** (2007) An ABC transporter gene of *Arabidopsis thaliana*, AtWBC11, is involved in cuticle development and prevention of organ fusion. *Plant Cell Physiol* **48**: 1790–802
- Ma Q, Grones P, Robert S** (2018) Auxin signaling: a big question to be addressed by small molecules. *J Exp Bot* **69**: 313–328
- Mao H, Nakamura M, Viotti C, Grebe M** (2016) A Framework for Lateral Membrane Trafficking and Polar Tethering of the PEN3 ATP-Binding Cassette Transporter. *Plant Physiol* **172**: 2245–2260
- Marchant A, Bhalerao R, Casimiro I, Eklöf J, Casero PJ, Bennett M, Sandberg G** (2002) AUX1 promotes lateral root formation by facilitating indole-3-acetic acid distribution between sink and source tissues in the *Arabidopsis* seedling. *Plant Cell* **14**: 589–97
- Marchant A, Kargul J, May ST, Muller P, Delbarre A, Perrot-Rechenmann C, Bennett MJ** (1999) AUX1 regulates root gravitropism in *Arabidopsis* by facilitating auxin uptake within root apical tissues. *EMBO J* **18**: 2066–2073
- Martinoia E, Klein M, Geisler M, Bovet L, Forestier C, Kolukisaoglu Ü, Müller-Röber B, Schulz B** (2002) Multifunctionality of plant ABC transporters - More than just detoxifiers. *Planta* **214**: 345–355
- Mashiguchi K, Tanaka K, Sakai T, Sugawara S, Kawaide H, Natsume M, Hanada A, Yaeno T, Shirasu K, Yao H, et al** (2011) The main auxin biosynthesis pathway in *Arabidopsis*. *Proc Natl Acad Sci* **108**: 18512–18517
- Meinke D, Koornneef M** (1997) Community standards for *Arabidopsis* genetics.

Plant J **12**: 247–253

Mellor N, Band LR, Pěnčík A, Novák O, Rashed A, Holman T, Wilson MH, Voß

U, Bishopp A, King JR, et al (2016) Dynamic regulation of auxin oxidase and conjugating enzymes AtDAO1 and GH3 modulates auxin homeostasis. Proc Natl Acad Sci U S A **113**: 11022–7

Morris SE, Cox MCH, Ross JJ, Krisantini S, Beveridge CA (2005) Auxin

dynamics after decapitation are not correlated with the initial growth of axillary buds. Plant Physiol **138**: 1665–72

Mravec J, Skůpa P, Bailly A, Hoyerová K, Krecek P, Bielach A, Petrásek J,

Zhang J, Gaykova V, Stierhof Y-D, et al (2009) Subcellular homeostasis of phytohormone auxin is mediated by the ER-localized PIN5 transporter. Nature **459**: 1136–40

Mravec, Kubes M, Bielach A, Gaykova V, Petrasek J, Skupa P, Chand S,

Benkova E, Zazimalova E, Friml J (2008) Interaction of PIN and PGP transport mechanisms in auxin distribution-dependent development. Development **135**: 3345–3354

Multani DS, Briggs SP, Chamberlin MA, Blakeslee JJ, Murphy AS, Johal GS

(2003) Loss of an MDR transporter in compact stalks of maize br2 and sorghum dw3 mutants. Science (80-) **302**: 81–4

Murphy AS, Hoogner KR, Peer WA, Taiz L (2002) Identification, purification, and

molecular cloning of N-1-naphthylphthalamic acid-binding plasma membrane-associated aminopeptidases from Arabidopsis. Plant Physiol **128**: 935–50

Nemhauser J, Feldman L, Zambryski P (2000) Auxin and ETTIN in Arabidopsis

- gynoecium morphogenesis. *Development* **127**: 3877–3888
- Nishimura T, Hayashi K, Suzuki H, Gyohda A, Takaoka C, Sakaguchi Y, Matsumoto S, Kasahara H, Sakai T, Kato J, et al** (2014) Yucasin is a potent inhibitor of YUCCA, a key enzyme in auxin biosynthesis. *Plant J* **77**: 352–366
- Noh B, Bandyopadhyay A, Peer WA, Spalding EP, Murphy AS** (2003) Enhanced gravi- and phototropism in plant *mdr* mutants mislocalizing the auxin efflux protein PIN1. *Nature* **423**: 999–1002
- Noh B, Murphy AS, Spalding EP** (2001) Multidrug Resistance-like Genes of *Arabidopsis* Required for Auxin Transport and Auxin-Mediated Development. *Plant Cell* **13**: 2441–2454
- Novák O, Hényková E, Sairanen I, Kowalczyk M, Pospíšil T, Ljung K** (2012) Tissue-specific profiling of the *Arabidopsis thaliana* auxin metabolome. *Plant J* **72**: 523–36
- Okada K, Ueda J, Komaki MK, Bell CJ, Shimura Y** (1991) Requirement of the Auxin Polar Transport System in Early Stages of *Arabidopsis* Floral Bud Formation. *Plant Cell* **3**: 677–684
- Oono Y, Chen QG, Overvoorde PJ, Köhler C, Theologis A** (1998) *age* Mutants of *Arabidopsis* exhibit altered auxin-regulated gene expression. *Plant Cell* **10**: 1649–62
- Ottenschlager I, Wolff P, Wolverson C, Bhalerao RP, Sandberg G, Ishikawa H, Evans M, Palme K** (2003) Gravity-regulated differential auxin transport from columella to lateral root cap cells. *Proc Natl Acad Sci* **100**: 2987–2991
- Pan L, Aller SG** (2015) Equilibrated atomic models of outward-facing P-

- glycoprotein and effect of ATP binding on structural dynamics. *Sci Rep* **5**: 7880
- Panikashvili D, Savaldi-Goldstein S, Mandel T, Yifhar T, Franke RB, Hofer R, Schreiber L, Chory J, Aharoni A** (2007) The Arabidopsis DESPERADO/AtWBC11 Transporter Is Required for Cutin and Wax Secretion. *Plant Physiol* **145**: 1345–1360
- Parry G, Calderon-Villalobos LI, Prigge M, Peret B, Dharmasiri S, Itoh H, Lechner E, Gray WM, Bennett M, Estelle M** (2009) Complex regulation of the TIR1/AFB family of auxin receptors. *Proc Natl Acad Sci* **106**: 22540–22545
- Parry G, Marchant A, May S, Swarup R, Swarup K, James N, Graham N, Allen T, Martucci T, Yemm A, et al** (2001) Quick on the Uptake: Characterization of a Family of Plant Auxin Influx Carriers. *J Plant Growth Regul* **20**: 217–225
- Peaucelle A, Morin H, Traas J, Laufs P** (2007) Plants expressing a miR164-resistant CUC2 gene reveal the importance of post-meristematic maintenance of phyllotaxy in Arabidopsis. *Development* **134**: 1045–50
- Peer WA, Blakeslee JJ, Yang H, Murphy AS** (2011) Seven things we think we know about auxin transport. *Mol Plant* **4**: 487–504
- Peer WA, Jenness MK, Murphy AS** (2014) Measure for measure: determining, inferring and guessing auxin gradients at the root tip. *Physiol Plant* **151**: 97–111
- Pérez-Pérez JM, Ponce MR, Micol JL** (2004) The ULTRACURVATA2 gene of Arabidopsis encodes an FK506-binding protein involved in auxin and brassinosteroid signaling. *Plant Physiol* **134**: 101–17
- Pérez-Pérez JM, Ponce MR, Micol JL** (2002) The UCU1 Arabidopsis gene encodes a SHAGGY/GSK3-like kinase required for cell expansion along the

proximodistal axis. *Dev Biol* **242**: 161–73

Petersson S V., Johansson AI, Kowalczyk M, Makoveychuk A, Wang JY, Moritz T, Grebe M, Benfey PN, Sandberg G, Ljung K (2009) An Auxin Gradient and Maximum in the Arabidopsis Root Apex Shown by High-Resolution Cell-Specific Analysis of IAA Distribution and Synthesis. *PLANT CELL ONLINE* **21**: 1659–1668

Petrasek J, Friml J (2009) Auxin transport routes in plant development. *Development* **136**: 2675–2688

Pighin JA, Zheng H, Balakshin LJ, Goodman IP, Western TL, Jetter R, Kunst L, Samuels AL (2004) Plant Cuticular Lipid Export Requires an ABC Transporter. *Science* (80-.). 306:

Pilu R, Cassani E, Villa D, Curiale S, Panzeri D, Badone FC, Landoni M (2007) Isolation and characterization of a new mutant allele of brachytic 2 maize gene. *Mol Breed* **20**: 83–91

Porco S, Pěňčík A, Rashed A, Voß U, Casanova-Sáez R, Bishopp A, Golebiowska A, Bhosale R, Swarup R, Swarup K, et al (2016) Dioxygenase-encoding AtDAO1 gene controls IAA oxidation and homeostasis in Arabidopsis. *Proc Natl Acad Sci U S A* **113**: 11016–21

Porter WL, Thimann K V. (1965) Molecular requirements for auxin action—I. : Halogenated indoles and indoleacetic acid. *Phytochemistry* **4**: 229–243

Prandi C, Occhiato EG, Tabasso S, Bonfante P, Novero M, Scarpi D, Bova ME, Miletto I (2011) New Potent Fluorescent Analogues of Strigolactones: Synthesis and Biological Activity in Parasitic Weed Germination and Fungal Branching.

European J Org Chem **2011**: 3781–3793

Prandi C, Rosso H, Lace B, Occhiato EG, Oppedisano A, Tabasso S, Alberto G,

Blangetti M (2013) Strigolactone Analogs as Molecular Probes in Chasing the (SLs) Receptor/s: Design and Synthesis of Fluorescent Labeled Molecules. *Mol Plant* **6**: 113–127

Qin P, Tu B, Wang Y, Deng L, Quilichini TD, Li T, Wang H, Ma B, Li S (2013)

ABCG15 encodes an ABC transporter protein, and is essential for post-meiotic anther and pollen exine development in rice. *Plant Cell Physiol* **54**: 138–154

Ranocha P, Dima O, Nagy R, Felten J, Corratge-Faillie C, Novak O, Morreel K,

Lacombe B, Martinez Y, Pfrunder S, et al (2013) Arabidopsis WAT1 is a vacuolar auxin transport facilitator required for auxin homoeostasis. *Nat Commun* **4**: 2625

Rasmussen A, Heugebaert T, Matthys C, Van Deun R, Boyer F-D, Goormachtig

S, Stevens C, Geelen D (2013) A Fluorescent Alternative to the Synthetic Strigolactone GR24. *Mol Plant* **6**: 100–112

Raven JA (1975) Transport of indoleacetic acid in plant cells in relation to Ph and

electrical potential gradients and its significance for polar IAA transport. *New Phytol* **74**: 163–172

Rees DC, Johnson E, Lewinson O (2009) ABC transporters: the power to change.

Nat Rev Mol Cell Biol **10**: 218–227

Remy E, Duque P (2014) Beyond cellular detoxification: a plethora of physiological

roles for MDR transporter homologs in plants. *Front Physiol* **5**: 201

Ren H, Gray WM (2015) SAUR Proteins as Effectors of Hormonal and

- Environmental Signals in Plant Growth. *Mol Plant* **8**: 1153–1164
- Rensing SA** (2014) Gene duplication as a driver of plant morphogenetic evolution. *Curr Opin Plant Biol* **17**: 43–48
- Romano P, Gray J, Horton P, Luan S** (2005) Plant immunophilins: functional versatility beyond protein maturation. *New Phytol* **166**: 753–769
- Roy A, Kucukural A, Zhang Y** (2010) I-TASSER: a unified platform for automated protein structure and function prediction. *Nat Protoc* **5**: 725–738
- Rubery PH, Sheldrake AR** (1974) Carrier-mediated auxin transport. *Planta* **118**: 101–121
- de Ruyter PG, Kuipers OP, de Vos WM** (1996) Controlled gene expression systems for *Lactococcus lactis* with the food-grade inducer nisin. *Appl Environ Microbiol* **62**: 3662–7
- Růžicka K, Strader LC, Bailly A, Yang H, Blakeslee J, Langowski L, Nejedlá E, Fujita H, Itoh H, Syono K, et al** (2010) Arabidopsis PIS1 encodes the ABCG37 transporter of auxinic compounds including the auxin precursor indole-3-butyric acid. *Proc Natl Acad Sci U S A* **107**: 10749–53
- von Sachs J** (1868) *Lehrbuch der Botanik*. Leipzig, Engelmann
- Santelia D, Vincenzetti V, Azzarello E, Bovet L, Fukao Y, Düchtig P, Mancuso S, Martinoia E, Geisler M** (2005) MDR-like ABC transporter AtPGP4 is involved in auxin-mediated lateral root and root hair development. *FEBS Lett* **579**: 5399–5406
- Sauer M, Kleine-Vehn J** (2011) AUXIN BINDING PROTEIN1: The Outsider. *Plant Cell* **23**: 2033–2043

- Sauer M, Robert S, Kleine-Vehn J** (2013) Auxin: simply complicated. *J Exp Bot* **64**: 2565–77
- Schinkel AH** (1997) The physiological function of drug-transporting P-glycoproteins. *Semin Cancer Biol* **8**: 161–170
- Shani E, Weinstain R, Zhang Y, Castillejo C, Kaiserli E, Chory J, Tsien RY, Estelle M** (2013) Gibberellins accumulate in the elongating endodermal cells of *Arabidopsis* root. *Proc Natl Acad Sci U S A* **110**: 4834–9
- Shitan N, Bazin I, Dan K, Obata K, Kigawa K, Ueda K, Sato F, Forestier C, Yazaki K** (2003) Involvement of CjMDR1, a plant multidrug-resistance-type ATP-binding cassette protein, in alkaloid transport in *Coptis japonica*. *Proc Natl Acad Sci U S A* **100**: 751–6
- Shitan N, Dalmas F, Dan K, Kato N, Ueda K, Sato F, Forestier C, Yazaki K** (2013) Characterization of *Coptis japonica* CjABCB2, an ATP-binding cassette protein involved in alkaloid transport. *Phytochemistry* **91**: 109–16
- Sidler M, Hassa P, Hasan S, Ringli C, Dudler R** (1998) Involvement of an ABC transporter in a developmental pathway regulating hypocotyl cell elongation in the light. *Plant Cell* **10**: 1623–36
- Simon S, Skůpa P, Viaene T, Zwiewka M, Tejos R, Klíma P, Čarná M, Rolčik J, De Rycke R, Moreno I, et al** (2016) PIN6 auxin transporter at endoplasmic reticulum and plasma membrane mediates auxin homeostasis and organogenesis in *Arabidopsis*. *New Phytol* **211**: 65–74
- Singh B, Röhm KH** (2008) Characterization of a *Pseudomonas putida* ABC transporter (AatJMQP) required for acidic amino acid uptake: *Biochemical*

- properties and regulation by the Aau two-component system. *Microbiology* **154**: 797–809
- Sokolowska K, Kizińska J, Szewczuk Z, Banasiak A** (2014) Auxin conjugated to fluorescent dyes - a tool for the analysis of auxin transport pathways. *Plant Biol* **16**: 866–877
- Spartz AK, Ren H, Park MY, Grandt KN, Lee SH, Murphy AS, Sussman MR, Overvoorde PJ, Gray WM** (2014) SAUR Inhibition of PP2C-D Phosphatases Activates Plasma Membrane H⁺-ATPases to Promote Cell Expansion in Arabidopsis. *Plant Cell* **26**: 2129–2142
- Stepanova AN, Robertson-Hoyt J, Yun J, Benavente LM, Xie D-Y, Doležal K, Schlereth A, Jürgens G, Alonso JM** (2008) TAA1-Mediated Auxin Biosynthesis Is Essential for Hormone Crosstalk and Plant Development. *Cell* **133**: 177–191
- Stepanova AN, Yun J, Robles LM, Novak O, He W, Guo H, Ljung K, Alonso JM** (2011) The Arabidopsis YUCCA1 Flavin Monooxygenase Functions in the Indole-3-Pyruvic Acid Branch of Auxin Biosynthesis. *Plant Cell* **23**: 3961–3973
- Stukkens Y, Bultreys A, Grec S, Trombik T, Vanham D, Boutry M** (2005) NpPDR1, a pleiotropic drug resistance-type ATP-binding cassette transporter from *Nicotiana glauca*, plays a major role in plant pathogen defense. *Plant Physiol* **139**: 341–52
- Subhani S, Jayaraman A, Jamil K** (2015) Homology modelling and molecular docking of MDR1 with chemotherapeutic agents in non-small cell lung cancer. *Biomed Pharmacother = Biomédecine pharmacothérapie* **71**: 37–45

- Surpin M, Zheng H, Morita MT, Saito C, Avila E, Blakeslee JJ, Bandyopadhyay A, Kovaleva V, Carter D, Murphy A, et al** (2003) The VTI family of SNARE proteins is necessary for plant viability and mediates different protein transport pathways. *Plant Cell* **15**: 2885–99
- Swarup R, Friml J, Marchant A, Ljung K, Sandberg G, Palme K, Bennett M** (2001) Localization of the auxin permease AUX1 suggests two functionally distinct hormone transport pathways operate in the Arabidopsis root apex. *Genes Dev* **15**: 2648–53
- Swarup R, Péret B** (2012) AUX/LAX family of auxin influx carriers-an overview. *Front Plant Sci* **3**: 225
- Szewczyk P, Tao H, McGrath AP, Villaluz M, Rees SD, Lee SC, Doshi R, Urbatsch IL, Zhang Q, Chang G** (2015) Snapshots of ligand entry, malleable binding and induced helical movement in P-glycoprotein. *Acta Crystallogr D Biol Crystallogr* **71**: 732–41
- Tan X, Calderon-Villalobos LIA, Sharon M, Zheng C, Robinson C V., Estelle M, Zheng N** (2007) Mechanism of auxin perception by the TIR1 ubiquitin ligase. *Nature* **446**: 640–645
- Tapken W, Murphy AS** (2015) Membrane nanodomains in plants: capturing form, function, and movement. *J Exp Bot* **66**: 1573–86
- Terasaka K, Blakeslee JJ, Titapiwatanakun B, Peer WA, Bandyopadhyay A, Makam SN, Lee OR, Richards EL, Murphy AS, Sato F, et al** (2005) PGP4, an ATP binding cassette P-glycoprotein, catalyzes auxin transport in Arabidopsis thaliana roots. *Plant Cell* **17**: 2922–2939

- Titapiwatanakun B, Blakeslee JJ, Bandyopadhyay A, Yang H, Mravec J, Sauer M, Cheng Y, Adamec J, Nagashima A, Geisler M, et al** (2009) ABCB19/PGP19 stabilises PIN1 in membrane microdomains in Arabidopsis. *Plant J* **57**: 27–44
- Titapiwatanakun B, Murphy AS** (2009) Post-transcriptional regulation of auxin transport proteins: cellular trafficking, protein phosphorylation, protein maturation, ubiquitination, and membrane composition. *J Exp Bot* **60**: 1093–1107
- Truong SK, McCormick RF, Rooney WL, Mullet JE** (2015) Harnessing Genetic Variation in Leaf Angle to Increase Productivity of Sorghum bicolor. *Genetics* **201**: 1229–38
- Tsuda E, Yang H, Nishimura T, Uehara Y, Sakai T, Furutani M, Koshiba T, Hirose M, Nozaki H, Murphy AS, et al** (2011) Alkoxy-auxins are selective inhibitors of auxin transport mediated by PIN, ABCB, and AUX1 transporters. *J Biol Chem* **286**: 2354–64
- Verrier PJ, Bird D, Burla B, Dassa E, Forestier C, Geisler M, Klein M, Kolukisaoglu U, Lee Y, Martinoia E, et al** (2008) Plant ABC proteins--a unified nomenclature and updated inventory. *Trends Plant Sci* **13**: 151–9
- Vriet C, Russinova E, Reuzeau C** (2013) From Squalene to Brassinolide: The Steroid Metabolic and Signaling Pathways across the Plant Kingdom. *Mol Plant* **6**: 1738–1757
- Wang B, Bailly A, Zwiewka M, Henrichs S, Azzarello E, Mancuso S, Maeshima M, Friml J, Schulz A, Geisler M** (2013) Arabidopsis TWISTED DWARF1

- functionally interacts with auxin exporter ABCB1 on the root plasma membrane.
Plant Cell **25**: 202–14
- Wang Y, Jiao Y** (2018) Auxin and above-ground meristems. J Exp Bot **69**: 147–154
- Weijers D, Benkova E, Jäger KE, Schlereth A, Hamann T, Kientz M, Wilmoth JC, Reed JW, Jürgens G** (2005) Developmental specificity of auxin response by pairs of ARF and Aux/IAA transcriptional regulators. EMBO J **24**: 1874–1885
- Weijers D, Wagner D** (2016) Transcriptional Responses to the Auxin Hormone. Annu Rev Plant Biol **67**: 539–574
- Weller B, Zourelidou M, Frank L, Barbosa ICR, Fastner A, Richter S, Jürgens G, Hammes UZ, Schwechheimer C** (2017) Dynamic PIN-FORMED auxin efflux carrier phosphorylation at the plasma membrane controls auxin efflux-dependent growth. Proc Natl Acad Sci U S A **114**: E887–E896
- Went F** (1926) On growth-accelerating substances in the coleoptile of *Avena sativa*. Proc K Ned Akad van Wet **30**: 10–19
- West NW, Golenberg EM** (2018) Gender-specific expression of GIBBERELLIC ACID INSENSITIVE is critical for unisexual organ initiation in dioecious *Spinacia oleracea*. New Phytol **217**: 1322–1334
- Wilkins S** (2015) Structure and mechanism of ABC transporters. F1000Prime Rep **7**: 14
- Won C, Shen X, Mashiguchi K, Zheng Z, Dai X, Cheng Y, Kasahara H, Kamiya Y, Chory J, Zhao Y** (2011) Conversion of tryptophan to indole-3-acetic acid by TRYPTOPHAN AMINOTRANSFERASES OF ARABIDOPSIS and YUCCAs

- in *Arabidopsis*. *Proc Natl Acad Sci* **108**: 18518–18523
- Wu G, Otegui MS, Spalding EP** (2010) The ER-localized TWD1 immunophilin is necessary for localization of multidrug resistance-like proteins required for polar auxin transport in *Arabidopsis* roots. *Plant Cell* **22**: 3295–304
- Xiong J, Feng J, Yuan D, Zhou J, Miao W** (2015) Tracing the structural evolution of eukaryotic ATP binding cassette transporter superfamily. *Sci Rep* **5**: 16724
- Xu Y, Zhang S, Guo H, Wang S, Xu L, Li C, Qian Q, Chen F, Geisler M, Qi Y, et al** (2014) OsABCB14 functions in auxin transport and iron homeostasis in rice (*Oryza sativa* L.). *Plant J* **79**: 106–17
- Yang H, Murphy AS** (2009) Functional expression and characterization of *Arabidopsis* ABCB, AUX 1 and PIN auxin transporters in *Schizosaccharomyces pombe*. *Plant J* **59**: 179–191
- Yang H, Richter GL, Wang X, Młodzińska E, Carraro N, Ma G, Jenness M, Chao D, Peer WA, Murphy AS** (2013) Sterols and sphingolipids differentially function in trafficking of the *Arabidopsis* ABCB19 auxin transporter. *Plant J* **74**: 37–47
- Zazimalová E, Murphy AS, Yang H, Hoyerová K, Hosek P** (2010) Auxin transporters--why so many? *Cold Spring Harb Perspect Biol* **2**: a001552
- Zhang J, Lin JE, Harris C, Campos Mastrotti Pereira F, Wu F, Blakeslee JJ, Peer WA** (2016) DAO1 catalyzes temporal and tissue-specific oxidative inactivation of auxin in *Arabidopsis thaliana*. *Proc Natl Acad Sci* **113**: 11010–11015
- Zhang J, Peer WA** (2017) Auxin homeostasis: the DAO of catabolism. *J Exp Bot*

68: 3145–3154

- Zhang K, Novak O, Wei Z, Gou M, Zhang X, Yu Y, Yang H, Cai Y, Strnad M, Liu CJ** (2014) Arabidopsis ABCG14 protein controls the acropetal translocation of root-synthesized cytokinins. *Nat Commun* **5**: 3274
- Zhao B, Lv M, Feng Z, Campbell T, Liscum E, Li J** (2016) TWISTED DWARF 1 Associates with BRASSINOSTEROID-INSENSITIVE 1 to Regulate Early Events of the Brassinosteroid Signaling Pathway. *Mol Plant* **9**: 582–592
- Zhao H, Liu L, Mo H, Qian L, Cao Y, Cui S, Li X, Ma L** (2013) The ATP-binding cassette transporter ABCB19 regulates postembryonic organ separation in Arabidopsis. *PLoS One* **8**: e60809
- Zhao Y** (2018) Essential Roles of Local Auxin Biosynthesis in Plant Development and in Adaptation to Environmental Changes. *Annu Rev Plant Biol* **69**: 1–12
- Zhou W, Wei L, Xu J, Zhai Q, Jiang H, Chen R, Chen Q, Sun J, Chu J, Zhu L, et al** (2010) Arabidopsis Tyrosylprotein Sulfotransferase Acts in the Auxin/PLETHORA Pathway in Regulating Postembryonic Maintenance of the Root Stem Cell Niche. *PLANT CELL ONLINE* **22**: 3692–3709
- Zou P, Mchaourab HS** (2009) Alternating Access of the Putative Substrate-Binding Chamber in the ABC Transporter MsbA. *J Mol Biol* **393**: 574–585